論文 / 著書情報
Article / Book Information

題目(和文)	
Title(English)	Allorecognition in jellyfish Cladonema radiatum
著者(和文)	TANGCrystal
Author(English)	Crystal Tang
出典(和文)	学位:博士(理学), 学位授与機関:東京工業大学, 報告番号:甲第12836号, 授与年月日:2024年9月20日, 学位の種別:課程博士, 審査員:立花 和則,岩崎 博史,川上 厚志,白木 伸明,折原 芳波
Citation(English)	Degree:Doctor (Science), Conferring organization: Tokyo Institute of Technology, Report number:甲第12836号, Conferred date:2024/9/20, Degree Type:Course doctor, Examiner:,,,,
学位種別(和文)	博士論文
Type(English)	Doctoral Thesis

Allorecognition in jellyfish *Cladonema radiatum*

A thesis submitted for the Degree of
Doctor of Science

in

the School of Life Science and Technology

at

Tokyo Institute of Technology

by

Crystal TANG

Submission date:	23rd August, 2024
Supervisor:	Dr. Kazunori Tachibana
Examination committee:	Professor Hiroshi Iwasaki Dr. Atsushi Kawakami Dr. Nobuaki Shiraki Dr. Kanami Orihara

Abstract

Allorecognition—the ability of an organism to discriminate between self and non-self—is crucial to colonial marine animals to avoid invasion by other individuals in the same habitat. The cnidarian hydroid *Hydractinia* has long been a major research model in studying invertebrate allorecognition, establishing a rich knowledge foundation. Here in this study, I introduce a new cnidarian model *Cladonema radiatum* (*C. radiatum*). *C. radiatum* is a hydroid jellyfish which also forms polyp colonies interconnected with stolons. Allorecognition responses, fusion or regression of stolons, are observed when stolons encounter. By transmission electron microscopy, I observe rapid tissue remodelling to connect gastrovascular system in fusion. Rejection responses are regulated by reconstruction of the chitinous exoskeleton perisarc, and induction of necrotic and autophagic cellular responses at cells in contact with the opponent. Genetic analysis identifies allorecognition genes: 6 *Alr* genes located on the putative Allorecognition Complex (ARC) and 4 immunoglobulin superfamily genes on a separate genome region. *C. radiatum* allorecognition genes show high conservation with *Hydractinia Alr* family. Stolon encounter assays of inbred lines reveal that genotypes of *Alr1* determine allorecognition outcomes in *C. radiatum*. Besides stolons, sign of incompatibility, in form of a ring-shaped scar on the jellyfish umbrella around the incompatible graft, is also observed in medusa. Association with Alr awaits investigations.

Acknowledgements

I would like to express my gratitude to my supervisor, Dr. Kazunori Tachibana, for his guidance and support during my doctoral study. I would also like to give special thanks to my collaborators, specifically Dr. Miwa Tamura-Nakano for her help in TEM observations, and Professsor Takehiko Ito, Dr. Rei Kajitani and Mr. Takao Onojima for their remarkable work on the genomic analysis. I would like to extend my heartfelt thanks to all my laboratory members, especially the Allorecognition team, for making these years an unforgettable experience. Special thanks to my family and friends for their support and understanding throughout these years.

Table of Contents

Chapter 1: Introduction

Multicellularity has evolved multiple times independently across lineages of eukaryotes (Niklas, 2014). One major advantage brought by multicellularity is the increase in size, which benefits acquisition of resources (Niklas, 2014; Bonner, 1998; Nicotra, 2019). Fusion between multicellular organisms when encountering was observed across the phyla of life. Similar to multicellularity, formation of chimeras enhances fitness by increasing body sizes. Chimerism may also increase survival rate by forming genetically heterogenous organisms (Carpenter et al., 2011; Rinkevich, 2002). However, chimerism also brings the risk of somatic cell/germline parasitism (Stoner & Weissman, 1996; Laird et al., 2005; De Tomaso, 2006). Fusion between different individuals allow the invasion of stem cells across the individuals. These stem cells may take over the production of somatic cells and also germ cells, which indeed leads to elimination of genetic diversity (Mueller & Rinkevich, 2020; De Tomaso, 2014; Rinkevich, 2002; Carpenter et al., 2011). Organisms therefore adapt various mechanisms to prevent or regulate these kinds of fusion. The general ability of an organism to discriminate between self and non-self, specifically within the same species, is referred to as allorecognition.

Marine sessile colonial invertebrates naturally encounter other individuals in the same habitat. Allorecognition therefore is important to prevent somatic cell/germline parasitism and also to regulate spatial competition between close colonies in the habitats (Buss, 1990; Bastiaans et al., 2015). Marine sessile animals, chiefly tunicate *Botryllus schlosseri* (hereafter *Botryllus*) and Cnidarian *Hydractinia symbiolongicarpus* (hereinafter *Hydractinia*; also *H. symbiolongicarpus*/Hsym in figures), have been classical research models for studying invertebrate allorecognition (Rosengarten & Nicotra, 2011).

Allorecognition in *Botryllus*

Botryllus belongs to ascidian, which is also known as sea squirt. *Botryllus* form colonies comprising multiple genetically identical individuals, called zooids. Zooids are embedded in a gelatinous extracellular matrix, tunic, and are interconnected by anastomosing blood vessel network. Zooids are arranged in star-shaped structures known as systems. Peripheries of colonies are surrounded by vascular protrusions called ampullae, which are the major site allorecognition responses take place. (De Tomaso, 2009). When two colonies encounter, the ampullae from each individual extend towards another and interact. When the two colonies are histocompatible, the ampullae fuses with formation of connecting vascular system (Rosengarten & Nicotra, 2011; De Tomaso, 2009). When the colonies are incompatible, localised inflammatory reaction occurs, which leads to destruction of the interacting ampullae (Rosengarten & Nicotra, 2011; De Tomaso, 2009).

Allorecognition of *Botryllus* is governed by a single highly polymorphic locus—FuHC (Fusion Histocompatibility) (De Tomaso & Weissman, 2003; De Tomaso et al., 2005). FuHC determines individuals' histocompatibility in a manner similar to the vertebrate major histocompatibility complex (MHC). FuHC codes for a membrane-bound protein that possesses two immunoglobin (Ig)-like domains (or IgSF), a common feature of cell-surface receptors involved in cell-cell recognition. Individuals sharing at least one allele are considered histocompatible and undergo fusion upon contact, while contact between individuals with no matching of alleles result in rejection (De Tomaso et al., 2005; Rosengarten & Nicotra, 2011). Another highly polymorphic locus, *fester*, has been identified near FuHC. Despite the high polymorphism, allorecognition outcomes are independent of the polymorphism. However, fester is reported to be involved in mediating the allorecognition responses. It is suggested that fester is a receptor of FuHC and may act as an effector in the allorecognition responses (Nyholm et al., 2006; McKitrick et al., 2011).

Allorecognition in *Hydractinia*

Hydractinia is another major research model for studying invertebrate allorecognition (Powell et al., 2007; Rosengarten & Nicotra, 2011). *Hydractinia* is a marine hydroid belonging to the Phylum Cnidaria and Class Hydrozoa (Figure 1A). *Hydractinia* specifically inhabits the shells of hermit crabs. *Hydractinia* colonies consist of polyps interconnected with gastrovascular canals known as stolons, which are webbed by stolon mat. Allorecognition responses have been documented at the encounter between different colonies. Initiation of allorecognition responses is accompanied by accumulation of nematocytes at the contact sites, in regardless of the allorecognition outcomes (Lange et al., 1989). Nematocytes are Cnidarian-specific specialized cells that produce and discharge stinging organelles nematocysts (a.k.a. cnidocysts), mainly for capturing prey and defence. During fusion, nematocytes, though once assemble, dismiss and connection of gastrovascular system occurs within hours after contact (Lange et al., 1989; Buss et al., 2012). In contrast, nematocytes are continuously recruited to the contact sites, usually including a growing stolon tip that encounters another stolons at its growing direction, and cause swelling of the stolons. These stolons are described as hyperplastic stolons. Rejection is recognised by the firing of nematocysts towards the opponent. Hyperplastic stolons also grow over the other colony and exploit the resources. End of rejection is marked with death of one of the colonies (Buss et al., 1984; Lange et al., 1989). Besides fusion and rejection, a special form of rejection—transitory fusion (also described as passive rejection in early publications) is also observed. In transitory fusion, colonies first temporarily fuse, with connection of gastrovascular system, but followed by rejection events. Rejection mechanisms with and without nematocyte involvement are both reported (Buss et al., 1984; Cadavid et al., 2004; Powell et al., 2007; Buss et al., 2012). Transitory fusion is categorised into two types: type I and type II. In type I transitory fusion, gastrovascular canals disconnect and stolon mat separates in one to three

days after the initial temporary fusion. Boundaries of the colonies are found to be physically barriered by a white fibrous material. Type II transitory fusion occurs in a similar manner as type I, except the two colonies remain in contact and gastrovascular systems re-connect, although with clear visible border (Powell et al., 2007). These allorecognition outcomes are determined genetically.

Early genetic analysis of inbred lines identified two key determinants—*Alr1* (*allorecognition 1*) and *Alr2* (Mokady & Buss, 1996; Cadavid et al., 2004). Alr1 and Alr2 are located in a genomic region called allorecognition complex (ARC). Both *Alr1* and *Alr2* code for membrane-bound proteins that contain highly polymorphic Ig-like domains (Nicotra et al., 2009; Rosa et al., 2010; Gloria-Soria et al., 2012). While both *Botryllus* FuHC and *Hydractinia* Alr1/2 have Ig-like domains, there is no evidence of evolutionary linkage between these allorecognition determinants, so as that with the vertebrate MHC (Grosberg & Plachetzki, 2010). Alr1 and Alr2 discriminate based on their homophilic binding with the Alr1 and Alr2 presented on cell surface of the opponents in contact (Karadge et al., 2015). Allorecognition outcomes can be predicted by the genotypes of the two genes. Colonies with at least one matching alleles in both *Alr1* and *Alr2* end up fusing. Colonies that have no matching allele in either *Alr1* or *Alr2* reject. Encounters between colonies sharing only one allele in either *Alr1* or *Alr2* result in transitory fusion (Cadavid et al., 2004; Powell et al., 2007). Genotypes of *Alr1* and *Alr2* perfectly predict the allorecognition outcomes in the inbred line study, but not that in the wild types (Shenk & Buss, 1991; Cadavid et al., 2004). Further genomic analysis has been carried out on the ARC. Recent published works identified the existence of 41 *Alr* family genes in the ARC (Huene et al., 2022), and at least 8 *IgSF* genes have association with allorecognition (Rodriguez-Valbuena et al., 2022). Functionality of each gene still await further investigation.

Allorecognition in *Podocoryne*

Allorecognition was also studied in another marine hydroid, *Podocoryne carnea* (Hereafter *Podocoryne*) (Tardent & Burhrer, 1982; Tardent & Jauch, 1983). *Podocoryne* belongs to Filifera III, the same sub-order as *Hydractinia* (Figure 1A). Similar to *Hydractinia*, *Podocoryne* also form colonies with polyps interconnected by stolon networks. *Podocoryne* also exhibit allorecognition in stolons. Fusion is similar to that in *Hydractinia*: compatible stolons fuse with connection of gastrovascular canals upon contact. However, aggressive rejection is not observed. Instead, encounters between incompatible stolons lead to thickening of exoskeleton, thus avoidance of further contact of the stolons (Tardent & Jauch, 1983). Cnidarian stolons are enclosed by a chitinous exoskeleton known as perisarc. This perisarc at the contact site thickens upon encounter between incompatible stolons, preventing cellular contact between the stolons. The approaching stolons eventually grow over or change direction to grow along the other stolons. Genetic mechanisms remain elusive.

Self/no-self recognition in *Hydra*

Interesting research on self/non-self recognition was also conducted with *Hydra*. *Hydra* also belongs to Hydrozoa but is solitary polyp living in freshwater (Figure 1A). Hydra does not form colonies nor have stolons, and so is unlikely to be in contact with other individuals in the natural habitat. Self/non-self recognition was studied with transplantation between polyps of different *Hydra* species. In early research, increased phagocytosing cells were reported at the epithelia of the contact sites in grafts between *Hydra attenuata* and *Hydra oligactis* (Bosch & David, 1986). Grafts between individuals of different species instead of those within the same species was examined, so the ability of recognition is not defined as allorecognition, but xenorecognition. Apoptosis was also observed in grafts between *Hydra vulgaris* and *Hydra oligactis*. However, the apoptosis observed was

suggested to be the consequence of detachment of epithelial cells from the extracellular matrix, instead of the xenorecognition (Kuznetsov et al., 2002). Furthermore, later publication showed that intraspecific grafts between genetically distinct strains of *Hydra vulgaris* did not induce phagocytosis nor elimination of foreign cells (Kuznetsov & Bosch, 2003). It suggested that Hydra does not possess ability of allorecognition, presumably due to its solitary nature.

Cladonema radiatum as new research model for allorecognition

In this study, I introduce *Cladonema radiatum* (hereinafter *C. radiatum*; also Crad in figures), as a new animal model for studying Cnidarian allorecognition. *C. radiatum* belongs to Hydrozoa, the same class as *Hydractinia*, *Podocoryne* and *Hydra* (Figure 1A). Life cycle of *C. radiatum* consists of sexual and asexual stages. *C. radiatum* reproduces sexually in the free-living medusae stage (Figure 1B). Male or female medusae are produced from polyps and these medusae spawn sperm or eggs, respectively. Fertilised eggs develop into larvae, called planulae, and metamorphose into primary polyps upon settlement on substrate. Stolons extend from the primary polyps and more polyps are budded on the stolons by asexual reproduction. These form the colonies of the sessile polyp stage (Figure 1C). *C. radiatum* has stolon networks similar to *Hydractinia*, but without stolonal mat (Figure 1D). In pilot experiments, fusion (Figure 1E) and rejection (Figure 1F) responses between stolons were observed at encounter between stolons of different colonies, suggesting allorecognition is conserved in *C. radiatum*.

C. radiatum belongs to the same class as the two studied Hydrozoans with observed allorecognition, *Hydractinia* and *Podocoryne*, but they are of different suborder clades: *Hydractinia* and *Podocoryne* are of Filifera III; *C. radiatum* is of Capitata. Comprehensive study on allorecognition was only reported on *Hydractinia*. There is inadequate information

for analysing the evolution or conservation of the *Hydractinia* allorecognition. Therefore in this study, by morphological and genetic analysis, I aimed to (1) characterise allorecognition in *C. radiatum* so as to establish *C. radiatum* as a new research model for studying Hydrozoan allorecognition, and (2) investigate the evolution and conservation of allorecognition by comparative analysis.

Allorecognition was first characterised in *C. radiatum* stolons. Morphological Investigation of allorecognition in stolons is organised in Chapter 2. Comprehensive morphological study using transmission electron microscopy (TEM) showed cellular detail of the fusion and rejection responses. Nematocysts were not involved in the allorecognition responses in *C. radiatum*. Rejection was mediated by (1) reconstruction of exoskeleton perisarc and (2) necrotic and autophagic cell damage at cellular contact site between incompatible individuals. Genetic analysis of *C. radiatum* allorecognition (in collaboration with Takao Onojima (Ito Lab, School of Life Science and Technology, Tokyo Institute of Technology)) is organised in Chapter 3. A total of 6 *Alr* family genes on the potential ARC and 4 IgSF-like genes on a separate region were identified. Stolon encounter assays using the inbred lines revealed *Alr1* being the determinant of allorecognition outcomes. Besides stolons, I also tried to investigate allorecognition in the medusae stage, which is absent in *Hydractina*. The results are discussed in Chapter 4. While there is no distinct rejection dependent on *Alr*, incompatibility between genetically distinct grafts, in form of a ring-shaped scar around the graft, was observed in grafted jellyfish.

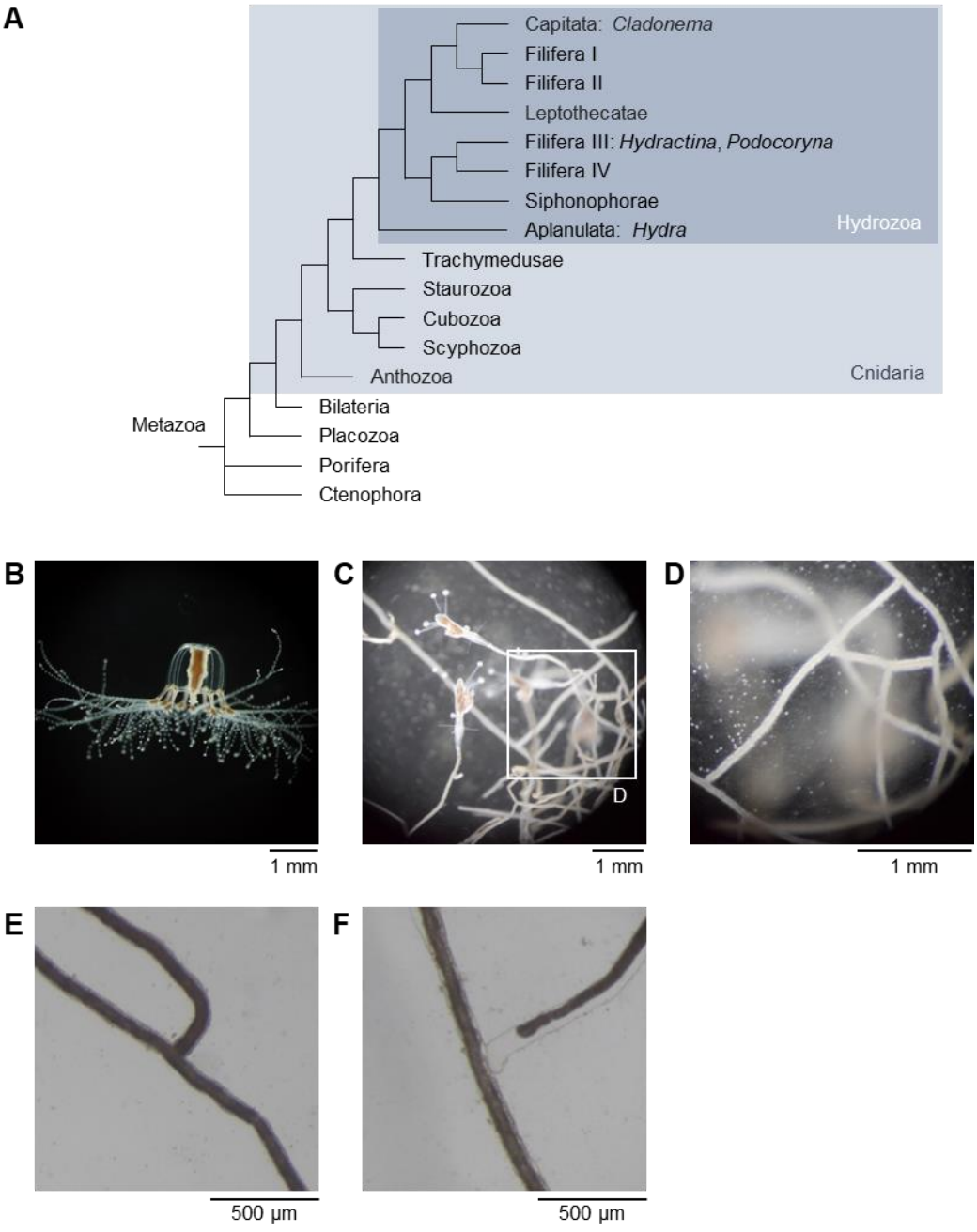

Figure 1. Allorecognition responses in Hydrozoan jellyfish *Cladonema radiatum*. (A) Phylogenetic relationships (based on Zapata et al. (2015) and Bentlage and Collins (2021)). (B) Medusa form. (C) Polyp colony. Close-up of the interconnecting stolons (white box) is shown in (D). (E) Fusion and (F) rejection between stolons.

Chapter 2: Allorecognition in *C. radiatum* stolons

TEM observation was performed in collaboration with Dr. Miwa Tamura-Nakano (Research Institute National Center for Global Health and Medicine). The main part of this chapter together with Chapter 3 are included in the publsihed manuscript, Tang, C., Tamura-Nakano, M., Kobayakawa, K., Ozawa, T., Onojima, T., Kajitani, R., Ito, T., Tachibana, K. (2024). A single gene determines allorecognition in hydrozoan jellyfish Cladonema radiatum inbred lines. *Journal of Experimental Zoology Part A: Ecological and Integrative Physiology*.

Introduction

Marine colonial invertebrates encounter other colonies occasionally in their habitats. As discussed in Chapter 1, fusion of different colonies benefits the survival of the colonies by increasing organism size and producing genetically heterogenous colonies. However, fusion also allows the invasion of stem cells and risks somatic/germ cell parasitism (Stoner and Weissman, 1996; Laird et al., 2005; De Tomaso, 2006). Therefore, effective allorecognition mechanisms are important in regulating this kind of fusion.

Morphological detail of allorecognition has been documented in *Hydractinia* (Powell et al., 2007; Rosengarten and Nicotra, 2011). One key feature of allorecognition responses in *Hydractinia* is the involvement of nematocytes. Nematocytes, the Cnidarian-specific stinging cells, are recruited to the contact sites immediately upon encounter, regardless of the allorecognition outcomes (Lange et al., 1989). Nematocytes are dismissed if the colonies are determined compatible, and nematocysts are discharged towards each other if the colonies are incompatible (Buss et al., 1984; Lange et al., 1989). Encounter of *Hydractinia* colonies usually occur with the approaching of a growing stolon tip (attacking) to a pre-existing stolon (defending). Nematocytes are recruited to both the attacking and defending stolons. The nematocyte accumulation causes the swelling of the growing stolon tips, which are described

as hyperplastic. These hyperplastic stolons grow over other encountered stolons and exploit the resources. Rejection continues until one of the colonies dies or there is no more contact between the colonies (Buss et al., 1984; Lange et al., 1989). The firing of nematocysts appears to a key step in differentiating fusion and rejection responses. However, there seems to be discrepancy between the morphological observation in different publications. In early publication, nematocytes recruitment at early contact was reported despite allorecognition responses. Rejection was therefore proposed to be the default response, and is suppressed when compatibility is recognised (Buss et al., 1984; Lange et al., 1989; Nicotra, 2022). However, in later publication, no nematocyte involvement was observed in any stages during transitory fusion (Buss et al., 2012). Nematocytes seem to be recruited upon intraspecific encounters, which include also those resulting in transitory fusion. There is inadequate discussion on whether the lack of nematocyte involvement in transitory fusion is an exception and if so, what the reasons for that are.

Another major difference between different allorecognition responses observed in *Hydractinia* is the remodelling and connection of gastrovascular canals in fusion and early transitory fusion. Gastrovascular systems are readily merged with connection of ectoderm and endoderm, within hours upon encounter, in cases of fusion and transitory fusion (Lange et al., 1989; Buss et al., 2012). In rejection, failure of adhesion of ectoderm is observed and gastrovascular canals never fuse (Lange et al., 1989).

Temporarily fused colonies separate in transitory fusion with autophagy and necrosis at the contact region (Buss et al., 2012). Necrosis was suggested to be a subsequent event of autophagy. Apoptosis was not observed. Application of pharmacological autophagic inhibitors suspended the separation of the colonies, establishing the involvement of autophagy and subsequent necrosis in the rejection process in transitory fusion.

Another feature of transitory fusion is the physical separation of the colonies by a

white fibrous, electron-dense, material (Buss et al., 1984; Cadavid et al., 2004; Powell et al., 2007; Buss et al., 2012). The contents of this material remain unidentified. In terms of physical barrier, *Podocoryne* also utilises the chitinous exoskeleton perisarc (also known as periderm) to avoid cellular contact in incompatible encounters. Fusion of *Podocoryne* stolons is similar to that in *Hydractinia*, with rapid connection of the gastrovascular canals. However, incompatible *Podocoryne* stolons develop thicker perisarc at the contact zone which prevents the stolons from contacting and eventually guides the approaching stolon to grow in a different direction, either across or along the defending stolon. Ectoderm cells with electron-dense granules were observed at the contact regions. Although the contents of the granules were not identified, the authors suggested these granules were responsible for enzymatic lysis and synthesis of the perisarc, and named these cells P-cells. However, there are only a few dated sources for studying the *Podocoryne* allorecognition. It may be inadequate to say these are the general allorecognition responses in *Podocoryne*, as these responses may vary among different strains or genotypes.

In this chapter, I summarised the results of morphological observations on the allorecognition responses in *C. radiatum* stolons. Pilot assays identified allorecognition responses at stolon encounter: fusion (Figure 1E) and rejection (Figure 1F). Progresses of the two responses were recorded by time-lapse observation by inverted stereomicroscope. Cellular morphologies of the responses were investigated by TEM. I found that nematocytes are not involved in *C. radiatum* stolon allorecognition. Fusion is accomplished rapidly with the connection of gastrovascular canals. Rejection is regulated by reconstruction of perisarc as physical barriers between the stolons. Necrotic and autophagic cell damage is also observed at contact site between incompatible stolons. These observations show that allorecognition responses in *C. radiatum* have similarities, but also evident differences compared to that in *Hydractinia* and *Podocoryne*.

Results

Morphological characteristics of *C. radiatum* stolons

To aid the observation by TEM and identification of changes occurring during allorecognition, I first characterised the morphology of a normal stolon. Stolons are generally around 80-100 μm thick, including the chitinous exoskeleton perisarc (Figure 2.1A,D). Perisarc at growing stolon tips is usually relatively thinner and is closely wrapping the ectoderm cells. Stolons consist of, from outside to inside, ectoderm, mesoglea, endoderm and gastrovascular canal (Figure 2.1E). Ectoderm cells are highly vacuolated and contain some small electron-dense granules (Figure 2.1D). Mesoglea is a thin non-cellular layer between ectoderm and endoderm. Endoderm cells have generally slightly electron-denser cytoplasm compared to ectoderm cells. Endoderm cells contain abundant large electron-dense granules, including lysosomes and lipid droplets. Crystal structures are frequently observed in these granules. There granules are presumably involved in food digestion and energy storage. Nematocysts are scattered in the ectoderm and also sometimes in endoderm. Nematocysts, due to its hardness and poor impermeability, often fell off from the resin sections, leaving an electron-lucent empty space in the TEM images (Figure 2.1A). Morphology of stolons was also observed with digital holographic microscopy (DHM), which allows non-invasive high-resolution imaging of live samples based on refractive index (Figure 2.1C,F). DHM images clearly captured the nematocysts in the ectoderm. DHM images also show the small and large granules in ectoderm and endoderm respectively.

No involvement of nematocysts in *C. radiatum* allorecognition responses

Allorecognition responses in stolons were monitored by time-lapse imaging on an inverted stereomicroscope. Fusion, characterised by the connection of gastrovascular canals,

was observed usually within 12 hours upon the contact between compatible stolons (Figure 2.2A). Rejection, in contrast, was a relative slow process (Figure 2.2B). Incompatible stolons stayed in contact, without developing connection of gastrovascular canals nor separation, for more than 24 hours, in some cases up to days. Rejection was most often noted by the regression of the attacking stolon leading to the separation of the two stolons. The separation was usually followed by repeated re-approaching and regression of the attacking stolons.

One notable observation is that nematocyte accumulation is never observed during the allorecognition processes in *C. radiatum*, unlike that in *Hydractinia*. To provide morphological observation in higher resolution, different time points of stolon encounters were sampled and observed with TEM. In none of the TEM observations made in any time points of fusion or rejection showed recruitment of nematocysts at the contact zones (Figure 2.3 and 2.4). Flattening and swelling of stolons, which resembles the hyperplastic stolons in *Hydractinia*, were observed when the attacking stolons approaching the defending stolons but nematocysts were absent (Figure 2.3A and 2.4A). Nematocysts are not involved in allorecognition in *C. radiatum* stolons.

Reconstruction of perisarc separates stolons during rejection

TEM observation reveals the dynamics of the cellular morphologies during stolon encounters. First morphological change observed was the increase in cytoplasmic density of the ectoderm cells of the attacking stolon tips (Figure 2.3A and 2.4A). Compared to highly vacuolated ectoderm cells in the typical stolon tip shown in Figure 2.1A,B, stolon tips were "densely packed" with polarised cells that have electron-dense granules accumulated at the contact side (Figure 2.3C and 2.4C). These electron-dense granule-containing cells may be equivalent to the P-cells observed in *Podocoryne* and contain enzymes that digest perisarc to allow cellular contact of the stolons. Electron-dense granules were also observed in ectoderm

of the defending stolons, but were slightly larger in size than those at the attacking stolon (Figure 2.3D). Live imaging by DHM showed evidence of release of high-refractive index granules into the space between the encountering stolons (Figure 2.5). Refractive index correlates with protein density. These granules were likely to contain perisarc lysing enzymes and were secreted to digest the own perisarc and also the perisarc of the opposing stolons.

Stolons came into cellular contact, after both perisarc of the attacking and defending stolons was lysed, at approximately 3 hours post-encounter (Figure 2.3E and 2.4E). The thick perisarc of defending stolons was lysed open to approximately the width of the attacking stolon, with blunt ends (Figure 2.3F and 2.4F), showing the digestion of the perisarc was resulted from localised enzymatic activity. Time required to lyse the perisarc varied with the thickness of the perisarc so time sequences of the samples does not directly represent event sequences. Fusion and rejection responses diverge upon cellular contact, presumably with Alr1 recognition. In fusion between compatible stolons, cells came into contact and boundary between cells of the attacking and defending stolons became ambiguous rapidly (Figure 2.3E.G). Ectoderm cells with electron-dense granules remained only at the sides but not at the centre of the contact site. Basement membrane of the attacking stolon remained intact. Cells on the defending side contains large lipid droplets and crystal structures, which are specific features of endoderm cells (Figure 2.3H). It showed that ectoderm cells at the centre of contact site were dismissed and endoderm cells were in direct contact. Dispersal of ectoderm cells indicates the remodelling process for connection of gastrovascular canals during fusion. Alteration of basement membranes were soon observed at 5 hours post-encounter (Figure 2.3I,J) and complete connection of gastrovascular canals with continuous basement membranes were recognised at 10.5 hours post-encounter (Figure 2.3K).

In contrast, incompatible stolons in rejection response remained in contact for prolonged periods of time without sign of connection of gastrovascular canals. Indeed,

perisarc separated the two stolons in most of the samples observed (Figure 2.4E-L). Ectoderm cells of the two stolons came into contact at 3 hours post-encounter after perisarc was digested while the border remained recognisable (Figure 2.4B,D). Stolons appeared to be in contact at 14 hours post-encounter (Figure 2.4E), but stolons were indeed separated by a thin layer of perisarc when observed at high magnification (Figure 2.4F). The thin perisarc was located between the broken thick perisarc and defending ectoderm, supposedly to be synthesised after the first contact so as to reconstruct the perisarc. The attacking stolon's perisarc was also recovered intact. Stolon encounters at 24 hours (Figure 2.4G,F), 48 hours (Figure 2.4I,J) and 62 hours post-encounter (Figure 2.4K,L) were also found separated by the newly synthesised perisarc. At 62 hours post-encounter, layers of newly synthesised perisarc, which made up the thickness of approximately the pre-existing thick perisarc, were observed. Reconstruction of perisarc apparently acts as a physical defence mechanism that avoid direct contact between incompatible individuals.

Necrotic and autophagic responses during early rejection

Rejection occurred upon cell contact at 3 hours post-encounter between incompatible individuals (Figure 2.6A). Cell process (Figure 2.6B) and loss of cell membrane integrity (Figure 2.6C) were observed at the contact sites. Necrosis, indicated by cellular materials leaking from the ruptured cell membrane into the extracellular space, was observed at the boundary cells (Figure 2.6E), especially at the regions in direct contact with the opponents' cells. No condensation of nucleus was observed so apoptosis was unlikely to contribute to the rejection response. Cytoplasmic vacuolisation (Figure 2.6D,F) occurred in the boundary cells, typically at the membrane-bound clefts along the endoplasmic reticulum (ER), forming small single-membrane vesicles. Multi-lamellar vesicles were often observed near these small vesicles, showing their formation might associate with the cytoplasmic vacuolisation.

Autophagic structures, including multi-lamellar vesicles, multi-vesicular bodies and autophagic vacuoles with digested cellular content, were present in boundary cells (Figure 2.6D,F,G), though only occasionally observed. Early autophagic features, like phagophores and autophagosomes were not found.

Increased cell debris in the extracellular space was observed at the boundary of stolon encounter sampled within 48 hours post-encounters (Figure 2.7A,F), presumably to be later stage of rejection compared to the 3-hour sample. Boundary between the two stolons became more obvious due to the accumulation of electron-dense cell debris, likely resulted from the proceeding necrosis. Disrupted mitochondria (Figure 2.7B,C,G) and autophagic vacuole-like vesicles containing partially digested cellular materials (Figure 2.7J) were observed in cell debris, showing autophagic cells might have been damaged by necrosis. Cells at the boundary had extensive projections towards the cell debris (Figure 2.7G). Increased autophagic features, like autophagosome, autolysosome-like vesicles with digest cellular materials (Figure 2.7D,E,H) were observed at the boundary cells. It is notable that cells with abundant autophagic vacuoles associated with extensive flaccidity of membrane structures (Figure 2.7H). Vacuolisation at clefts along the ER were also observed (Figure 2.7I). This membrane flaccidity might be the sign of necrosis-like cell death that resulted in release of cell contents into the extracellular space.

Although connection of mesoglea of attacking and defending stolons, which was observed during remodelling in fusion, never occurred in rejection, mesoglea near to contact sites was often disrupted (Figure 2.7K,L). The disruption might be initiated in a similar manner as in fusion as a response to encounters between individuals of the same kind, prior to determination of histocompatibility. The disruption might also be induced by the cell damage occurred during rejection to facilitate the restoration of ectoderm.

At late stage of stolon contact in rejection, a large empty cavity was developed

between the front lines of the two stolons (Figure 2.8A). No cell debris is observed in the extracellular space. Boundary cells of the defending stolon contain abundant electron-dense substances in their cytoplasm (Figure 2.8B-D). The nature or the sources of these substances were undetermined. They might possibly be cell debris internalised or newly synthesised materials for perisarc reconstruction. The attacking stolon cells also contained some of these electron-dense materials, but the overall cell morphology was similar to that before stolon encounter (Figure 2.8E). The empty cavity marked the beginning of separation of the two stolons and subsequent recovery of the perisarc divided the stolons.

Involvement of phagocytosis in removing unwanted materials from stolons

Phagocytosis-like cell engulfment was observed in both late fusion and rejection. Round engulfed cells were observed particularly in the endoderm (Figure 2.9). This cell engulfment was observed in both the attacking and also the defending stolons. Cells were typically engulfed by cells with distinctive morphology: smooth cytoplasm only a few cytoplasmic organelles. Some engulfed cells were identified spanning across the mesoglea. These observations resemble the removal of epithelial cells by phagocytosis of digestive cells in endoderm in Hydra (Campbell, 1976). It shows that recycling of unwanted cells and materials by cell engulfment of endoderm cells is conserved across Hydrozoa. The cell engulfment observed might not be directly related to allorecognition responses. However, it might be triggered by the cellular stress, e.g. increase of necrotic cell debris (Westman et al., 2020), experienced during the rejection response. It might also be the underlying mechanism in removing unwanted ectoderm cells during remodelling in fusion response.

Attempt to detect enzymes associating with the perisarc dynamics

Digestion of perisarc to allow initial cellular contact and rescontruction of the perisarc

to block further contact in rejection are important processes in *C. radiatum* stolon allorecognition responses. Increased electron-dense granules, possibly containing perisarc-lysing/synthesising enzymes, were observed in the boundary cells. Compositions of the perisarc are not fully understood and probably vary among species. Main common components of Cnidarian perisarc are chitin, proteins and a melanin-like pigment (Hwang et al., 2013; Mendoza-Becerril et al., 2016; Mendoza-Becerril et al., 2017). Enzymes that associate with the perisarc morphology are likely to enzymes that degrade or synthesise chitin. Chitin is linear polymer of β-(1,4)-linked D-glucosamine (GlcNAc). Digestion of perisarc was the initial process in allorecognition to allow cellular response. I first attempted to investigate the enzymes that lyse chitin: Chitinase. Chitinases are enzymes that hydrolyse GlcNAc linkages, thus degrade chitin to oligosaccharides. *Hydractinia echinata* Chitinase 1 (HyChit1 (termed Hydroid Chitinase 1 in Mali et al., 2004); UniProt Q6ZYN0; GenBank CAG25409), which belongs to the family 18 glycosyl hydrolases, was found expressed in the ectoderm of *Hydractinia* stolon. *HyChit1* had specific expression patterns—elevated expression was observed at putative branching spots, sub-apical region of growing stolons and having elevated expression at allorecognition-induced hyperplastic stolons, suggesting roles in stolon development and allorecognition (Mali et al., 2004).

Putative homologs of *HyChit1* in *C. radiatum* was identified by local BLAST against the *C. radiatum* library ("all.fasta"; a mixed database containing cDNA library from medusae and eggs of *C. raditum* wild types and inbred lines). "TRINITY_DN108060_c3_g1_i1" (corresponding to "female_contig_2336.48.mrna1" in the whole genome database) showed the highest similarity with *HyChit1* (Figure 2.10), and was designated as *C. radiatum Chitinase 1* (*CrChit1*) candidate 1. CrChit1 candidate 1 (494 aa) is of comparable size as HyChit1 (464 aa) and has perfectly conserved active site residues (DxxDxDxE) (Renkema et al., 1998) (Figure 2.10C). Secretory signal peptide

“MKNLVVISVGGFQRATMKFIVAFILAASACAVINA” (first 35 aa at the N-terminus) was predicted by SignalP-6.0.

Expression of *CrChit1* candidate 1 was examined by in-situ hybridisation. Unexpectedly, *CrChit1* candidate 1 was expressed entirely in the endoderm of stolons, but not in the ectoderm as in *Hydractinia* (Figure 2.11A). Also, reduced, instead of increased, expression was detected at the attacking stolon tips during incompatible stolon encounters (Figure 2.11B,C). As the expression pattern is totally different from that reported in *Hydractinia*, further examination was done by in-situ hybridisation on paraffin sections of stolons and also medusae. In stolons, as shown in whole-mount stolons, *CrChit1* candidate 1 was expressed in the endoderm (Figure 2.11F,G). In medusa, *CrChit1* candidate 1 showed clear expression exclusively in the endoderm, specifically near the mesoglea (Figure 2.11H). The results suggested that this *CrChit1* candidate 1 is not homolog, at least not functional homolog, of *HyChit1*, and *CrChit1* candidate 1 is not involved in allorecognition.

To identify the homolog of *HyChit1*, I searched through the annotated genes in the whole genome dataset and selected annotated genes with best BLAST hits (against Non-redundant protein sequences (nr) database) being Chitinase-related genes. Candidates were further narrowed down to genes sharing highest similarities with *HyChit1* and containing the crucial residues in the chitinase active site: the last D (Asp) and the last E (Glu) in the DxxDxDxE motif (Tsuji et al., 2010) (Figure 2.12A). Three candidates were selected:

CrChit1 candidate 2: female_contig_2336.49.mrna1

CrChit1 candidate 3: female_contig_1866.6.mrna1

CrChit1 candidate 4: female_contig_2026.47.mrna1

Note that the second Asp in the active site DxxDxDxE of “female_contig_2026.47.mrna1” (candidate 4) was substituted by Ser (S). As the second Asp was reported to have a minor role, this gene is also included in the candidates.

Expression of these candidates were detected by in-situ hybridisation on whole-mount stolons. I failed to amplify the template for the synthesis of the in-situ hybridisation RNA probes of *CrChit1* candidate 3, which might be due to a low copy number in the cDNA template or failure in the primer design. In-situ hybridisation results of candidates 2 and 4 are shown in Figure 2.12B-F. No signal of either candidate 2 or 4 was detected in usual grown stolons or growing stolon tips, even with prolonged hybridisation at varied hybridisation temperature (37°C, 55°C and 65°C) and prolonged signal colour development. These candidates were expressed at low levels in stolons. Signal of candidate 4 was detected in newly branched stolon (Figure 2.12F), which might indicate a possible of candidate 4 in development of new stolon branches. However, this signal might be a false signal due to accumulation of RNA probes, anti-DIG antibodies or NBT/BCIP due to the impermeability of the stolons (further discussed in Appendix 2). As none of the *CrChit1* candidates showed resemblance to *HyChit1* in expression pattern or expressed at the stolon encounters, Chitinase or other enzymes involved in chitin lysis in *C. radiatum* remain to be further investigated.

Discussion

Moderate but effective allorecognition mechanisms in *C. radiatum*

This study reported *C. radiatum* stolons demonstrate effective allorecognition mechanisms, that share some similarities, but also have significant differences compared to the two Hydrozoan models. Fusion between compatible stolons is comparable to that in *Hydractinia* and *Podocryne*, featured by tissue remodelling and connection of gastrovascular canals. However, rejection occurs in a different manner. First, nematocysts are not involved, which is different from the rejection response in *Hydractina*. In *Hydractinia*, rejection is mediated by nematocyst discharge and is accomplished with the death of one of the colonies.

In contrast, rejection in *C. radiatum* typically results in regression of only the single attacking stolons without affecting other stolons in the colony. Both colonies survive for months since first stolon contact (Figure 2.13). The tolerance towards colonies living in the same habitat may be due to less competition of living space and resources in the nature habitat. *Hydractinia* specifically survive only on shells of hermit crabs and have high competition of survival space in the natural environment (Cunningham et al., 1991; Buss and Yund, 1988) while there is no report of particular requirement for settlement or survival for *C. radiatum*. The high tolerance may allow survival of more individuals in environment with excessive resources.

Second, perisarc acts as physical barrier between incompatible stolons during rejection. Rejection in *C. radiatum* is relatively comparable to transitory fusion in *Hydractinia*. Stolons are apparently in contact but are actually separated by some form of barrier. Formation of a white fibrous border is reported in *Hydractinia* (Buss et al., 1984; Cadavid et al., 2004; Powell et al., 2007; Buss et al., 2012), while perisarc is reconstructed in *C. radiatum*. However, continuity of gastrovascular systems is observed before the separation in *Hydractinia* (Cadavid et al., 2004; Powell et al., 2007), but not in *C. radiatum*. In *C. radiatum*, only compatible individuals, with at least 1 match of *Alr1* alleles, establish connection of gastrovascular canals. Regulation of allorecognition responses by counteracting perisarc lysis is also reported in *Podocoryne* (Tardent and Jauch, 1983). Direct cellular contact was not observed and encounters between incompatible stolons produce outcomes similar to the "ignoring" observed in this study. I here presented evidence of cellular contact in advance of determination of allorecognition outcomes in *C. radiatum*. The comparison of allorecognition mechanisms between *C. radiatum* and other Hydrozoans provides insight into the evolution and conservation of the Cnidarian allorecognition.

Interestingly, It was observed in stolon encounters between *C. radiatum* and *C.*

pacificum that stolons rapidly grew over or bypassed (=ignoring) each other (Kobayakawa, master's project), without pausing of the stolon tips upon contact. Attacking stolons grew across the defending in around 3 hours, which is approximately the time requirement for perisarc digestion to allow cellular contact. Therefore, I speculate that, in inter-specific stolon encounters between *C. radiatum* and *C. pacificum*, perisarc was never digested. There might be transfer of materials across the perisarc that enable discrimination between stolons of the same or different species, and induce digestion of perisarc upon encounter of the same species.

Necrotic and autophagic responses as primary consequences of incompatible stolon encounters

Necrotic and autophagic responses were observed at contact regions between incompatible stolons, which were also reported in *Hydractinia* transitory fusion (Buss et al., 2012). This indicates that these necrotic and autophagic responses may be fundamental cellular responses responsible for rejection, triggered downstream of Alr recognition. Increased autophagic features, especially double-membrane-bound autophagosomes, were observed at the boundary cells as rejection proceeded. It might indicate elevated autophagy was induced by the necrotic cell debris, perhaps as a form of inflammatory response. Although there is no direct evidence showing how the extracellular cell debris was removed, the disappearance of this debris in later rejection stages suggested that boundary cells might possess measures of ingestion and degradation of these materials. The accumulation of autophagosomes might also be a result of reduced autophagic flux, due to deficient digestion of autophagosome content by lysosomes (Boya et al., 2005, Zhang et al., 2013). Indeed, cells with abundant autophagosomes had relatively reduced electron-dense granules, of which a proportion might be lysosomes.

Regression predominantly occurs at attacking stolon tips, regardless of *Alr1* genotypes, showing *Alr1* genotypes do not possess hierarchy. Competitive hierarchy was observed in *Hydractinia* (Ivker, 1972) and *Podocoryne* (McFadden, 1986), in which colony of a "stronger" genotype overgrows that of a "weaker" genotype. The "overgrower" colony developed hyperplastic stolons and starved the opponent colonies by tangling and monopolising its feeding polyps. Rejection in *C. radiatum* is comparatively simple, in which only the stolon tips in contact with the opponents regressed, with mild to no effect on the surrounding stolons. TEM observation revealed necrotic and autophagic cells were present at boundary cells of both attacking and defending sides. Stolon tips may be more prone to morphological changes when experiencing cellular stress. Indeed, stolon tips are the first to show signs of weakening during abnormal health conditions, e.g. starvation and contamination. Typical stolon tips consist of highly vacuolated ectoderm cells. While vacuoles reduce in volume in boundary cells with abundant electron-dense granules during allorecognition response, membrane of the vacuoles remained and eventually became elongated clefts, usually along rough ER. These clefts may serve as the source of membrane for formation of autophagic bodies. In addition, attacking stolon resulted in a change of growing direction instead of regression when it approached at an angle, indicating regression response may be limited to stolon tip.

Regulation of perisarc morphology was observed to be an important mechanism in *C. radiatum* stolon allorecognition. Regulatory expression of enzymes associating with perisarc was expected be part of the allorecognition responses. Not only in allorecognition, the initial digestion of perisarc to allow cellular contact also appears to be an important differentiating step in xenorecognition. In our observation so far, perisarc was only digested during encounters between stolons of the same species, but not that between different species, e.g. between *C. radiatum* and *C. pacificum*. As *HyChit1* with suggested role in allorecognition

was reported, I tried to identify homolog of *HyChit1* in *C. radiatum*. Despite CrChit1 candidate 1 highly resembled HyChit1, with similar size, presence of putative signal peptides, and flawlessly conserved catalytic active site residues, it showed completely different expression patterns. HyChit1 was expressed exclusively in ectoderm while CrChit1 candidate 1 was expressed only in endoderm. In a recent preprint, *Chitinase 1* (Hydractinia genome project portal: HyS0041.99), which is 93.8% identical to *HyChit1* in terms of amino acid sequence, was used as a cell marker for endodermal gland/secretory cell in *Hydractinia symbiolongicarpus* (Schnitzler et al., 2023). Chitinase was also identified in three other hydroids: *Hydra attenuata*, *Hydra circumcincta*, and *Podocoryne carnea* and its expression was limited in the endoderm of polyps (stolons were not studied) (Klug et al., 1984). CrChit1 candidate 1 might be homolog of this type of chitinase. Chitinase expressed in endoderm is expected to participate in food digestion. It is not clear if the ectodermally expressed property of *HyChit1* was acquired after divergence or *C. radiatum* also has this ectodermally expressed chitinase but is not yet identified. Except candidate 1, candidates 2-4 were not detected in usual stolons in in-situ hybridisation. Optimisation of the in-situ hybridisation protocols might be necessary. In later analysis by SignalP 6.0, candidate 2 was found not containing secretory signal peptide so it might be excluded from the candidate list. Besides the 4 candidates, there are still 20 more annotated genes related to chitinase and many of them contain the conserved DxxDxDxE active site motif. Further screening is needed to identify the putative allorecognition-associating chitinase in *C. radiatum*.

Besides digestion of chitin, reconstruction of perisarc is also a key process in rejection. Chitin synthases (CHSs) are glycosyltransferases expressed on plasma membranes that catalyse the polymerisation of GlcNAc to produce chitin. CHSs were identified and characterised in the sea anemone *Nematostella vectensis* (Anthozoa, Cnidarian) (Vandepas et al., 2023; Vandepas, 2018). While putative genes were identified in all classes of Cnidarian,

including Hydrozoan *Hydractinia* and *Hydra* (Vandepas, 2018), expression and functionality were undefined. Putative homologs of CHSs were identified in *C. radiatum* but there was too little information for filtering potential candidates. Further genetic or structural analysis of the putative candidates, or screening are required for the identification of *C. radiatum* CHSs.

Overall, this chapter summarised the morphological observations of the allorecognition response in *C. radiatum* and discussed the comparative analysis of the allorecognition responses between *C. radiatum* and other reported Hydrozoans. While fusion is similar in all studied animals, rejection occurs in different manners, summarised in Table 2.1, enhancing the understanding of the evolution of allorecognition in Cnidarian.

Table 2.1. Comparative morphological features of allorecognition responses in Hydrozoan stolons. R: rejection, TF: transitory fusion.

	C. radiatum	*Hydractinia* (R)	*Hydractinia* (TF)	*Podocoryne*
Nematocyte involvement	✗ Nematocyte are never recruited	✓ Nematocytes are recruited to contact zone and fired to opponents	✓/✗ Nematocyte involvement is reported in some but not all publications	
Digestion of perisarc	✓	✓	✓	✗
Cellular contact	✓	✓	✓	✗
Gastrovascular canal connection	✗	✗	✓	✗
Autophagy and necrosis	✓		✓	
Physical barrier after contact	✓ Reconstruction of perisarc		✓ White fibrous material along boundary	✓ Thickening of perisarc

Materials and Methods

Animals

Two strains of *C. radiatum*: GNW (female; F0♀) and Chu (male; F0♂) were collected in Makiminato Bay (Ginowan City, Okinawa Prefecture, Japan) and Yamakawa fishery harbor (Motobu Town, Okinawa Prefecture, Japan), respectively. Another strain (OGW),

which was collected in Ogasawara Island, Tokyo, Japan, was purchased from a local breeder. Animals were maintained in artificial seawater (ASW) at 26–28°C and were fed three to four times per week with freshly hatched to 1-day old brine shrimp nauplii. Seawater was changed >2 hours after feeding. Two strains of *C. pacificum*, Strain 1 (6W) and Strain 2 (B3-9) used in this study were described previously (Tachibana et al., 2020).

TEM and digital holographic microscope (DHM) imaging

Stolon encounters on PET sheets were prefixed with 2.5% glutaraldehyde in 30 mM HEPES buffer (pH 7.4) containing 100 mM NaCl, 2 mM $CaCl_2$ and 0.45 M sucrose for 24 hours at 4 °C and postfixed with 1% osmium tetroxide (OsO_4) and 10 mM potassium ferricyanide ($K_3Fe(CN)_6$) in 30 mM HEPES buffer (pH 7.4) containing 100mM NaCl, 2 mM $CaCl_2$ for 1.5 hours at room temperature. After fixation, samples were rinsed three times with Milli-Q water. Samples were dehydrated in a graded ethanol series, and embedded in epoxy resin (Quetol 651, Nisshin EM Co. Ltd., Tokyo, Japan). Each sample was serially sectioned with an ultramicrotome (EM UC7, Leica, Wetzlar, Germany). Ultra-thin sections at 70 nm were stained with uranyl acetate and lead citrate, and examined using a JEM-1400 electron microscope (JEOL, Tokyo, Japan). Images were stitched either manually or using Adobe Photoshop Lightroom Classic (Adobe) to produce wide-field images of higher resolution. Homotomographs of Stolon encounters on glass-bottom dish were observed with a DHM, HT-X1i (Tomocube, Daejeon, South Korea). Brightness and contrast of the TEM and DHM images were adjusted with ImageJ or Photoshop (Adobe).

In-situ hybridisation

Whole-mount in-situ hybridisation using DIG-labelled RNA probes was carried out with reference to the published protocol (Sea Anemone protocol). Animals were fixed in 4%

paraformaldehyde/PBS overnight at 4°C. Animals were then dehydrated in a methanol/PBST series (25%, 50%, 75%, and 100%). Samples were then stored at -30°C until use. Samples were bleached with 0.3% hydrogen peroxide/methanol for 30-45 minutes, followed by rehydration through a descending methanol/PBST series (100%, 75%, 50%, and 25%). All pre-treatment steps before pre-hybridisation were performed at room temperature. Samples were treated with 0.2 N HCl for 20 minutes at room to eliminate endogenous alkaline phosphatase, and permeabilised with an incubation in 10 µg/ml proteinase K/PBST for 30-45 minutes, followed by a brief post-fixation with 4% paraformaldehyde/PBS for 20 minutes. Acetylation was performed with 0.3% and 0.6% Acetic anhydride in 0.1 M TEA buffer for 5 minutes each. Samples were pre-hybridised with hybridisation buffer (50% deionised formamide, 5X Saline-sodium citrate (SSC), 50 µg/ml tRNA, 50 µg/ml heparin, 2X Denhardt's reagent, 10% dextran sulphate, 0.1% Tween-20) at hybridisation temperature (55-65°C) overnight. Hybridisation was performed with 0.1-1.0 µg/ml DIG-RNA probes, synthesized with Roche DIG DNA Labeling Kit, in hybridisation buffer at hybridisation temperature for 48-72 hours. Primers used for DIG-RNA probe synthesis are summarised in Table 2.2. Post-hybridisation washes were performed by 30-60-minute incubation at hybridisation temperature in buffers of increasing stringencies: wash solution 1 (50% formamide, 5X SSC, 0.1% Tween-20), wash solution 2 (50% formamide, 2X SSC, 0.1% Tween-20), 2X SSC+T (2X SSC, 0.1% Tween-20), and 0.2X SSC+T (0.2X SSC, 0.1% Tween-20). Samples were then blocked with 2% blocking reagent (11096176001, Roche) in maleic acid buffer for 2 hours at room temperature, followed by overnight incubation at 4°C with 1:5000 Anti-Digoxigenin-AP, Fab fragments (11093274910, Roche) in blocking solution. The signals were visualised with 1:100 dilution of NBT/BCIP Stock Solution (11681451001, Roche) in AP buffer (0.1 M Tris-HCl (pH9.5), 0.1 M NaCl, 2 mM Levamisole, 1% Tween-20) at room temperature or 4°C for prolonged incubation. Colour

development was quenched by PBST washes. Samples were cleared with 99.5% ethanol at room temperature for 10 minutes, and subsequently equilibrated in 50% glycerol/PBST. Images were obtained with Olympus BX51 (Olympus, Japan).

Paraffin sections were prepared under standard tissue processing procedures. Samples were fixed in 4% paraformaldehyde/PBS overnight at 4°C, and dehydrated in an ethanol/PBST series (25%, 50%, 75%, and 100%). Samples were then cleared in xylene and embedded in Paraplast Plus (P3683, Sigma-Aldrich). Paraffin-embedded samples were sectioned into 4-μm sections with a rotary microtome (RX-860, Yamato Kohki Industrial Co. Ltd., Saitama, Japan) and were mounted on a hydrophilic polyester film (9901P, 3M Japan Ltd.). After rehydration with a reversed ethanol/PBST series (100%, 75%, 50% and 25%), in-situ hybridization was performed as described above with shortened incubation time.

Table 2.2. List of primers used in amplifying cDNA templates for synthesis of in-situ hybridisation RNA probe. cand: candidate, bp: base pairs, "cagtgaattg"=extra nucleotides, "taatacgactcactatag"=T7 promoter, "atttaggtgacactatag"=SP6 promoter.

Target		Forward	Reverse	Product (bp)
CrChit1 cand 1	1st PCR	TTAGCTGTCGGTGGATGGAA	GCTTCACGGGTGTATCTTCC	644
	2nd PCR	cagtgaattg-taatacgactcactatag-TCATGAGAATGGGAACGCAC	cagtgaattg-atttaggtgacactatag-AGCTCGACCATATGTTCCCA	588
CrChti1 cand 2	1st PCR	GTCTCCAATGCAGTTCCGTC	TCGTCTAATGCAAGGCTCCA	999
	2nd PCR	cagtgaattg-taatacgactcactatag-CCAAGACGGTCAGTGATGAT	cagtgaattg-atttaggtgacactatag-TGTCGAAACCTATCCATGCTT	770
CrChti1 cand 3	1st PCR	GAGTTGGTGGCTGGAATCAC	AGCTTCAGATGACGTTGAGGA	950
	2nd PCR	cagtgaattg-taatacgactcactatag-GGAAGACGTGACCACTTTCA	cagtgaattg-atttaggtgacactatag-GTTGTTGATGTTGACGTTGGC	787
CrChti1 cand 4	1st PCR	GTTCACCACCATCGGACAAG	TCCTTACCATGCACCAACGT	601
	2nd PCR	cagtgaattg-taatacgactcactatag-AGTGCCTTTCAAGCTGATGG	cagtgaattg-atttaggtgacactatag-GGACTTTGTATCATACCCTACCC	563

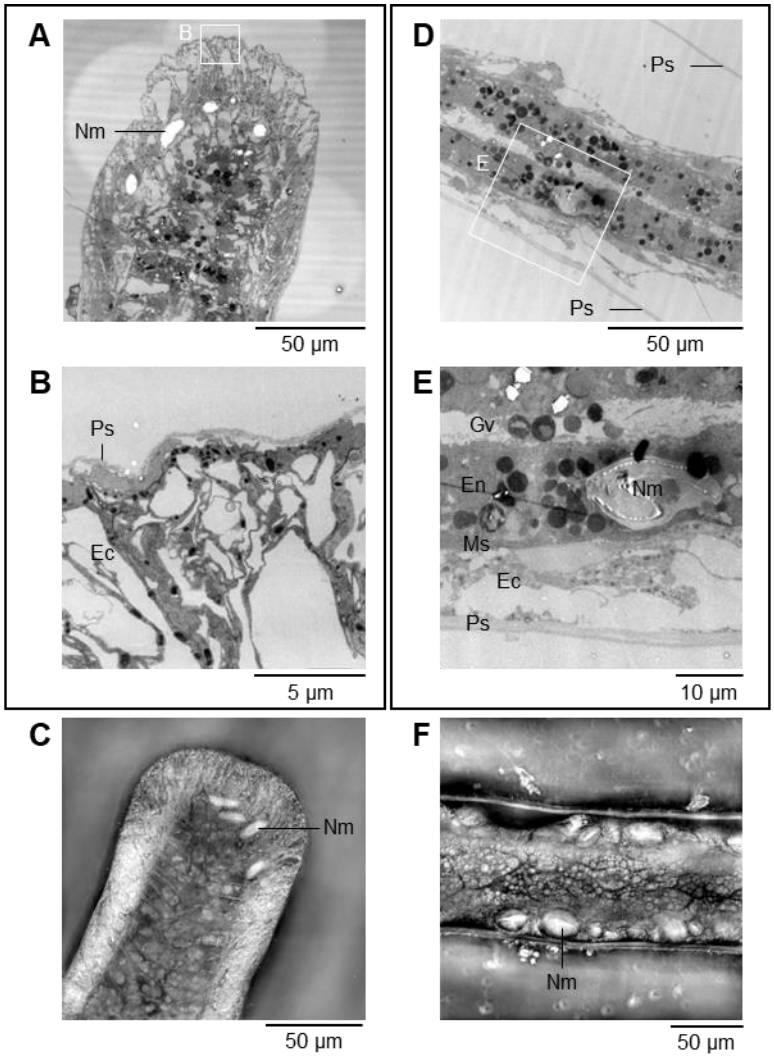

Figure 2.1. Morphology of typical growing stolons. (A and B) TEM images of a growing stolon tip (F0 ♂). The oval empty cavities are nematocysts that detached during sectioning. White boxed area is enlarged in (B) to show vacuolation of ectoderm cells. (C) DHM image of a growing stolon tip (F0 ♂). (D and E) Ultra-thin TEM images of a typical stolon (F0 ♂). White boxed area is enlarged in (E) to show the detail of the morphological features. (F) DHM image of a typical stolon (F0 ♂). Ec: ectoderm; En: endoderm; Gv: gastrovascular canal; Ms: mesoglea; Nm: nematocyst.

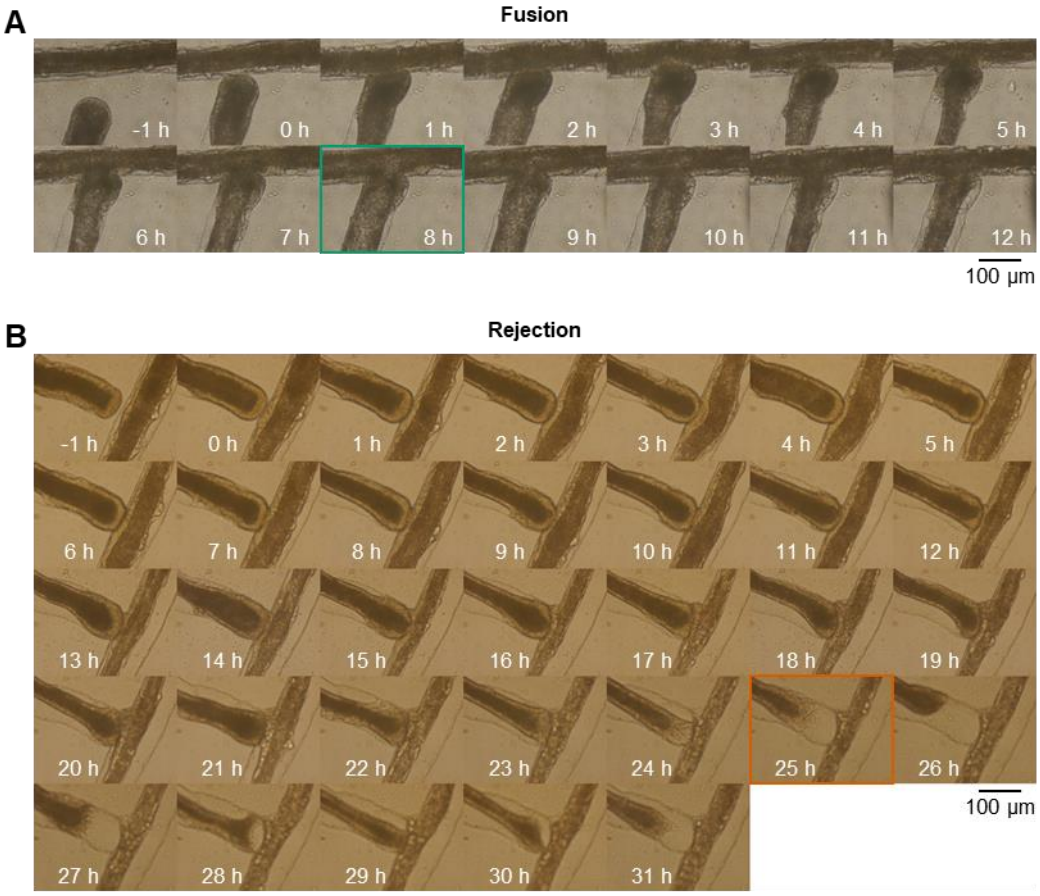

Figure 2.2. Overview of the stolon fusion and rejection responses. Time-lapse montages of (A) stolon fusion and (B) rejection. Boxed panels show the timing of fusion (green), indicated by the connection of gastrovascular canals and rejection (red), indicated by the separation of the two stolons.

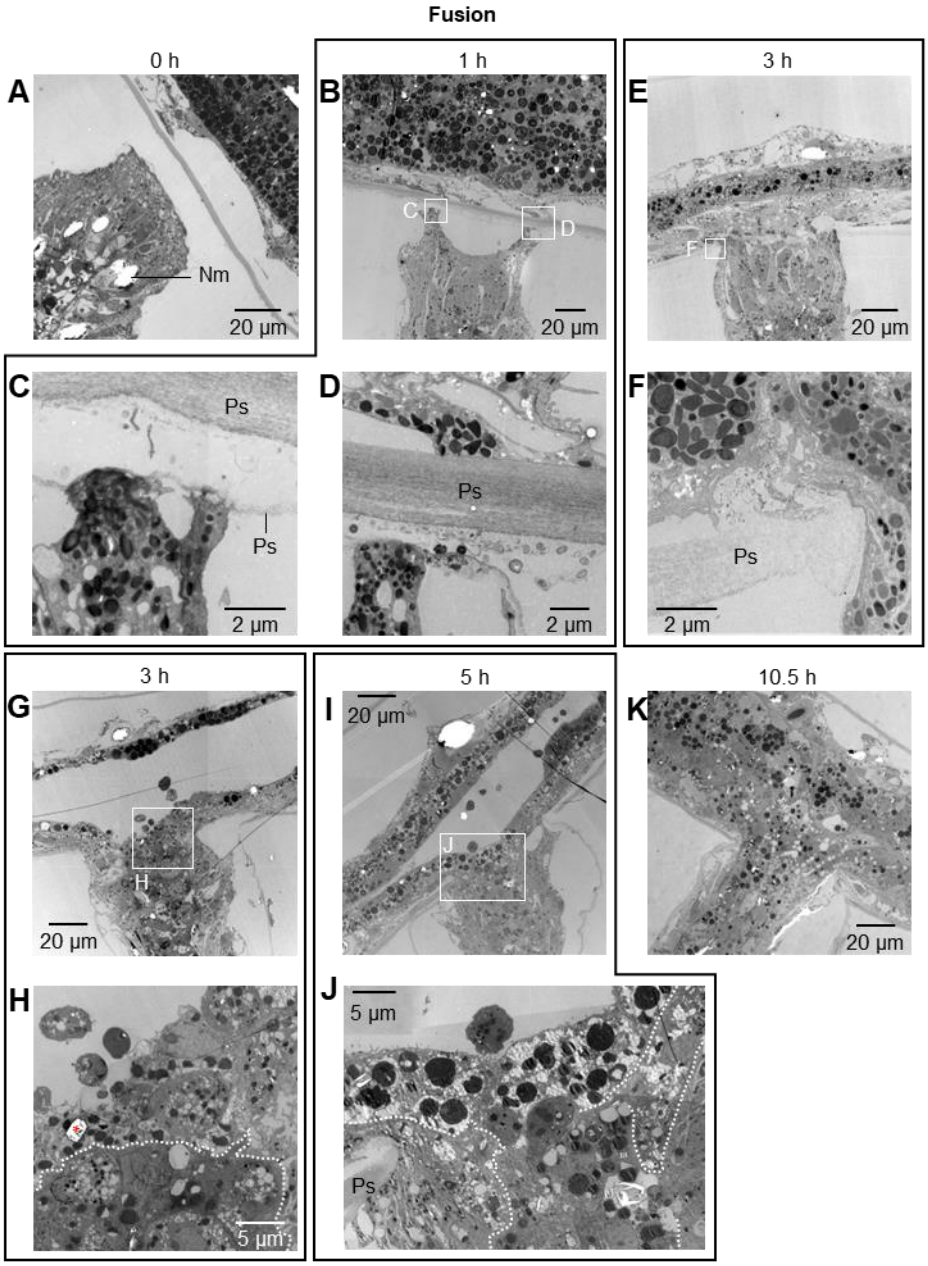

Figure 2.3. TEM images of fusion between compatible stolons. (A) F0 ♀ approaching F0 ♀. Stolons appeared to be in contact under digital microscope. (B) 1 hour post-encounter between two F0 ♀ stolons. Higher magnification of the white boxed area is shown in (C) to show the association of electron-dense granules in the ectoderm cells with the perisarc at the attacking stolon tip, and (D) to show accumulation of granules at both attacking and defending ectoderm. (E) 3 hours post-encounter between F0 ♂ stolons. White boxed areas are enlarged in (F) to show the blunt end of the broken perisarc of the defending stolon. (G) Fused F0 ♂ stolons at 3 hours post-encounter. White-boxed area is enlarged in (H) showing the contact boundary between the endoderm of attacking and defending stolons. White dotted line indicates the boundary. Red asterisk indicates the endoderm-specific crystal structure. (I) 5 hours post-encounter between two F0 ♀ stolons. White-boxed area is enlarged in (J) (manually stitched images) to show remodelling of cell layers during fusion. Basement membranes are outlined with white dotted lines. (K) 10.5 hours post-encounter between two F0 ♂ stolons.

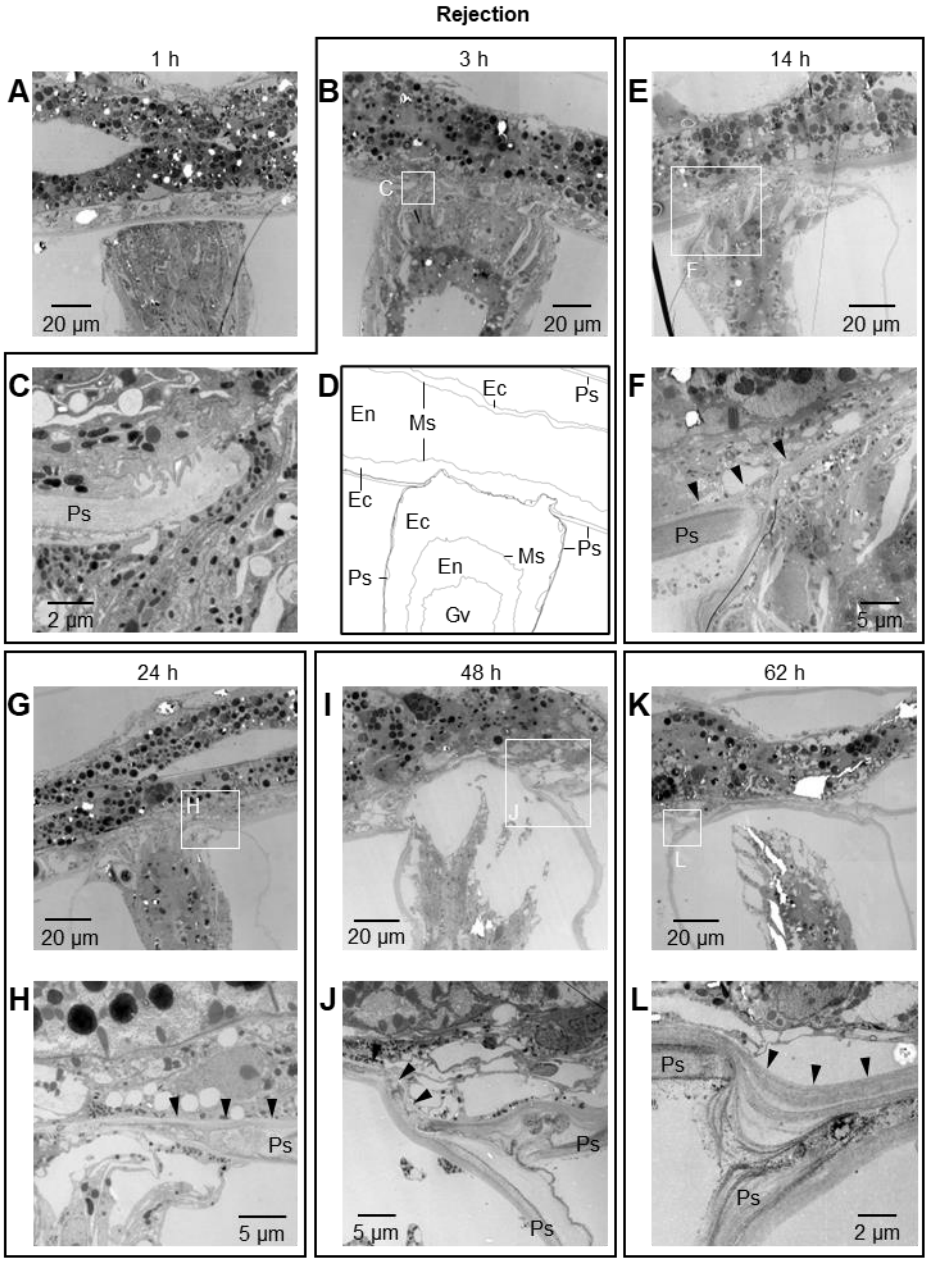

Figure 2.4. TEM images of rejection between incompatible stolons. (A) 1 hour post-encounter between F0 ♂ (attacking) and F0 ♀ (defending). (B) 3 hours post-encounter between F0 ♀ (attacking) and F0 ♂ (defending). Blunt broken end (white box) of the perisarc of the defending F0 ♂ stolon is magnified in (C). (D) shows an illustration outlining the simplified morphological features of (B). (E) 14 hours post-encounter between F0 ♂ (attacking) and F0 ♀ (defending). White boxed area is enlarged in (F) to show the newly synthesised thin perisarc layer (black arrows). (G) 24 hours post-encounter between F0 ♂ (attacking) and F0 ♀ (defending). Stolons are separated by perisarc. White boxed area is magnified in (H). (I) 48 hours post-encounter between F0 ♀ (attacking) and F0 ♂ (defending). Stolons are separated by perisarc. White boxed area is magnified in (J). (K) 62 hours post-encounter between F0 ♀ (attacking) and F0 ♂ (defending). Stolons are separated by perisarc. Magnified white boxed area is shown in (L) to show the layers of newly synthesised (black arrows).

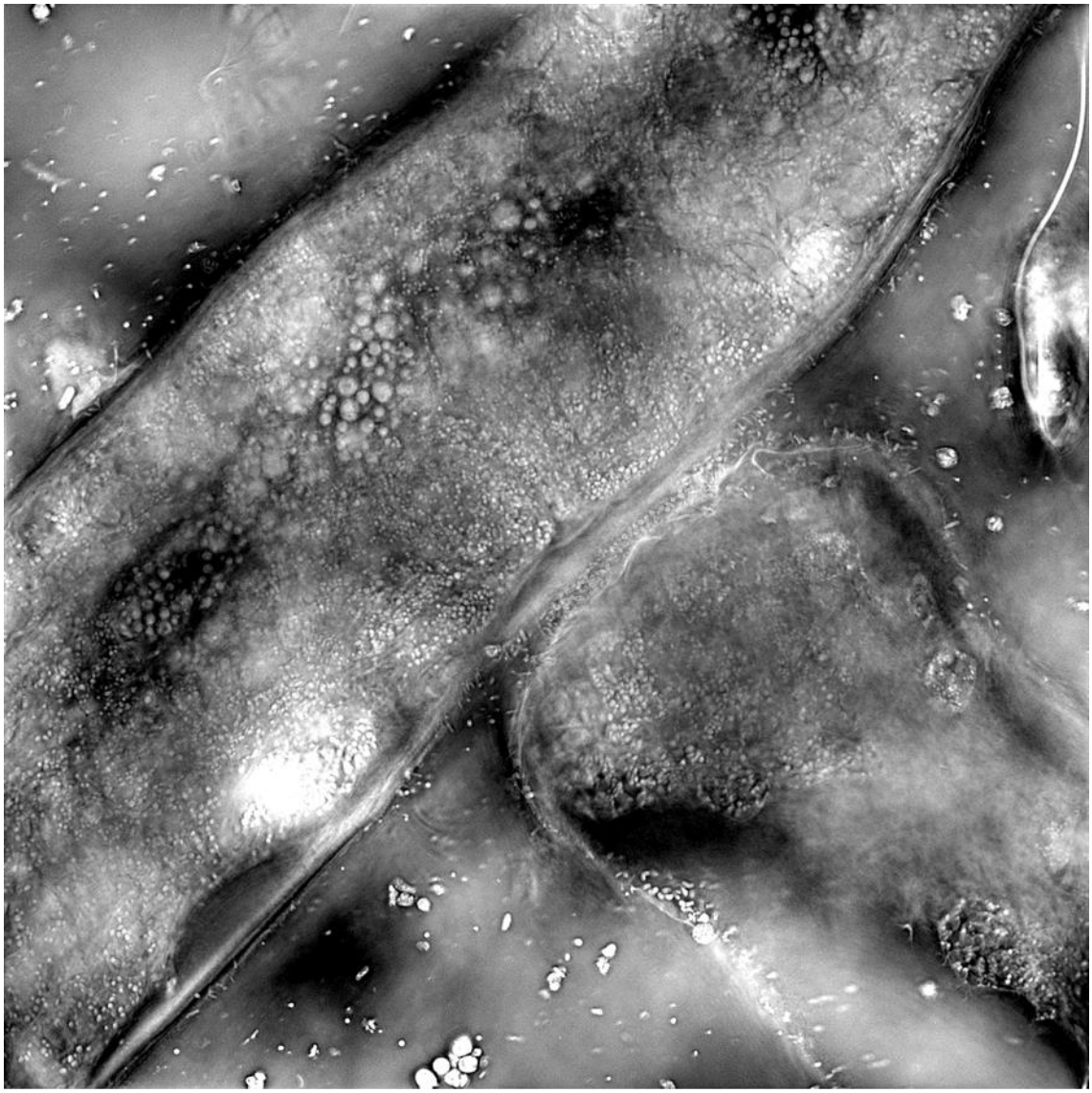

Figure 2.5. Degranulation at stolon encounter. DHM image of incompatible stolon encounter (attacking: F0 ♀ and defending: F0 ♂). Granules of high retractive index (high protein density) at between the contacting stolons.

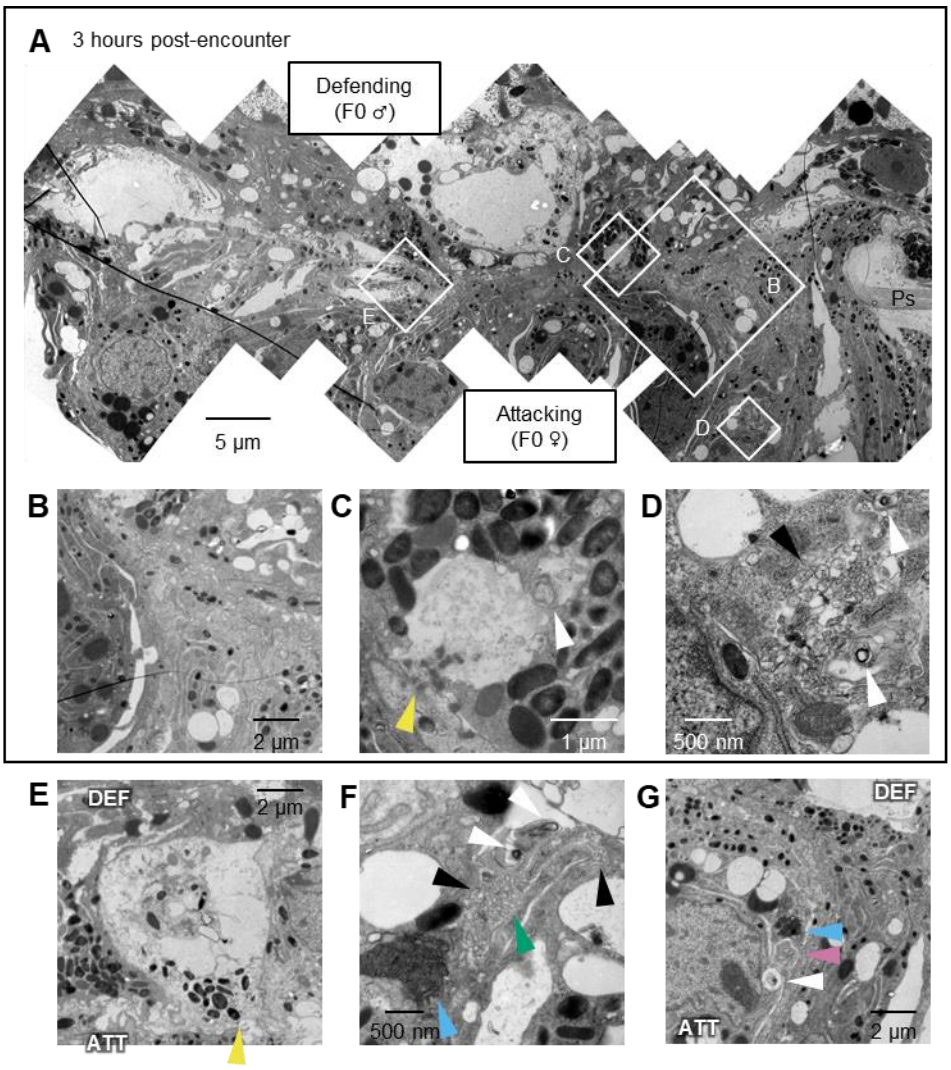

Figure 2.6. Necrotic and autophagic responses during early rejection.

(A) Stitched TEM image of the contact boundary at 3 hours post-encounter between incompatible F0 ♀ (attacking) and F0 ♂ (defending). White boxed areas are enlarged in (B-G). (B) Cell process from both attacking and defending cells at the contact faces. (C) loss of cell membrane integrity (yellow arrow) and release of cellular content into extracellular space. (D) Cytoplasmic vacuolisation (black arrow) and multi-lamellar structure (white arrows) formation from the vesicles.

(E-G) TEM images of another ultra-thin section of the sample as (A). (E) Disrupted cell membrane (yellow arrow) and leakage of cell content. (F) Autophagic vesicle-like membranous structures (white arrows) and vacuolization (black arrows) associating with membrane-bound clefts along rough endoplasmic reticulum (green arrow). Autolysosome-like vesicle (blue arrow) with digested material is also observed. (G) Autophagic membranous structures (white arrow), multi-vesicular body (pink arrow) and autophagic vesicle with digested cell content (blue arrow).

ATT: attacking, DEF: defending

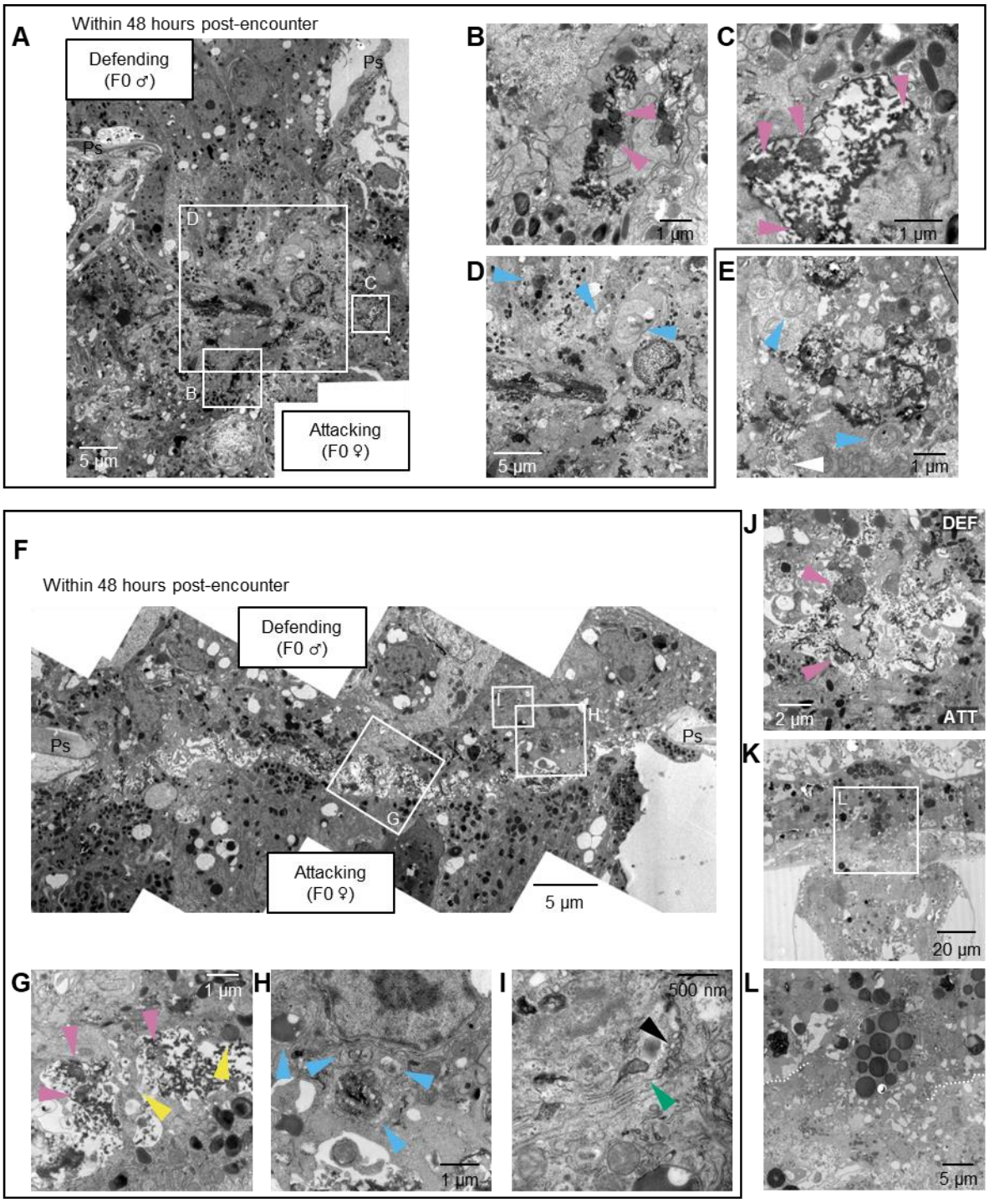

Figure 2.7. Increased cell debris and increased autophagic features as rejection proceeds.

(A) Stitched TEM image of the contact boundary sampled within 48 hours post-encounter between incompatible F0 ♀ (attacking) and F0 ♂ (defending). Increased electron-dense cell debris is observed at the contact site. (B and C) Cell debris with disrupted mitochondria (pink arrows) in extracellular space. (D) Ectoderm cells at contact boundary contain autophagic vacuoles at different stages (blue arrows). (E) TEM images of another ultra-thin section of the sample as (A), showing autophagic vesicles (blue arrows) and multi-lamellar vesicles (white arrow).

(F) Stitched TEM images of another sample of encounter between incompatible individuals (attacking: F0 ♀ ; defending: F0 ♂) collected within 48 hours post-encounter. Extensive cell process and increased cell debris at the extracellular space between attacking and defending stolons' cells are observed. White boxed areas are enlarged in (G-I). (G) Cell debris with mitochondria (pink arrows) in extracellular space. Boundary cells have processes towards the cell debris with partial loss of cell membrane integrity (yellow arrows). (H) Boundary cells with multiple autophagic vesicle-like double membrane-bound compartments (blue arrows). Note the flaccidity of the membranes. (I) Vacuolization (black arrow) associating with membrane-bound clefts along rough endoplasmic reticulum (green arrow). (J) TEM images of another ultra-thin section of the sample as (F). Partially digested autophagic vacuoles (blue arrow) in extracellular space. (K) TEM images of another ultra-thin section of the sample as (F and J). White boxed area is enlarged in (L) to show disruption of basement membrane, outlined with white dotted lines.

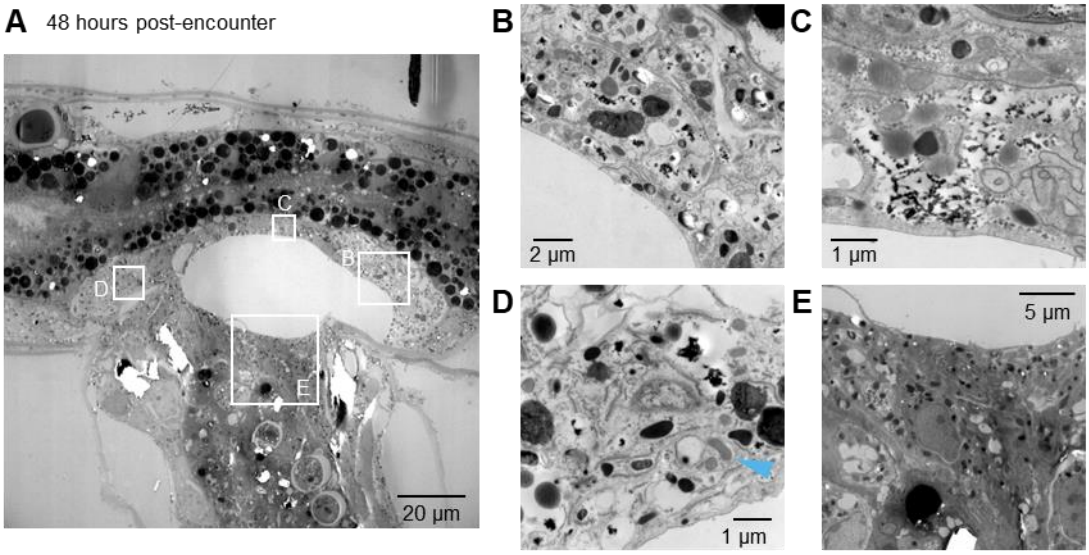

Figure 2.8. Clearance of extracellular cell debris and increased electron-dense materials in defending stolons before separation of stolons. (A) Large-field TEM image of stolon encounter between incompatible F0 ♂ (attacking) and F0 ♀ (defending) at 48 hours post-encounter. There is no perisarc or cell debris but a large empty cavity between the stolons. White-boxed areas are enlarged in (B-E). (B-D) show electron-dense materials in the cytoplasm of the ectoderm cells of the defending stolon. Phagophore-like membrane structure is observed but with flabby membrane (blue arrow). (E) Cellular morphology of the attacking stolon.

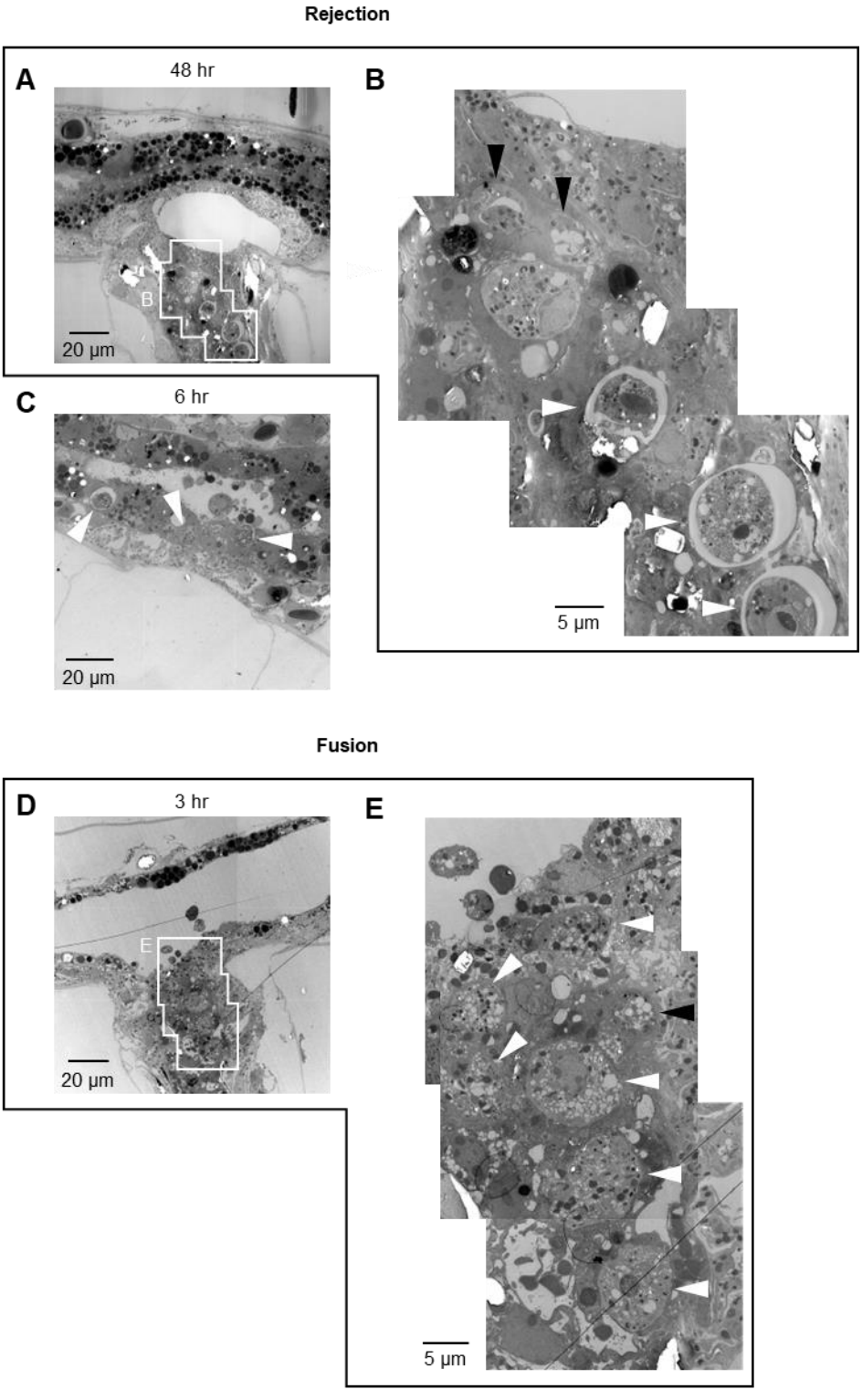

Figure 2.9. Cell engulfment in late rejection and fusion. (A) A duplicate of Fig. 2.8A (rejection between incompatible F0 ♂ (attacking) and F0 ♀ (defending) at 48 hours post-encounter). (B) Manually stitched TEM images showing the magnified view of the white boxed area in (A). (C) TEM image of stolon encounter between incompatible F0 ♂ (attacking) and F0 ♀ (defending). (D) A duplicate of Fig. 2.4G (Fused F0 ♂ stolons at 3 hours post-encounter). (E) Manually stitched TEM images showing the magnified view of the white boxed area in (D). White arrows indicate engulfed cells and black arrows indicates cells engulfed by cell projection from endoderm across the mesoglea.

A

TRINITY_DN108060_c3_g1_i1 (1717 nt):

```
ATTAATTCTTTTCTGGATTCACACTCTCAGAAACTTAACAGATCTTAATTTTTTTAATAGTTAATTTTAAGTTATACAAAACATCTTT
GAAAACCCATGTTTTGATGTTAAACTTGCGTCACCTGTAACATATGTGTCAATAGTTACGAAGGCTAATAAAATAAAGCATGAAGAAC
TTAGTTGTCATTTCAGTTGGTGGATTTCAAAGAGCGACGATGAAGTTTATCGTCGCATTCATTCTTGCTGCTTCGGCATGCGCTGTCA
TCAATGCAAATTATGTTCGAAATTGTTACTATACAAATTGGGCGCAATATCGTCCACCACCCATGAAATATTTCCCAGAAAATCTTGA
TCCATTCCTCTGTACTCATATCTTTTATGCTTTTGCTAAGATCGGAAGAGGAAGCACATTAGCAATGTACGAATGGAATGATGATAAG
ATGTATCCAAGAATGATGGCTATGAAGAAACAAAATCCTGATCTCAAAGTTCTTTTAGCTGTCGGTGGATGGAATCATGAGAATGGGA
ACGCACAGGGGAAGTTCTCCGTTATGGTTAACAACGATTCATTACGAAAGGGATTTATCGATTCAGCTGTTGCACTTTTAAGAAAATG
GGGATTTGATGGTCTCGATTTGGACTGGGAATACCCAGGATCACGTGACAGTGGAAAAAATCACCCAGGAGATAAACAAAAATTTACA
CAATTATGCAAAGAGCTTCTCCATGCATTTGAAACTGATGCTGCAAAACGTCAGATGCCAAGACTTTTACTTACTGCAGCTGTTGCTG
CTGGTAAACCAACTATTGATGCCGGATATGAAGCTAAAGAACTTGGAAACTGCTTAGATTACTTAAACTTGATGGCTTACGATTTACA
CGGAGCTTGGGATACAGTAACTGGTCATCACACTGCCATGAAATGGGACGGCGTTGAAGGTGAAAACAGAAAAGAATTTACCGTGACG
TATGCTGTTGAGTATTGGATTAGCAAAGGATTCCCTGCTTCAAAAATTGCTCTTGGAATGGGAACATATGGTCGAGCTTTCCGATTAA
AAGATGGTGCACAAAATGGTTTAGGAGCACCAGTAACAAGCGGTTGGCCACAACCACCAAAAGGAAGATACACCCGTGAAGCTGGTTT
CTTGGCTTACTATGAAATCTGCAACCGAAAAGATTTAACGTACGTAGATGAGACTGCAGTCGATGCCCCGTATGCATACAGCTCATCA
ACCAAAGAATGGATTGGTTATGATAACAAGAAAAGTTTGAAACTTAAAGTTGATAAACTGATCAAAGGCAAGAACCTTGCGGGAGCTA
TGTTTTGGTGTTTGGACTTAGACGATTTTACTGAAAAATGCGGTGAGGGAAAATATCCTTTGATGAGCAGTGTTGCCCAAGAATTAGG
TGGGTACAACCCTCCAACACCCAAAATACCACGGTCACCACCACCAACACTACCAACCGAAAAACCACCACCACCTGGACAATCAACA
GTAAAACCTCCACCAGTTAAAACCAACGCACCACCACCCGGTGGAAAAGGATGTAAGTCTATTGGTCGATGGAGAGGAATTCCAAATA
TGGATGAATGGTGTATAACAAACTGTGCAGCTGGTAACTGTCCATCAGATATGTGTAAATGTACATGAATGCATGTTTTTAGAGAAAA
TATATTATAAAAAAATAAAAAAAAAAAAAAAAAAAAAAAAAAAAGA
```

B

Deduced amino acid sequence (494 aa):

```
MKNLVVISVGGFQRATMKFIVAFILAASACAVINANYVRNCYYTNWAQYRPPPMKYFPENLDPFLCTHIFYAFAKIGRGSTLAMYEWN
DDKMYPRMMAMKKQNPDLKVLLAVGGWNHENGNAQGKFSVMVNNDSLRKGFIDSAVALLRKWGFDGLDLDWEYPGSRDSGKNHPGDKQ
KFTQLCKELLHAFETDAAKRQMPRLLLTAAVAAGKPTIDAGYEAKELGNCLDYLNLMAYDLHGAWDTVTGHHTAMKWDGVEGENRKEF
TVTYAVEYWISKGFPASKIALGMGTYGRAFRLKDGAQNGLGAPVTSGWPQPPKGRYTREAGFLAYYEICNRKDLTYVDETAVDAPYAY
SSSTKEWIGYDNKKSLKLKVDKLIKGKNLAGAMFWCLDLDDFTEKCGEGKYPLMSSVAQELGGYNPPTPKIPRSPPPTLPTEKPPPPG
QSTVKPPPVKTNAPPPGGKGCKSIGRWRGIPNMDEWCITNCAAGNCPSDMCKCT
```

C

```
CrChit1_candidate_1   MKNLVVISVGGFQRATMKFIVAFILAASACAVINANYVRNCYYTNWAQYRPPPMKYFPEN   60
HyChit1_Q6ZYN0        ---------------MIKLTTA-IFLTLCAVAAAKNYVRVCYYTNWAQYRPPPMKFFPEN   44
                                      :*: .* *: : ....   **** ***************:****

CrChit1_candidate_1   LDPFLCTHIFYAFAKIGRGSTLAMYEWNDDKMYPRMMAMKKQNPDLKVLLAVGGWNHENG   120
HyChit1_Q6ZYN0        LDPLLCTHVVYSFAKIGRGHTLQMYEWNDDKMYPRMMALKQQNPALKVLLAVGGWNHENG   104
                      ***:****:.*:******** ** ***************:*:*** ***************

CrChit1_candidate_1   NAQGKFSVMVNNDSLRKGFIDSAVALLRKWGFDGLDLDWEYPGSRDSGKNHPGDKQKFTQ   180
HyChit1_Q6ZYN0        GT-SKFSVMVNSDSNRKAFIDSSVALLRKWGFDGLDLDWEYPGGRG--NSPAGDKQRFTQ   161
                      .: .*******.** **.****:**********************.*.  :.  ****:***

CrChit1_candidate_1   LCKELLHAFETDAAKRQMPRLLLTAAVAAGKPTIDAGYEAKELGNCLDYLNLMAYDLHG-   239
HyChit1_Q6ZYN0        LCRELIEAFDKDAAEKQKPRLMLTAAVAAGFKTIDGGYEIQKIAKYLDILNFDGFLIYTV   221
                      **:**:.**:.***::* ***:********  ***.*** ::::.: ** **: .: ::

CrChit1_candidate_1   AWDTVTGHHTAMKWDGVEGENRKEFTVTYAVEYWISKGFPASKIALGMGTYGRAFRLKDG   299
HyChit1_Q6ZYN0        TGEKISGHHTAWDFDGAPGDDRNKLTVTYAVDYWIKGGFPANKIALGMGTYGRAFKLKDA   281
                      : :.::****** .:**. *::*:::******:***. ****.*************:***.

CrChit1_candidate_1   AQNGLGAPVTSGWPQPPKGRYTREAGFLAYYEICNRKDLTYVDETAVDAPYAYSSSTKEW   359
HyChit1_Q6ZYN0        SNNGLGAPK-ADWQKPPKGQFTREAGFLSYYEICKM-GLTVVKDNAVKSPYGYK--GQDW   337
                      ::******  :.* :*****::*******:*****:  .** *.:.**.:**.*.   ::*

CrChit1_candidate_1   IGYDNKKSLKLKVDKLIKGKNLAGAMFWCLDLDDFTEKCGEGKYPLMSSVAQELGGYNPP   419
HyChit1_Q6ZYN0        IGYDDQESLVHKVNTLIKGKGLMGAMFWALDLDDFRGVCGEGKYPLISAVSKALGGYTPP   397
                      ****:::**  **:.*****.* *****.******   ********:*:*:: ****.**

CrChit1_candidate_1   TPKIPRSPPPTLPTEKPPPPGQSTVKPPPVKTNAPPPGGKGCKSIGRWRGIPNMDEWCIT   479
HyChit1_Q6ZYN0        PEPTHGPRPPSKAPTKAPSRG------PT-NKPVTSGPGGKCHAIGVWKGNANMDSWCVA   450
                             **:    * *  *      *  :. .    *  *::** *:*  ***.**::

CrChit1_candidate_1   NCAAGNCPSDMCKCT  494
HyChit1_Q6ZYN0        NCARNNCPADTCAC-  464
                      *** .***:* * *
```

Figure 2.10. Identification of *C. radiatum Chitinase 1* candidate 1. (A) Nucleotide sequence and (B) deduced amino acid sequence of *CrChit1* candidate 1 (TRINITY_DN108060_c3_g1_i1). (C) Multiple sequence alignment of amino acid sequences of CrChit1 candidate 1 and HyChit1 (UniProt Q6ZYN0) by CLUSTAL O (1.2.4). Putative signal peptide is underlined in orange, catalytic domain is unlined in black, and active sites are boxed in green (Mali et al., 2004).

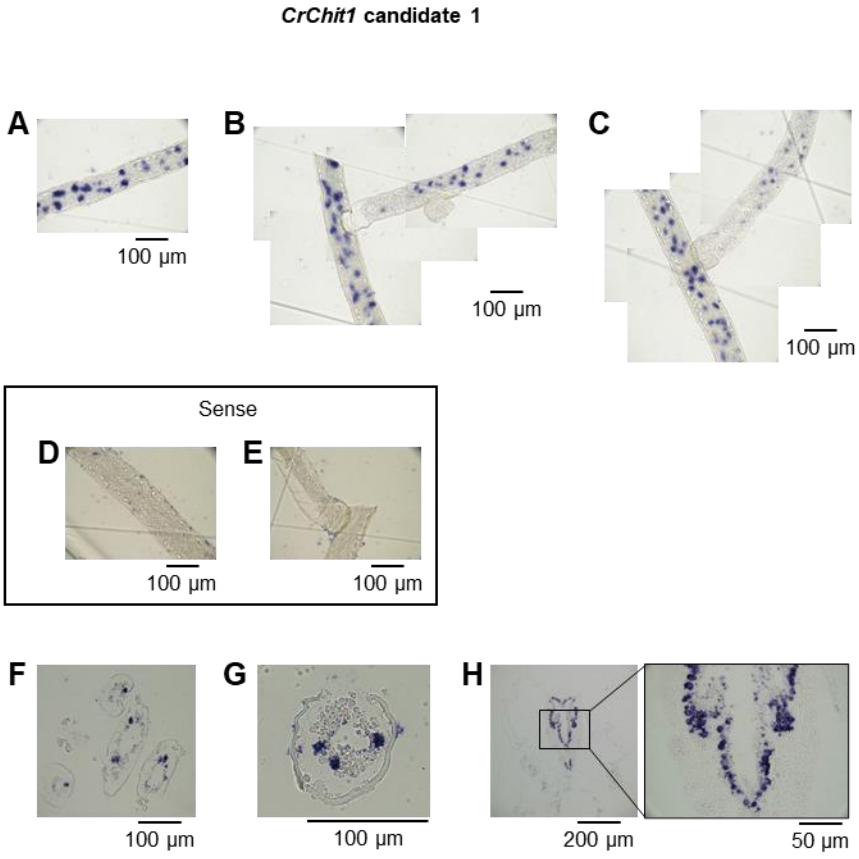

Figure 2.11. Detection of involvement of *Chitinase 1* in allorecognition. (A-D) In-situ hybridisation of *CrChit1* candidate 1 on stolons with anti-sense probe. (A) Typical signal pattern of *CrChit1* candidate 1 in stolons. (B,C) *CrChit1* candidate *1* signal patterns at incompatible stolon encounters (between F0 ♂ and F0 ♀). (D,E) Negative control with sense probe in typical stolon (D) and incompatible stolon encounter (F0 ♂ and F0 ♀) (E). (F,G) Representative images showing *CrChit1* candidate *1* expression on stolon cross sections. (H) Representative images showing *CrChit1* candidate *1* expression on medusa cross section.

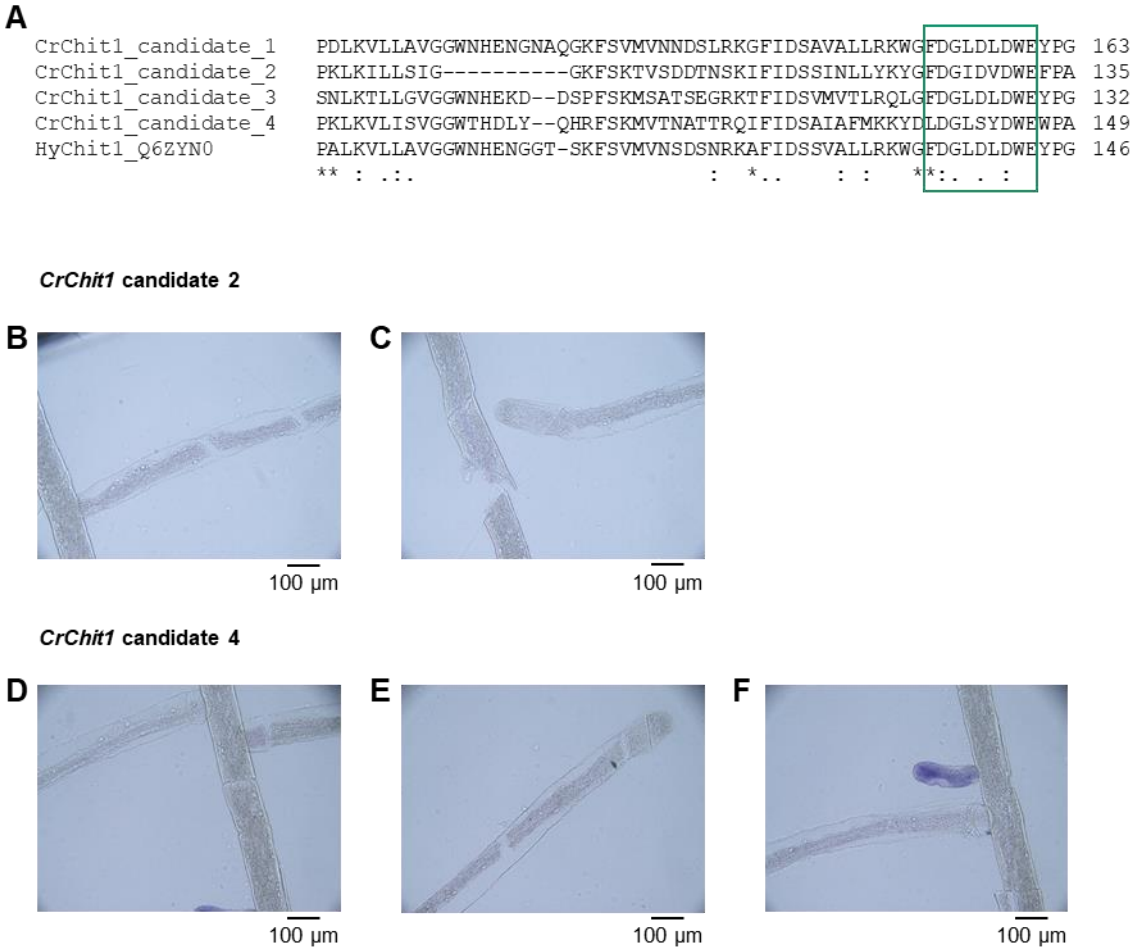

Figure 2.12. Other candidates of *C. radiatum Chitinase 1*. (A) Multiple sequence alignment of amino acid sequences of CrChit1 candidates 1-4 and HyChit1 (UniProt Q6ZYN0) by CLUSTAL O (1.2.4). Active sites are boxed in green (Mali et al., 2004). (B,C) Representative images showing in-situ hybridisation of *CrChit1* candidate 2 on stolons. (D-F) Representative images showing in-situ hybridisation of *CrChit1* candidate 4 on stolons.

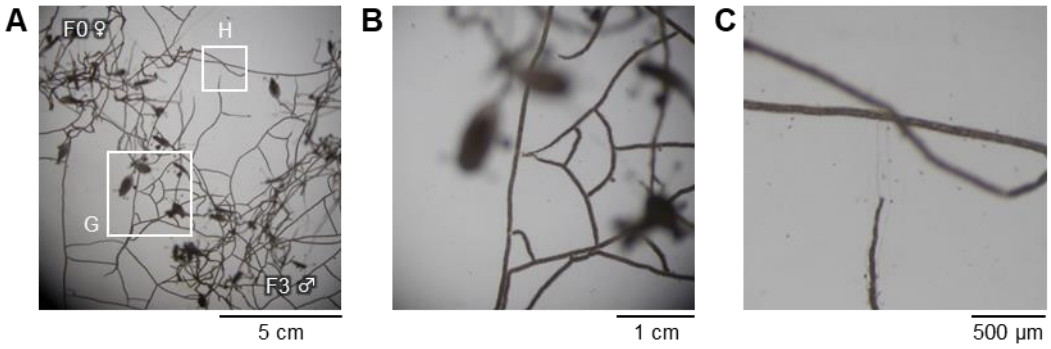

Figure 2.13. Photos demonstrating incompatible colonies growing in the same environment for prolonged period of time. (A) Wide-field image of two incompatible colonies (F0 ♀ and F3 ♂) growing in the same container for over one month. (B) and (C) show rejecting stolon encounters, boxed in white in (A).

Chapter 3: Genetic analysis of *C. radiatum* allorecognition

The work in this chapter was done in collaboration with Takao Onojima (Ito Lab, School of Life Science and Technology, Tokyo Institute of Technology). Stolon encounter assay results included data obtained by Kenta Kobayakawa and Zuyu Han (master students, Tachibana Lab). The main parts of this chapter and Chapter 2 are included in the published manuscript, Tang, C., Tamura-Nakano, M., Kobayakawa, K., Ozawa, T., Onojima, T., Kajitani, R., Ito, T., Tachibana, K. (2024). A single gene determines allorecognition in hydrozoan jellyfish Cladonema radiatum inbred lines. *Journal of Experimental Zoology Part A: Ecological and Integrative Physiology*.

Introduction

Genetics of allorecognition has been extensively in *Hydractinia*. Genetic analysis of histocompatibility of inbred lines identified that a single chromosomal region, ARC, determined allorecognition responses in *Hydractinia* (Mokady & Buss, 1996). Colonies sharing of at least one allele of ARC, of which genotypes were assigned *f*/*r*/*q* (this *f*/*r* genotype system was applicated in afterward studies), fuse and colonies with no shared allele reject. Later, the observation of transitory fusion, at a low frequency in a population, suggested that allorecognition was not completely explained by genotypes of a single locus (Cadavid et al., 2004). An additional locus was identified inside the ARC. The first determinant locus was termed *Alr1* and the second identified locus was termed *Alr2* (Cadavid et al., 2004). Predictions of allorecognition outcomes by genotypes of *Alr1* and *Alr2* was updated as below (Cadavid et al., 2004; Powell et al., 2007):

(1) Colonies sharing at least one matching allele in both *Alr1* and *Alr2* fuse.

(2) Colonies sharing no matching allele in either *Alr1* or *Alr2* reject.

(3) Colonies sharing only one allele in either *Alr1* or *Alr2* result in transitory fusion.

While allorecognition outcomes were predicted by the genotypes of *Alr1* and *Alr2* in the inbred line study, exceptions were observed in the wild types (Cadavid et al., 2004; Rosa et al., 2010). Understanding of ARC was advanced by sequencing and genomic analysis. Recent publication reported ARC is at least 11.8 Mb and contains 41 *Alr* family genes (Huene et al., 2022), and at least eight genes within the ARC associate with allorecognition (Rodriguez-Valbuena et al., 2022). Functionality and association with allorecognition of each gene are undetermined.

Most of the *Alr* genes code for transmembrane proteins with highly polymorphic IgSF-like domains (Nicotra et al., 2009; Rosa et al., 2010; Gloria-Soria et al., 2012; Huene et al., 2022; Rodriguez-Valbuena et al., 2022). IgSF domains of Alr proteins contain unique V-set and I-set domains, with significant differences compared to those identified metazoan IgSF domains (Huene et al., 2022). IgSF domains were also recognised in Botryllus allorecognition determinant FuHC but there is no evidence of evolutionary relationships between FuHC and Alr, as well as with the vertebrate MHC (Grosberg & Plachetzki, 2010). This demonstrates the diversification of IgSF proteins during metazoan evolution.

While the genomics of allorecognition is extensively studied in *Hydractinia*, there is almost no information for that in other Cnidarian. Putative homologs with notable similarities were identified in *Hydra* by NCBI BLAST but *Hydra* does not seem to possess allorecognition. There is inadequate information for interpreting if *Alr* genes are conserved. Therefore, studying genetics of allorecognition in *C. radiatum* could potentially provide insights in to conservation and evolutionary aspects of Cnidarian allorecognition.

This chapter organised genomic and genetic analysis of *C. radiatum* ARC. *Alr*-related genes and ARC were identified by homology search of the whole genome sequencing data of inbred lines. A total of 10 *Alr*-like genes was identified. Six of these genes, including the putative *Alr1* homolog, were located on the putative ARC. The other four genes were located

on a separate genomic region. The Alr-like proteins contain IgSF domains like *Hydractinia* Alr. Allorecognition outcomes in the inbred lines were predicted solely by the genotypes of *Alr1*.

Results

Identification of *C. radiatum Alr* genes

To assess the genetic basis of allorecognition in *C. radiatum*, genetic search was performed in the genomes of two inbred lines: a female F20 11-2 and a male F20 8-1 (Onojima et al., in preparation), and identified a total of 10 *Alr*-like genes by *ab initio* gene predictions and sequence similarity to the *Hydractinia Alr1* and *Alr2*. The identified *Alr*-like gene with the highest amino acid similarity to *Hydractinia Alr1* was presumed to be the homolog and was annotated as *Alr1* (Figure 3.1). This *Alr1* gene is located on the contig 0247, together with 5 more *Alr*-like genes, which were annotated as *Alr2-6* (Figure 3.2A). Please note that these *Alr2-6* are not homologous to the *Hydractinia Alr2-6*. The genomic region occupied by these genes was the putative ARC of *C. radiatum*. The remaining 4 *Alr*-like genes were found on a different contig (1843), and were denoted as *IgSF1-4* (Figure 3.2B). Besides *C. radiatum*, a number of *Alr*-like genes were identified in *Cladonema pacifium* (*C. pacificum*; also Cpac in figures), a close relative species of the same genus of *C. radiatum*, and in other Hydrozoans (Hydractinia and Hydra) in the same class, using *Alr*-like genes identified in *C. radiatum* as queries. Phylogenetic tree of these Hydrozoan *Alr*-like genes revealed that *C. radiatum Alr1-4* and a group of *C. pacificum Alr*-like genes, including the potential homolog of *Alr1*, were grouped into distinct clades, respectively (Figure 3.3). In contrast, each *IgSF* gene of *C. radiatum* clustered in pair with its corresponding homolog of *C. pacificum*. It suggests that *Alr1-4* arose by gene duplication after the divergence of the two

species while duplication of the *IgSF* genes occurred before the divergence.

Alternative splicing was identified in *Alr1* of both *C. radiatum* (derivatives were designated as *Alr1.1* and *Alr1.2*) and *C. pacificum* (Figure 3.1C), and the splicing patterns were highly similar to that in *Hydractinia* (Huene et al., 2022), suggesting these genes descended from a common evolutionary origin. While there is evidence of homology of the *Alr1* genes, the other 9 *Alr*-like genes varied greatly in length, encoding proteins of from ~300 to ~1200 amino acids, and did not show strong evidence of direct homology to *Hydractinia Alr1* or *Alr2* in multiple sequence alignments. Domain analysis of the encoded proteins was performed to provide information for function prediction of the *Alr*-like genes.

Conserved domain architecture among Hydrozoan Alr

C. radiatum Alr were mainly composed of signal peptides, Ig domains, extracellular spacers (ECS), transmembrane domains and cytoplasmic tails (Figure 3.4), as reported in *Hydractinia* (Nicotra et al., 2009; Rosa et al., 2010; Huene et al., 2022.) Ig domains were grouped into V-set and I-set domains. An additional Ig-like Fibronectin type III (Fn3)-like domains were identified in the ECS.

Ig domains are the keys in determining allorecognition. The Ig domains of the *C. radiatum* Alr-like proteins was comprehensively analysed by multiple sequence alignments with *Hydractinia* Alr Ig domains. The V-set domains contained residues corresponding to the canonical residues (Figure 3.5), Arg75, Leu89 and Asp98, which are highly conserved in V-set Ig domains across species. Substitutions of Cys23 by Trp, and Trp41 and Cys104 by Met/Leu/Ile /Val were observed, which is consistent with that in *Hydractinia* (Huene et al., 2022). In addition, Huene et al. demonstrated that *Hydractinia* Alr proteins contains unique conserved cysteines, which were suggested to contribute to structural stability. These cysteines were also highly conserved in *C. radiatum*. For the I-set domains, canonical motif

Pro (ix) (Wang, 2013) was totally conserved in both *C. radiatum* and *Hydractinia* (Figure 3.6). Furthermore, cis-Pro (v) and Trp35 were conserved in the Alr family, but not in the IgSF groups. The ECS of *C. radiatum* Alr-like proteins also displayed conservation with the *Hydractinia* ECS (Figure 3.7). *Hydractinia* Alr-specific cysteines were shared among almost all the ECS in *C. radiatum*. Ig-like Fn3-like folds were reported in most of the *Hydractinia* Alr ECS. Similarly, conservation of canonical residues (Halaby et al., 1999) was observed in *C. radiatum*: a proline at the beginning of strand A, a tryptophan at the end of strand B, and a tyrosine at the beginning of strand C. *C. radiatum* showed a higher level of conservation of the consensus residues. Tyrosine at the end of the strand C was almost conserved in all ECS. Leucine at the EF loop, which is not conserved in *Hydractinia*, was identified in Alr1-4. Topohydrophobic positions, another characterised feature of Fn3, were also highly conserved. These observations demonstrated the conservation of linkage between *C. radiatum* and *Hydractinia* Alr ECS.

In the cytoplasmic tail, multiple *Hydractinia* Alr proteins contain the signalling motifs immunoreceptor tyrosine-based activation motifs (ITAMs; YxxI/Lx6-12YxxI/L) (Barrow et al., 2006) and immunoreceptor tyrosine-based inhibition motifs (ITIMs; S/I/V/LxYxxI/V/L) (Murphy et al., 2008), which are highly conserved in immunoreceptors and adaptor proteins. Motifs were searched in cytoplasmic tails of Alr and IgSF proteins of *C. radiatum*. ITIMs were found in five of the Alr-like proteins (Figure 3.8). Alr1.1 and Alr1.2 each contains two ITIMs. ITAM, to the contrary, was not found in Alr-like proteins of *C. radiatum*. Overall, *C. radiatum* and *Hydractinia Alr*-like proteins exhibited significant levels of domain architecture conservation.

Alr1 and *Alr2* as candidate genes for allorecognition

Allelic polymorphism at the Ig domains is fundamental in defining individuals'

identities, thus allowing allorecognition at high specificity. Therefore, the allelic variation of the Ig domains was examined to assess the functionality of the *Alr*-like genes. To obtain more data for analysing the allelic variations of the Ig domains, strand-specific RNA-sequencing (RNA-seq) data was generated from medusae of the two wild-type founder strains of the inbred lines, F0 ♀ and F0 ♂, and another wild-type strain OGW. These sequences were mapped to the entire genome. I failed to obtain sequence data of *Alr3* and *Alr4* due to their low expression in medusae. Pairwise comparison was made between the encoded amino acid sequences of the V-set (Figure 3.9A), I-set (Figure 3.9B) and ECS (Figure 3.9C) domains of all haplotypes identified. For the V-set domains, *Alr1* and *Alr2* showed distinctly high variation between alleles. Alleles of *Alr1* and *Alr2* had low similarities with medians of 68% and 69%, respectively, while all other genes had similarities of above 85%. While *Alr1* and *Alr2* still exhibit relatively higher variation, similarities between alleles of all *Alr*-like genes at I-set and ECS domains had similarities above 85%. The high allelic variation of *Alr1* and *Alr2* indicates their potential as the determinants in allorecognition.

Allorecognition outcomes in inbred lines depend on the genotypes of *Alr1*

To test the functionality of *Alr1* and *Alr2*, I observed stolon encounters between individuals of different genotypes in our inbred lines. RNA-seq data showed that F0 ♀ was homozygous at *Alr1* with only 1 haplotype (genotype: AA) and F0 ♂ was heterozygous with 2 haplotypes (genotype: CD) (Table 3.1, Figure 3.10). For *Alr2*, F0 ♀ displayed 2 haplotypes, but with amino acid similarity of 99.8%. They were unlikely to produce different phenotypes, so they were considered the same haplotype (A). F0 ♂ only had 1 haplotype (C) (Table 3.1, Figure 3.11). I also included *IgSF2*, as a representative of the *IgSF* groups. The *IgSF* genes were very closely located (<100 kb) so I assume they were inherited together in the inbred lines. Both F0 ♀ and F0 ♂ had 2 haplotypes, but of high similarities in between them (99.7%

and 98.2% respectively), so the 2 haplotypes of each strain were considered the same haplotype. Haplotypes of F0 ♀ and F0 ♂ were denoted as A and C, respectively (Table 3.1, Figure 3.12). All alleles that categorised as the same haplotype have no more than one different amino acid in the V-set domains. With the genomic sequences and genetic information from the RNA-seq data, primers were designed for genotyping the inbred lines by Polymerase Chain Reaction (PCR) (Table 3.3). A region at Intron 4 between Exon 4 and Exon 5 was targeted to generate PCR products of different sizes for each haplotype of *Alr1*. Results were confirmed with additional primer sets that amplified only at specific haplotypes. *Alr2* was also genotyped by PCR targeting a region at Intron 4 between Exon 4 and Exon 5. Haplotypes were discriminated by the different PCR product sizes. *IgSF2* was genotyped by PCR amplifying a region at the cytoplasmic region to generate products of different sizes. Genotyping results were summarised in Figure 3.13. An additional cross between F2 ♀ and F5 ♂ was generated to obtain individual with *Alr1* genotype DD. *Alr1* and *Alr2* became homozygous in F9, while IgSF2 became homozygous in F6. Coincidentally, All *Alr1*, *Alr2* and *IgSF2* alleles in the late progenies were all inherited from F0 ♀.

Table 3.1. Amino acid sequence comparison of alleles of *Alr1*, *Alr2* and *IgSF2*. HT: designated haplotype. "Identical amino acids/total number of amino acids" is shown in brackets. Multiple sequence alignments of all alleles are shown in Figure 3.10-12.

A

Gene_strain_allele	HT	Alr1_F0♀_allele1	Alr1_F0♂_allele1	Alr1_F0♂_allele2
Alr1_F0♀_allele1	A	100% (529/529)		
Alr1_F0♂_allele1	C	85.3% (451/529)	100% (527/527)	
Alr1_F0♂_allele2	D	83.7% (443/529)	88.6% (466/527)	100% (527/527)

B

Gene_strain_allele	HT	Alr2_F0♀_allele1	Alr2_F0♀_allele2	Alr2_F0♂_allele1
Alr2_F0♀_allele1	A	100% (631/631)		
Alr2_F0♀_allele2		99.8% (630/631)	100% (631/631)	
Alr2_F0♂_allele1	C	86.9% (549/632)	86.7% (548/632)	100% (632/632)

C

Gene_strain_allele	HT	IgSF2_F0♀_allele1	IgSF2_F0♀_allele2	IgSF2_F0♂_allele1	IgSF2_F0♂_allele2
IgSF2_F0♀_allele1	A	100% (734/734)			
IgSF2_F0♀_allele2		99.7% (732/734)	100% (734/734)		
IgSF2_F0♂_allele1	C	97.4% (715/734)	97.4% (715/734)	100% (734/734)	
IgSF2_F0♂_allele2		96.7% (710/734)	96.7% (734/734)	98.2% (721/734)	100% (734/734)

Association between the *Alr* genes and allorecognition was examined by observing responses at stolon encounters between the inbred lines. Stolons encounters were observed for a period of 14 days, and the outcomes are categorised as "fusion"—connection of gastrovascular canals (Figure 3.14A), "rejection"—separation of the contacting stolons (Figure 3.14B) and "ignoring/pending"—attacking stolon changed its growing direction so it grows alongside (Figure 3.14C) or across the defending stolon (Figure 3.14D) (ignoring), or the stolons stayed in contact without fusion or rejection until the end of 14-day observation (Figure 3.14E) (pending).

Stolon encounter assay results show that *Alr1* is the determinant in allorecognition. One matching allele of *Alr1* allowed fusion of stolons (Figure 3.15). Stolons with at least one shared allele had high rates of fusion (>60%) (Table 3.2). Rejection occurred at low rates (<30%), which were apparently the results of naturally occurring stolon regression. Stolons without any shared allele of *Alr1* never fused, even if common alleles were shared at *Alr2* and *IgSF*. These stolon encounters either ended up in rejection (47-100%) or ignoring/pending (0-

53%). Rejection was typically recognised by the regression of the attacking stolons. As observation was conducted on daily basis and regression usually occurred for a few hours, followed by re-approaching of the attacking stolon tips to the defending stolons, some regression events might be omitted and were counted as pending. Consistent with the *Hydractinia Alr* genes, All *Alr1* alleles are codominant. As long as there is one match of *Alr1* genotypes, regardless of the combination, stolons fuse. Unfortunately, I did not have combinations that share *Alr1* alleles but not *Alr2* alleles so I could not assert genotypes of *Alr1* alone decide the allorecognition outcomes. In summary, stolon encounter assay results, together with the genetic analysis, suggested *Alr1* being the major determinant in *C. radiatum* allorecognition.

Table 3.2. Inbred line stolon encounter assay results. n: number of counts.

		Genotype						Allorecognition outcome			
Combination		*Alr1*	match	*Alr2*	match	*IgSF2*	match	Fusion	Rejection	Ignoring/pending	n
F0 ♀	F0 ♀	AA AA	**2**	AA AA	**2**	AA AA	**2**	100.0%	0.0%	0.0%	23
F0 ♂	F0 ♂	CD CD	**2**	CC CC	**2**	CC CC	**2**	91.7%	4.2%	4.2%	24
F1 ♀	F1 ♀	AC AC	**2**	AC AC	**2**	AC AC	**2**	100.0%	0.0%	0.0%	20
F2 ♂	F2 ♂	AD AD	**2**	AC AC	**2**	AC AC	**2**	80.0%	20.0%	0.0%	25
F3 ♂	F3 ♂	CD CD	**2**	CC CC	**2**	AC AC	**2**	86.4%	13.6%	0.0%	22
F5 ♀	F5 ♀	CC CC	**2**	CC CC	**2**	AA AA	**2**	80.0%	0.0%	20.0%	25
DD	DD	DD DD	**2**	AC AC	**2**	AC AC	**2**	73.0%	27.0%	0.0%	37
F0 ♀	F2 ♂	AA AD	**1**	AA AC	**1**	AA AC	**1**	75.0%	0.0%	25.0%	24
F0 ♂	F2 ♂	AA AD	**1**	AA AC	**1**	AA AC	**1**	61.9%	14.3%	23.8%	21
F0 ♀	F7 ♀	AA AC	**1**	AA AC	**1**	AA AA	**2**	81.8%	4.5%	13.6%	22
F1 ♀	F2 ♂	AC AD	**1**	AC AC	**2**	AC AC	**2**	75.0%	25.0%	0.0%	20
F1 ♀	F5 ♀	AC CC	**1**	AC CC	**1**	AC AA	**1**	94.4%	0.0%	5.6%	36
F2 ♂	"DD"	AD DD	**1**	AC AC	**2**	AC AC	**2**	80.8%	11.5%	7.7%	26
F0 ♂	F5 ♀	CC CD	**1**	CC CC	**2**	AA CC	0	82.1%	10.3%	7.7%	39
F0 ♂	F7 ♀	CD AC	**1**	CC AC	**1**	CC AA	0	72.7%	13.6%	13.6%	22
F0 ♀	F0 ♂	AA CD	0	AA CC	0	AB CC	0	0.0%	75.0%	25.0%	20
F0 ♀	F3 ♂	AA CD	0	AA CC	0	AA AC	**1**	0.0%	82.8%	17.2%	29
F0 ♀	F5 ♀	AA CC	0	AA CC	0	AB AA	**2**	0.0%	100.0%	0.0%	32
F0 ♀	DD	AA DD	0	AA AC	**1**	AA AC	**1**	0.0%	71.7%	28.3%	46
F1 ♀	DD	AC DD	0	AC AC	**2**	AC AC	**2**	0.0%	78.6%	21.4%	28
F5 ♀	DD	CC DD	0	CC AC	**1**	AA AC	**1**	0.0%	75.0%	25.0%	36
DD	F7 ♀	DD AC	0	AC AC	**2**	AC AA	**1**	0.0%	47.1%	52.9%	34

Alr1 expression pattern in *C. radiatum*

Alr1 is involved in the allorecognition by direct binding with Alr1 of the opposing individual, is thus expected to be presented at the stolon ectodermal epithelia. However, there is no study on the expression pattern of Alr1. *Alr1* transcripts were detected in RNA-seq data of eggs and also medusae, which constructed the *C. radiatum* local BLAST database. *Hydractinia Alr1* transcript was also reported expressed in not only in adult colonies and stolon mat, but also in all examined stages, including eggs, embryos (blastula) and planula larvae (Nicotra et al., 2009; Rosa et al., 2010). However, allorecognition was not observed in all, but only after late larval stage (Lange et al., 1992). Expression of Alr1 is essential to but

may not correlate with allorecognition. To examine the expression pattern of *Alr1*, in-situ hybridisation was performed on *C. radiatum* stolons and medusa (Figure 3.16). *Alr1* transcripts were detected in both stolons and medusa, in both ectoderm and endoderm. Intense signals were observed at one of the incompatible stolon encounters (Figure 3.16A). However, this was considered a rare case, as it is not observed at another encounter in Figure 3.16A, and the overall in-situ hybridisation signals were uneven throughout the stolons. The intense signals might be a result of uneven distribution of reagents during in-situ hybridisation (discussed in detail in Appendix 2) or signals could only be detected at specific timing during the encounter, as the allorecognition processes are dynamic.

Discussion

Genetic analysis of *C. radiatum* ARC provides evolutionary information of Hydrozoan allorecognition

Alr-related genes and ARC of *C. radiatum* were identified. Compared to *Hydractinia* ARC, *C. radiatum* ARC is apparently simple, with only 6 *Alr* genes. 4 additional *IgSF* genes are located in a separate genomic region. Phylogenetic analysis revealed the 6 *Alr* genes diverge after the divergence between *C. radiatum* and the close relative *C. pacificum*. Most of the *Alr* genes are presumably paralogs of one of the *Alr* genes, putatively *Alr1*, which shows relatively high homology to *Hydractinia* and *C. pacificum Alr1*. Conserved alternative splicing patterns were also observed in *C. radiatum Alr1*, although functional differences between the derivatives still remain to be investigated.

Domain architectures of the Alr proteins are conserved. High allelic variation of Ig domains, which gives rise to the allorecognition ability, is also observed. Downstream signalling pathways after Alr recognition had long been a mystery. In *Hydractinia*, ITAM

was first identified in cytoplasmic region of Alr1 (Rosa et al., 2010) and ITIM was found in the Alr2 (Nicotra et al., 2009; Rodriguez-Valbuena et al., 2022). ITAMs associate with the activation of immune cells in vertebrates, while ITIMs usually downregulate the immune responses (Underhill and Goodridge, 2007). They work harmony in maintaining a balanced immune response of lymphoid and myeloid cells in vertebrate immune (Ravetch and Lanier, 2000). Huene et al. (2022) reported the presence of ITAMs and ITIMs in multiple Alr proteins, and proposed a conserved ITAM/ITIM-mediated signalling pathway in regulating the allorecognition responses—ITAMs in default initiate rejection response and ITIMs inhibit it upon homophilic binding of Alr proteins. In *C. radiatum*, ITIMs were identified in Alr1 and Alr3, but no ITAM was found in any of the Alr-like proteins. The absence of the ITAMs may explain the differences between the allorecognition responses between *C. radiatum* and *Hydractinia*, e.g. nematocyst assembly and discharge. Allorecognition is still effective in *C. radiatum*, indicating that ITIMs instead of ITAMs may be more primary in differentiating fusion and rejection responses, on the premise that ITAM/ITIM signalling pathway is the dominant signalling pathway. However, how rejection is induced in *C. radiatum* remains unknown. Indeed, on contrary to its name, ITIMs may actually be activating (Barrow et al., 2004; Barrow and Trowsdale, 2006). The actual role of ITIMs and presence of other potential signalling pathways demand further investigation.

Although genomic sequences of the ARC are completely assembled, there are still a lot of remaining questions awaiting investigation in the ARC. *Alr* genes in the ARC are hypothesised to be products of gene duplication. It is unclear why gene duplication was promoted. Gene duplication was also suggested to contribute to the presence of abundant *Alr* genes in *Hydractinia* (Nicotra et al., 2009; Huene et al., 2022). However, underlying mechanisms were unclear. Functionality of most of the genes are uninvestigated and it is unknown whether they provided survival advantage to the individuals that drove evolution

towards the complication of the ARC. The sequence diversity between *Alr* genes, along with their conserved domain architecture, also suggests that there might be frequent duplication and recombination events within the ARC (Huene, 2022). Interestingly, unexpectedly high recombination rates were observed between *Alr1* and *Alr2* during genotyping of the inbred lines. *Alr1* and *Alr2* are separated by around 2 Mb (Figure 3.2A), which were expected to have a recombination rate at around 2%, based on 1 cM/Mb. However, I observed at least recombination at one of the parental strains in almost every cross between the inbred lines until F6, after which recombination was not detectable. Recombination hotspots might be present in the ARC of *C. radiatum*. *Hydractinia* was the only Hydrozoan model with genetic analysis of the ARC. Valuable discoveries, for example, presence of Ig-like domains in Hydrozoans that shared similarity with other invertebrates and even vertebrates, and putative ITAM/ITIM signalling, shed light on the evolutionary importance of Hydrozoan/Cnidarian allorecognition in understanding the evolution of animal immunity. Genomic and genetic information of *C. radiatum* ARC in this study provided materials for comparative analysis and thus insights into the evolutionary basis of the Hydrozoan ARC.

Results in Chapters 1 and 2 are summarised in Figure 3.17. Upon encounter between stolons, electron-dense granules are assembled at the epithelial cells and perisarc separating the stolons is digested at the contact zone. After perisarc is open, cells of the two stolons come into contact and allorecognition occurs from this point via Alr1 binding. With at least one allele match of *Alr1*, tissue remodelling rapidly takes place to connect the gastrovascular canals between the stolons. Without *Alr1* match, autophagy and necrosis are induced at the contact cells to evade further contact with the opponents' cells. Contacting cells are removed and perisarc is reconstructed to physically separate the two stolons. Overall, Chapters 1 and 2 characterised the morphological and genetic features of allorecognition in stolons.

Materials and Methods

Inbreeding in the laboratory

Jellyfish breeding in the laboratory was carried out in 6-cm polystyrene dishes filled with 20 ml of artificial seawater. Spawning was induced by exposing the sexually mature jellyfish to light. Mature eggs and sperm were released 15-20 minutes after the light-on under our experimental condition at 26–28°C. Within 2 days post fertilisation (dpf), planula larvae settled to the bottom of the dish and metamorphosised into primary polyps 3 dpf. Sliced brine shrimp was fed to the primary polyps once every 2 days in the first week. Single polyp from each colony was transferred to a fresh dish to isolate single clones. Typically, 25 females and 25 males among the offspring were obtained from cross. A medusae-polyp life cycle of *C. radiatum* is around 4-5 weeks. To select healthy offspring, each clone was observed for 3-4 weeks. Offspring to be intercrossed to generate the next generation were selected according to the criteria described previously (Tachibana et al., 2020). It took 7-9 weeks to produce one generation. F0♀ and F0♂ were crossed to generate F1 progeny. Then, F1♀ was backcrossed to F0♂ to generate F2 (F2) strains as F0♂ generally showed better health and growth than F0♀. Subsequent generations of the inbred lines were generated by full-sib-mating from F2-F21.

Genomic DNA preparation and genotyping

Genomic DNA was extracted from 5-10 medusae using DNeasy Blood & Tissue Kit (Qiagen, Hilden, Germany) according to the manufacturer's instruction. A 25-µl multiplex PCR reaction mix was prepared with 10-20 ng genomic DNA, 0.4 mM dNTPs, 500 nM forward and reverse primers (listed in supplementary table 3.3), 1X KOD FX buffer and 2.5 units KOD FX DNA polymerase (Toyobo, Osaka, Japan), and was subjected to 30 rounds of

amplification, using the following conditions: 95°C for 10 sec, 55°C for 1 min, and 72°C for 1 min. 5 μl of each PCR product was analysed with 5% polyacrylamide gel electrophoresis.

Table 3.3. List of primers used in genotyping *Alr1, Alr2* and *IgSF2*. bp: base pairs.

			PCR product Length (bp)		
Target (HT)	Forward	Reverse	A	C	D
Alr1 (A, C, D)	GTGTGTGGTGTAATATTGTTG	GATTTAACAGGAATAGTACC	1015	399	414
Alr1 (C)	AACAGTCAGATAAGAAACCT	TATATGCAAAAGGAAAACTC		135	
Alr1 (D)	AACACTCACGTAAGACAACT	TTGTTTTTTTACTTTTTGTC			152
Alr2 (A, C)	ACCTCAGTTGAGAGATGAGAAATG	CTTGGAGCTTAATAAGCAATTACC	108	94	
IgSF2 (A,C)	AATACTAAATAAATAGTTGGCCTG	AGAAGAGTTAAACTGAGAGGAAACC	149	131	

RNAseq

Total RNA was extracted from 5-10 jellyfish medusae using MagExtractor RNA (Toyobo). Total RNA with an RNA integrity number value exceeding 9.7 was used for subsequent analysis. Using 1 μg of total RNA as an input, the libraries for RNA-seq were prepared using a SureSelect Strand-Specific RNA Library Preparation Kit (Agilent, Santa Clara, CA, USA) according to the manufacturer's protocol. Then, 150-bp paired-end reads were obtained using a HiSeq2500 platform (Illumina, San Diego, CA, USA).

Stolon allorecognition assay

Polyps of interest were transferred into a plastic culture container, and were allowed to settle for one day without disturbance before usual husbandry. Stolon growth was monitored on daily basis and encounters were recorded for 14 days with a Leica MZ10F stereomicroscope. For time-lapse record, polyps were either settled on a glass slide or on a transparent PET sheet, which was maintained in a petri dish during the time-lapse imaging with an inverted microscope Zeiss Axiovert 135 (Carl Zeiss, Oberkochen, Germany).

In-situ hybridisation

Assays were performed as described in Chapter 2. Primers used for DIG-RNA probe synthesis are summarised in Table 3.4.

Table 3.4. List of primers used in amplifying cDNA templates for synthesis of in-situ hybridisation RNA probe. cand: candidate, bp: base pairs, "cagtgaattg"=extra nucleotides, "taatacgactcactatag"=T7 promoter, "atttaggtgacactatag"=SP6 promoter. Alr1 (1) and Alr1 (2) were used in in-situ hybridisation on medusa and stolon, respectively.

Target		Forward	Reverse	Product (bp)
Alr1 (1)	1st PCR	TGATAACGTTCAAGCAGGCT	TCACCAGACATTGCCCAAAC	816
	2nd PCR	cagtgaattg-taatacgactcactatag-CCCTAACGATCGATTGGTTGT	cagtgaattg-atttaggtgacactatag-ATCGCCAACATCAAGTGCTG	624
Alr1 (2)	2nd PCR	cagtgaattg-taatacgactcactatag-GGAGGTCCTGTGTCATGTAAC	cagtgaattg-atttaggtgacactatag-CACCAGACATTGCCCAAACT	591

Figure 3.1. *C. radiatum Alr1*. (A) Deduced amino acid sequence of *C. radiatum Alr1* (F0 ♀ allele 1) and its alignment with *C. pacificum* and *Hydractinia* (*H. symbiolongicarpus*) *Alr1* amino acid sequences. Identical amino acids are boxed, and gaps introduced for optimal alignment are indicated by dashes. Underlined red: signal peptide (SP), green: V-set Ig (Immunoglobulin), blue: I-set Ig, yellow: ECS (extracellular spacer), purple: TM (transmembrane), black: CT (cytoplasmic tail). (B) Domain architecture. (C) Alternative splicing of *Alr1* from *C. radiatum* (top) and *C. pacificum* (bottom). To compare splicing patterns, see Huene et al. (2022) Fig. S4 (A) alternative splicing of *Hydractinia Alr1*.

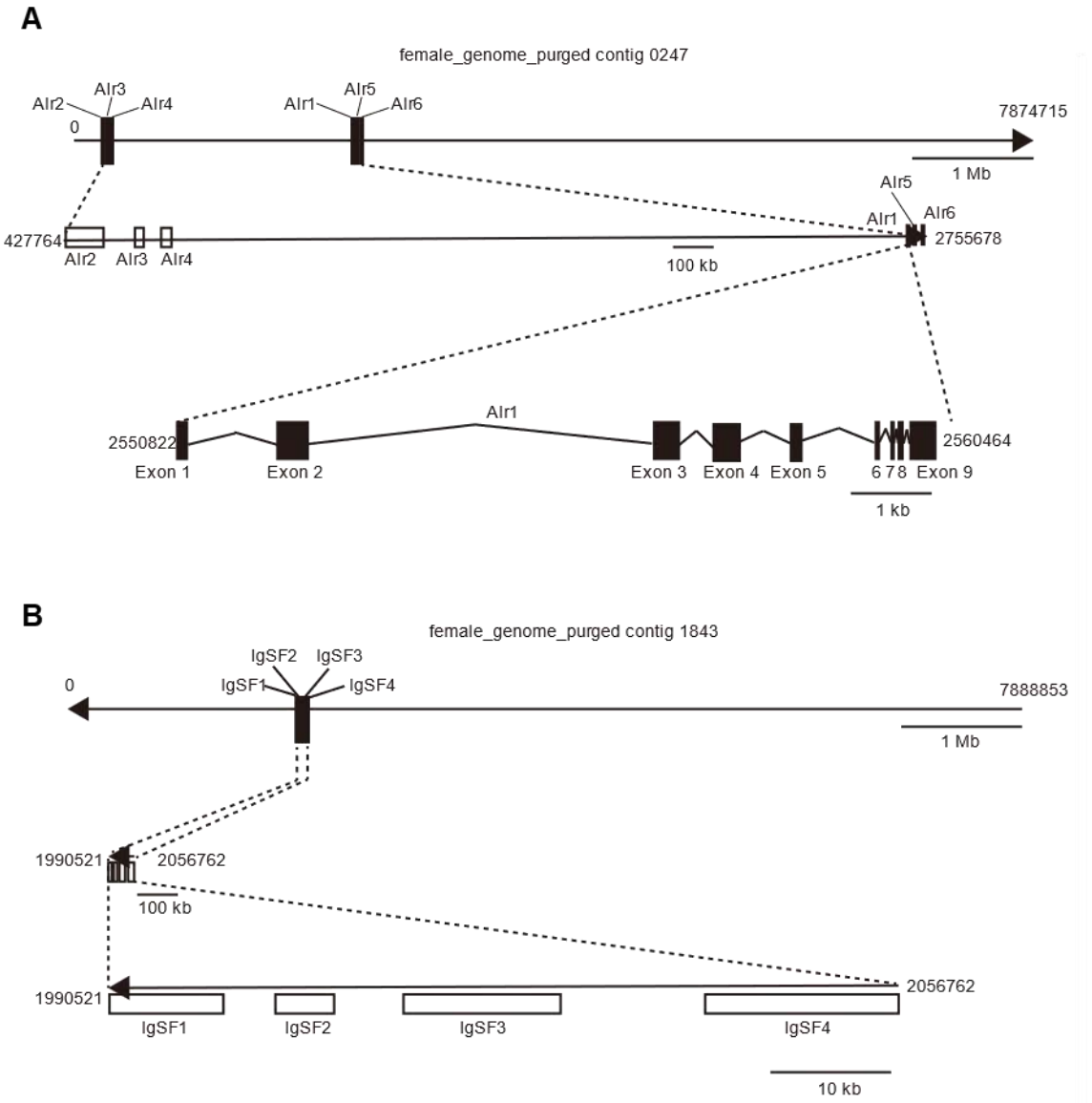

Figure 3.2. Assembly of Alr-like genes in *C. radiatum*. **A**. Six *Alr*-related genes: *Alr1-6* were found within 3 Mb region in contig 0247. **B.** Four *Alr*-related genes: *IgSF1-4* were found in contig 1843.

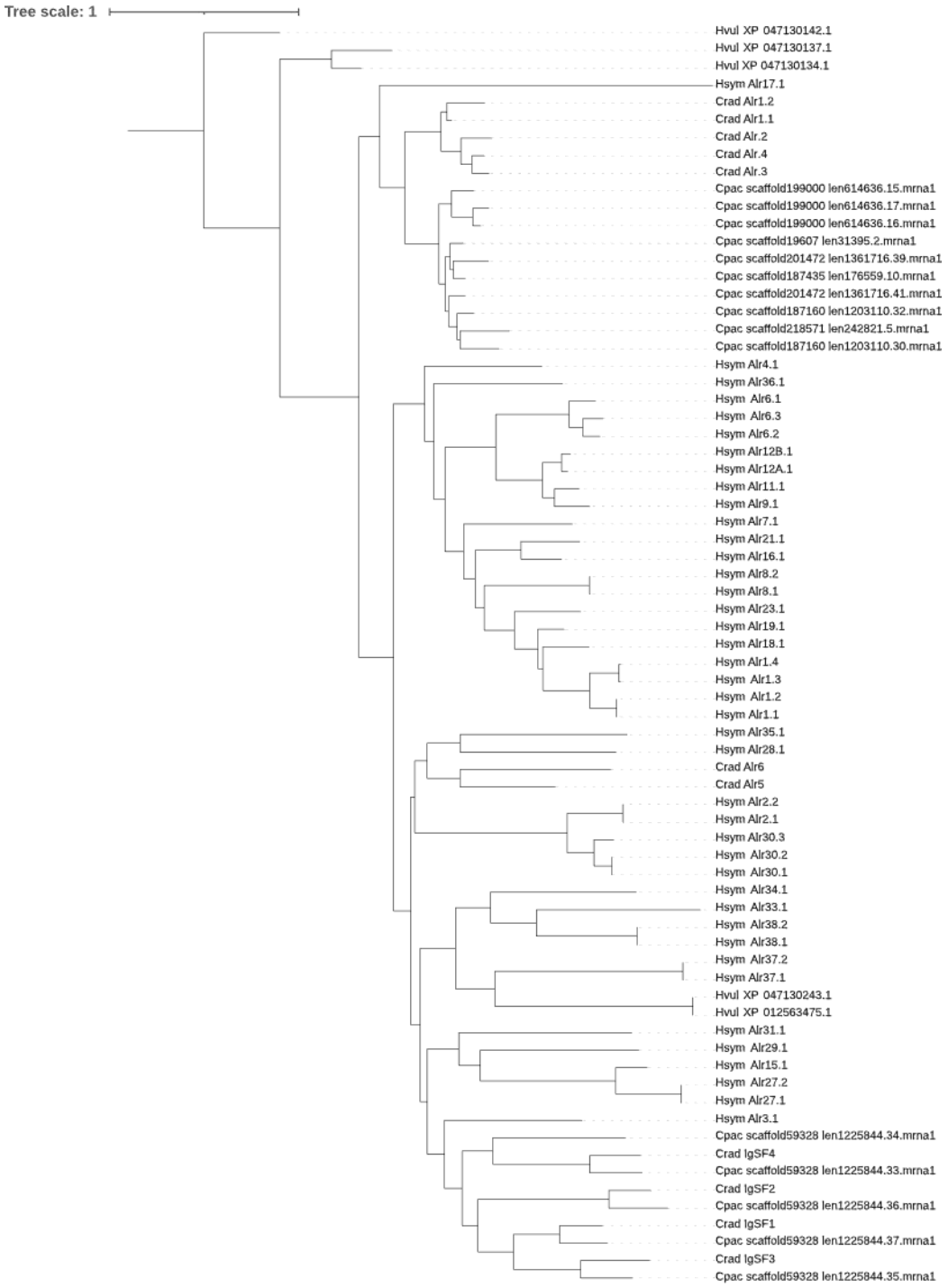

Figure 3.3. Phylogeny of Hydrozoan *Alr*-like genes. Maximum-likelihood probabilities and Bayesian posteriors of the node support below (0.5) are not shown. The values are the likelihoods and posteriors respectively. Hvul: *Hydra vulgaris*.

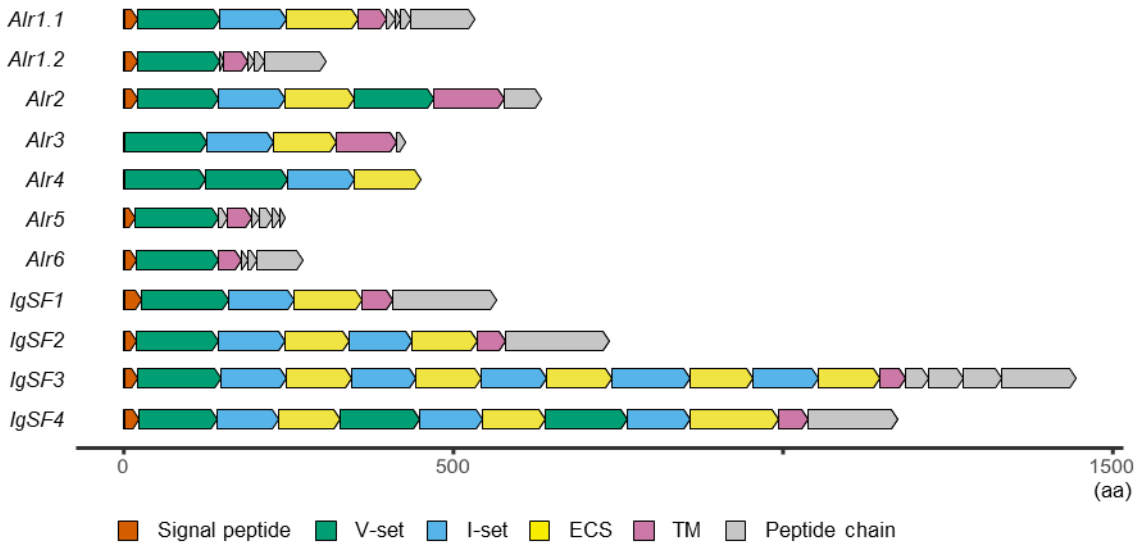

Figure 3.4. Domain architecture of *Alr* and *IgSF* proteins..

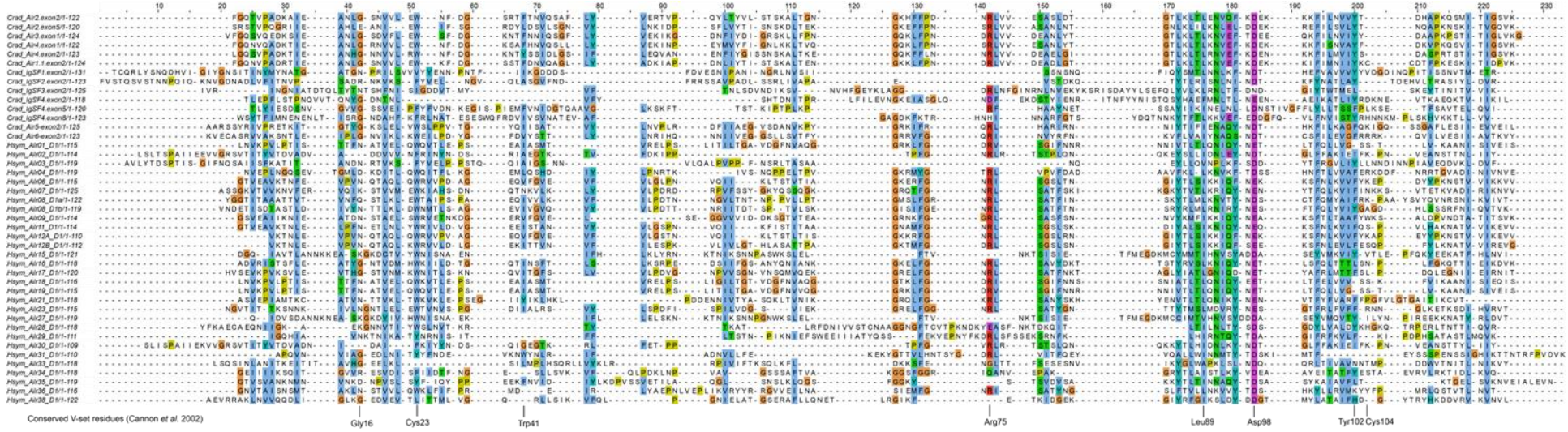

Figure 3.5. Multiple sequence alignment of V-set Ig domains of *H. symbiolongicarpus* and *C. radiatum* Alr-like gene V-set domains. Alr sequences V-set Ig domains from pfam. Conserved V-set residues (Cannon et al., 2002) are shown below the alignment. Residues are highlighted by sequence conservation and chemical property with CLUSTALX colors as implemented in Jalview.

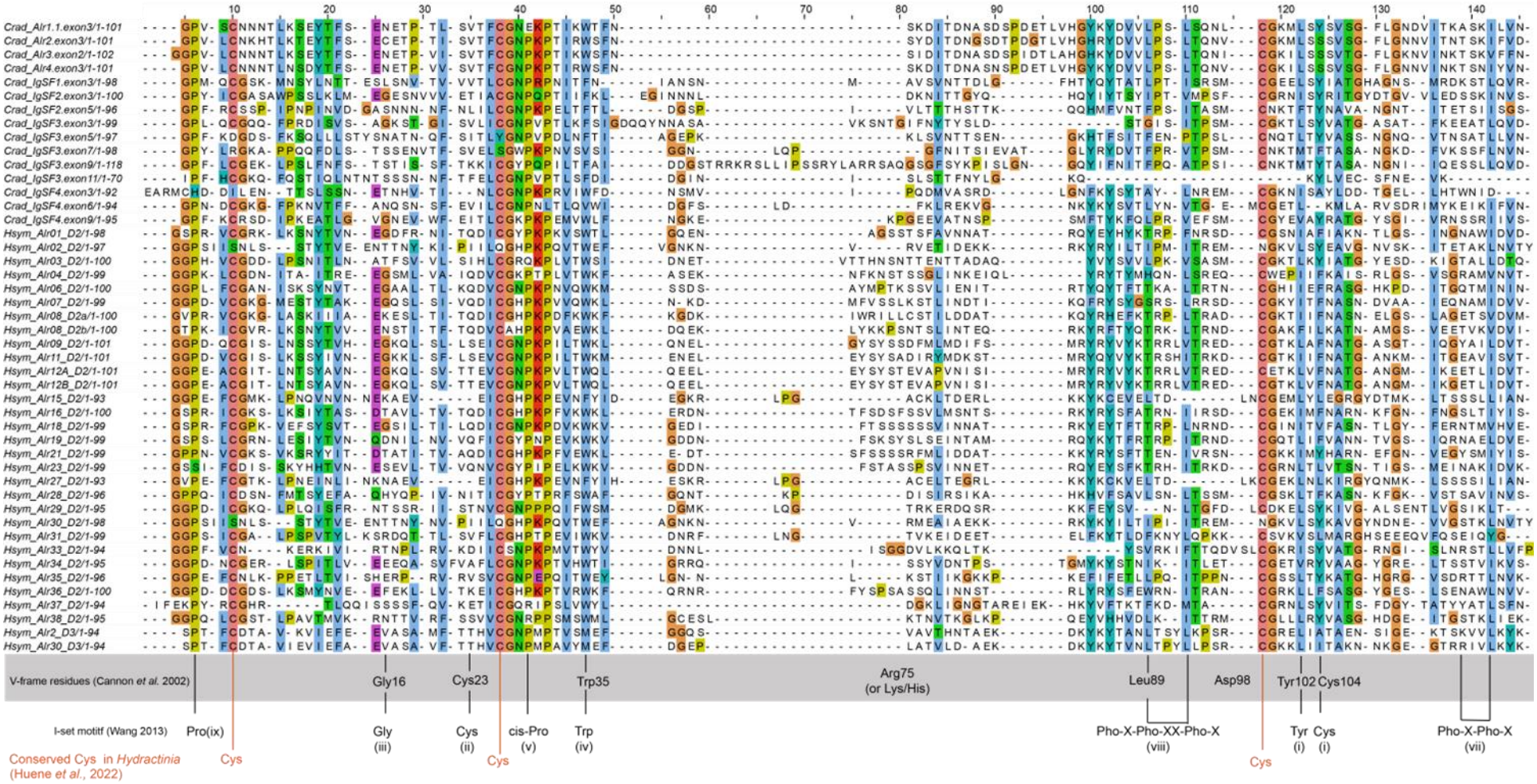

Figure 3.6. Multiple sequence alignment of I-set Ig domains. Alr I-set sequences I-set from pfam. Conserved V-set residues (Cannon et al., 2002; Wang, 2013) and conserved cysteine residues in *Hydractinia* Alr (Huene et al., 2022) are indicated below the alignment. Residues are highlighted by sequence conservation and chemical property with CLUSTALX colors as implemented in Jalview.

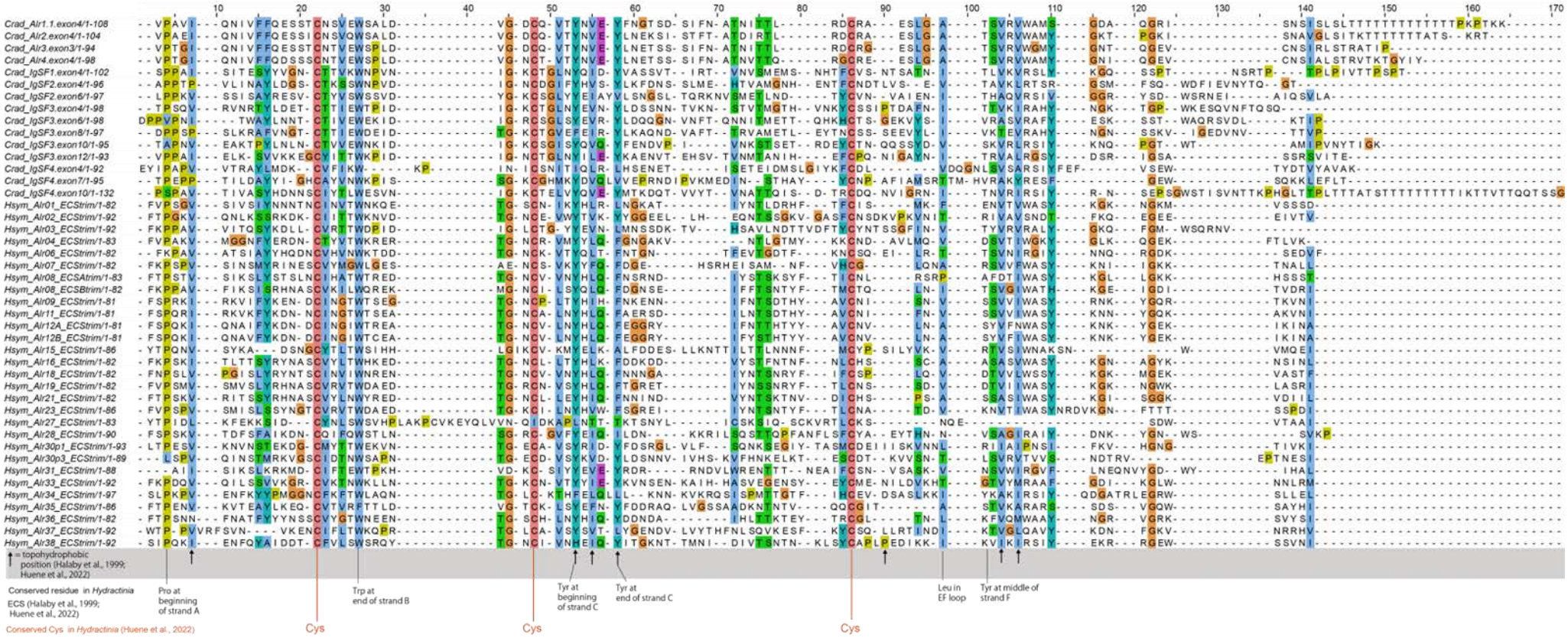

Figure 3.7. Multiple sequence alignment of ECS domains. Alr ECS domain sequences from pfam. Conserved Fn3-like domain residues (with reference to Halaby et al., 1999; Huene et al., 2022) and *Hydractinia*-specific conserved cysteine residues (Huene et al., 2022) are indicated below the alignment. Residues are highlighted by sequence conservation and chemical property with CLUSTALX colors as implemented in Jalview.

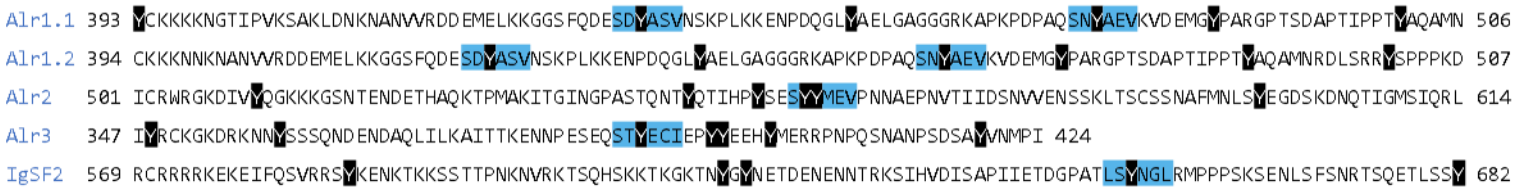

Figure 3.8. ITIMs in Alr-like proteins. Cytoplasmic tails of Alr-like proteins with ITIMs (blue shaded). All tyrosines are shaded in black.

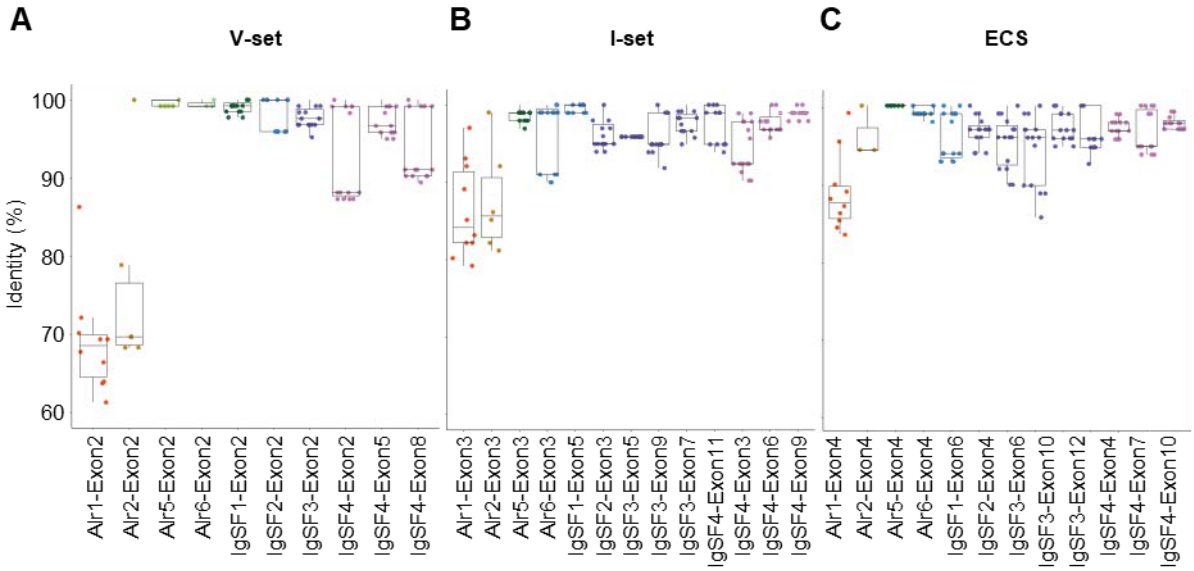

Figure 3.9. High allelic variation of *Alr1* and *Alr2*. Exons coding V-set (A), I-set (B), and ECS (C) domains of all determined haplotypes of *Alr* and *IgSF* genes were compared by pairwise alignment. Identity was calculated with match/alignment length*100. Sequences used in this analysis are shown in Supplemental sequence (exon_separate).

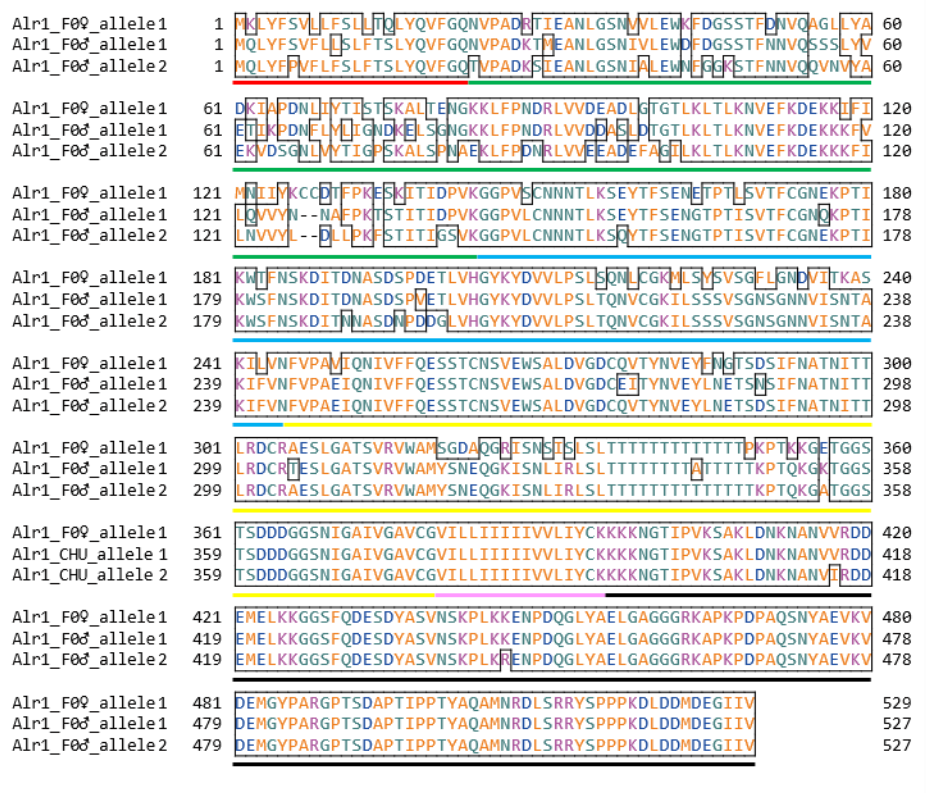

Figure 3.10. Multiple sequence alignment of *Alr1* alleles. CLUSTALX comparison of *Alr1* amino acid sequences *Alr* alleles from F0♀ and F0♂ founder strains. Residues are highlighted by sequence conservation and chemical property with colors as implemented in Jalview. Underlined red: signal peptide, green: V-set Ig, blue: I-set Ig, yellow: ECS (extracellular spacer), purple: transmembrane, black: cytoplasmic tail

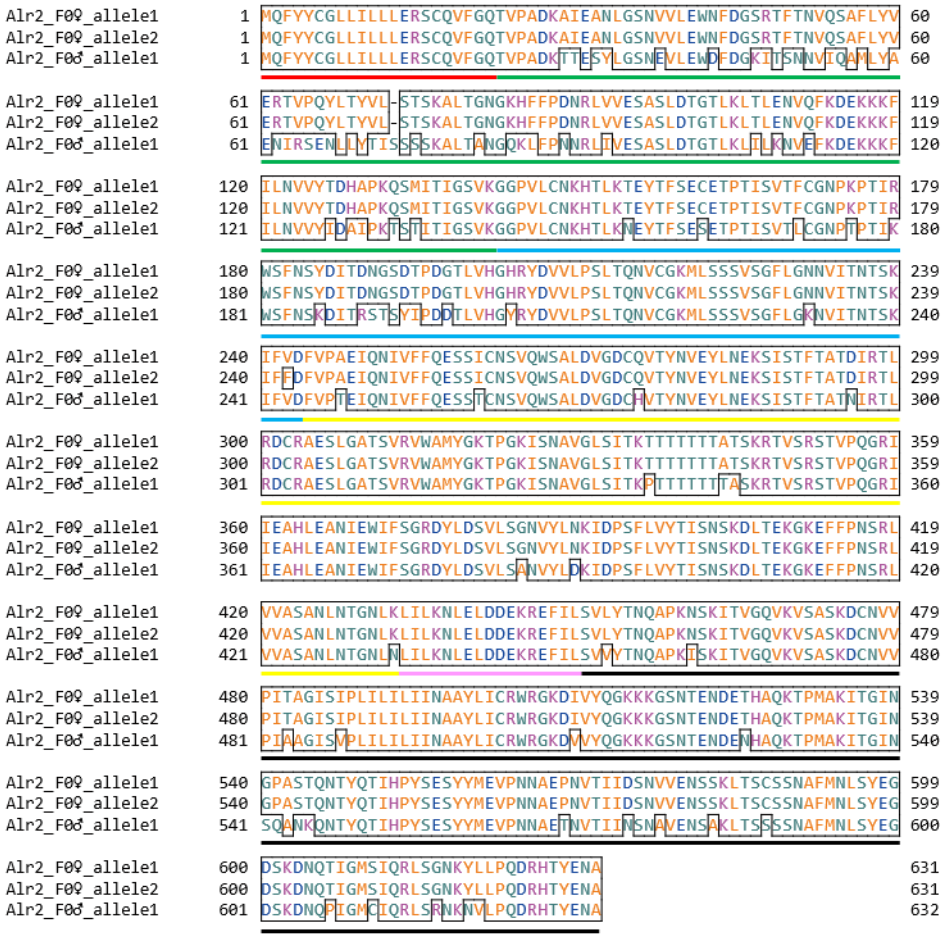

Figure 3.11. Multiple sequence alignment of *Alr2* alleles. CLUSTALX comparison of *Alr2* amino acid sequences *Alr* alleles from F0♀ and F0♂ founder strains. Residues are highlighted by sequence conservation and chemical property with colors as implemented in Jalview. Underlined red: signal peptide, green: V-set Ig, blue: I-set Ig, yellow: ECS (extracellular spacer), purple: transmembrane, black: cytoplasmic tail

Figure 3.12. Multiple sequence alignment of *IgSF2* alleles. CLUSTALX comparison of *IgSF2* amino acid sequences *A/r* alleles from F0♀ and F0♂ founder strains. Residues are highlighted by sequence conservation and chemical property with colors as implemented in Jalview. Underlined red: signal peptide, green: V-set Ig, blue: I-set Ig, yellow: ECS (extracellular spacer), purple: transmembrane, black: cytoplasmic tail

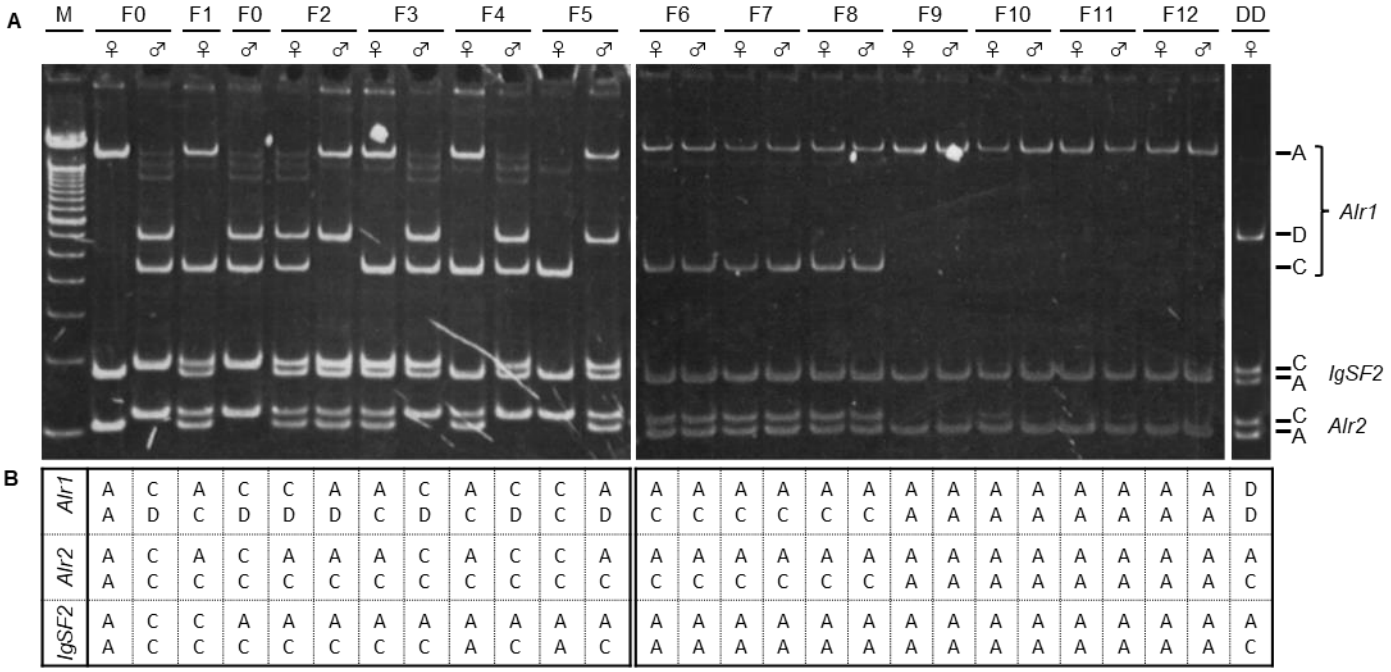

Figure 3.13. Genotyping analysis of Alr1, Alr2 and IgSF2. (A) Electrophoresis profile. For genotyping multiple PCR using primer sets for Alr1, Alr2 and IgSF2 listed in Table S1 and unanalyzed Polyacrylamide gel electrophoresis. M: Maker (100-bp ladder Invitrogen 15628019) **(B)** Genotypes identified.

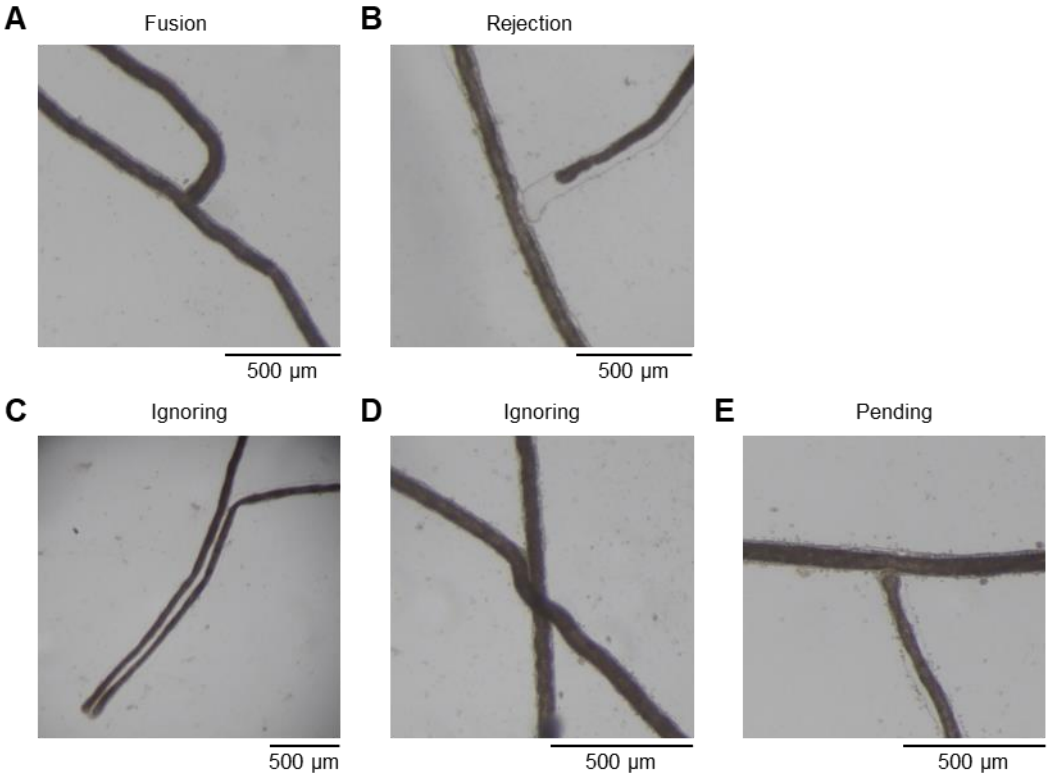

Figure 3.14. Photos demonstrating typical allorecognition outcomes. (A) Duplicate of Figure1A. "fusion" between F1 ♀ (attacking) and F5 ♀ (defending). (B) Duplicate of Figure 1B. "Rejection" between F7 ♀ (attacking) and "DD" (defending). (C) "Ignoring" (attacking stolon changed growing direction) between F3 ♂ (attacking; lower) and F0 ♀ (defending; upper). (D) "Ignoring" (attacking stolon grow across the defending stolon) between F0 ♀ (attacking) and "DD" (defending). (E) "Pending" (stolons stay in contact without connection of gastrovascular canals or stolon regression) between "DD" (attacking) and F0 ♀ (defending).

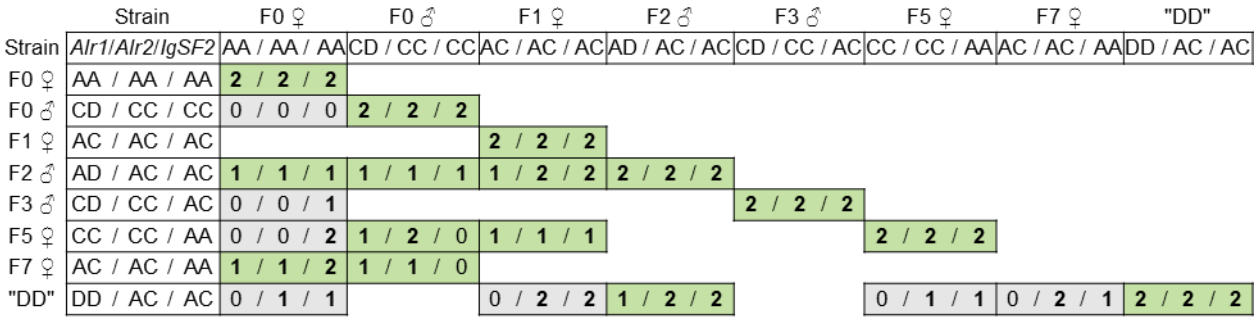

Strain	Strain	F0 ♀	F0 ♂	F1 ♀	F2 ♂	F3 ♂	F5 ♀	F7 ♀	"DD"
	Alr1/*Alr2*/*IgSF2*	AA / AA / AA	CD / CC / CC	AC / AC / AC	AD / AC / AC	CD / CC / AC	CC / CC / AA	AC / AC / AA	DD / AC / AC
F0 ♀	AA / AA / AA	**2 / 2 / 2**							
F0 ♂	CD / CC / CC	0 / 0 / 0	**2 / 2 / 2**						
F1 ♀	AC / AC / AC			**2 / 2 / 2**					
F2 ♂	AD / AC / AC	**1 / 1 / 1**	**1 / 1 / 1**	**1 / 2 / 2**	**2 / 2 / 2**				
F3 ♂	CD / CC / AC	0 / 0 / **1**				**2 / 2 / 2**			
F5 ♀	CC / CC / AA	0 / 0 / **2**	**1 / 2** / 0	**1 / 1 / 1**			**2 / 2 / 2**		
F7 ♀	AC / AC / AA	**1 / 1 / 2**	**1 / 1** / 0						
"DD"	DD / AC / AC	0 / **1 / 1**		0 / **2 / 2**	**1 / 2 / 2**		0 / **1 / 1**	0 / **2 / 1**	**2 / 2 / 2**

Figure 3.15. *Alr1* genotypes determine allorecognition outcomes in inbred lines stolon encounter assays. Table showing results of stolon encounter assays between the inbred lines. Number of matching alleles of *Alr1*/*Alr2*/*IgSF2* are presented. Number of matching alleles >0 is emphasised by bold font. Combinations resulting in fusion (>50%) are coloured in green and those without fusion (0%) are in grey.

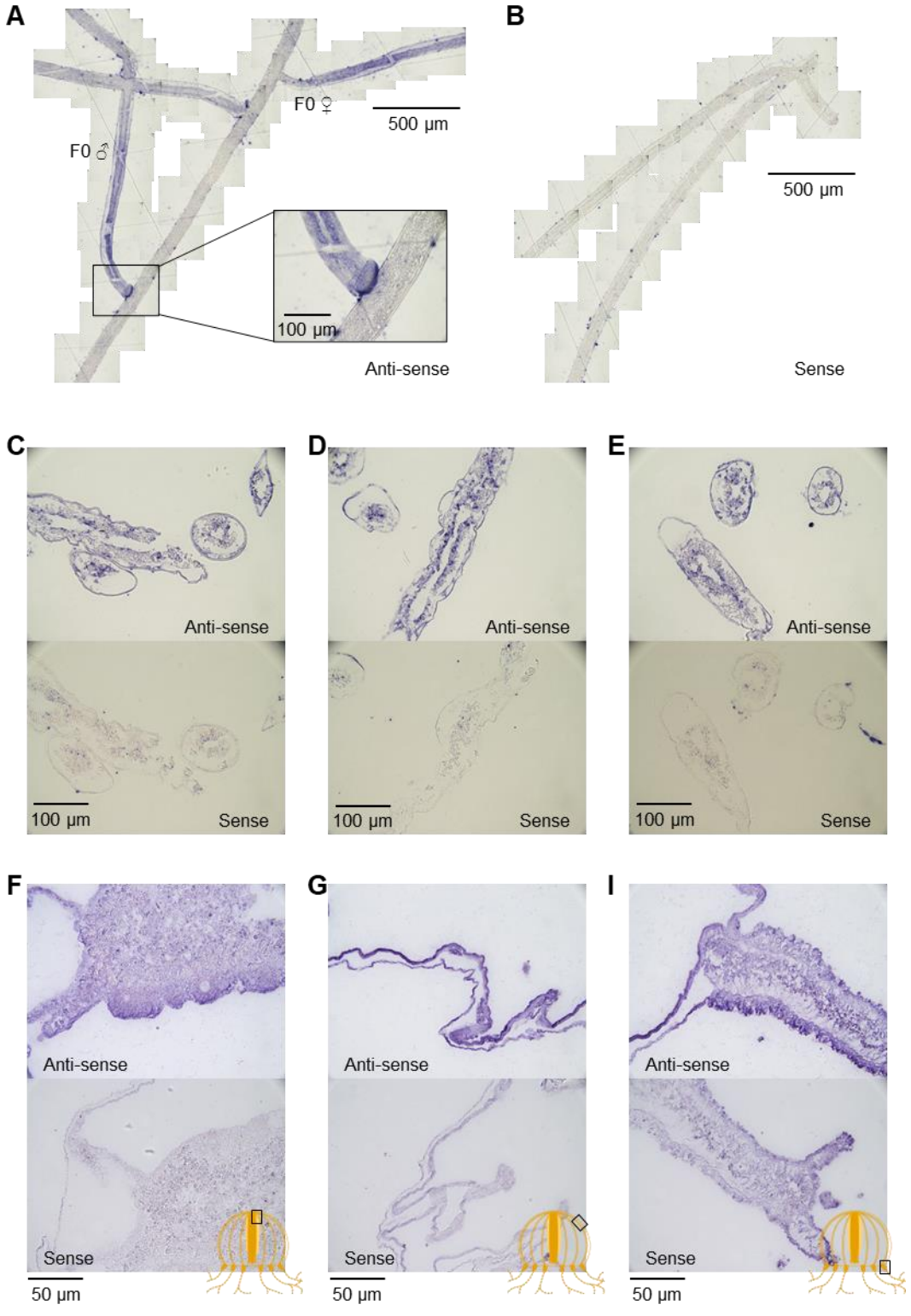

Figure 3.16. *Alr1* expression in *C. radiatum*. (A) Representative image showing in-situ hybridization of *Alr1* in whole-mount incompatible stolon encounters. (B) Negative control with sense probe. (C-E) Representative images showing in-situ hybridization of *Alr1* on stolon cross sections. (F-I) Representative images showing in-situ hybridization of *Alr1* on medusa cross sections. The illustration icons at the lower right corners indicate the approximate positions (black box) of the images.

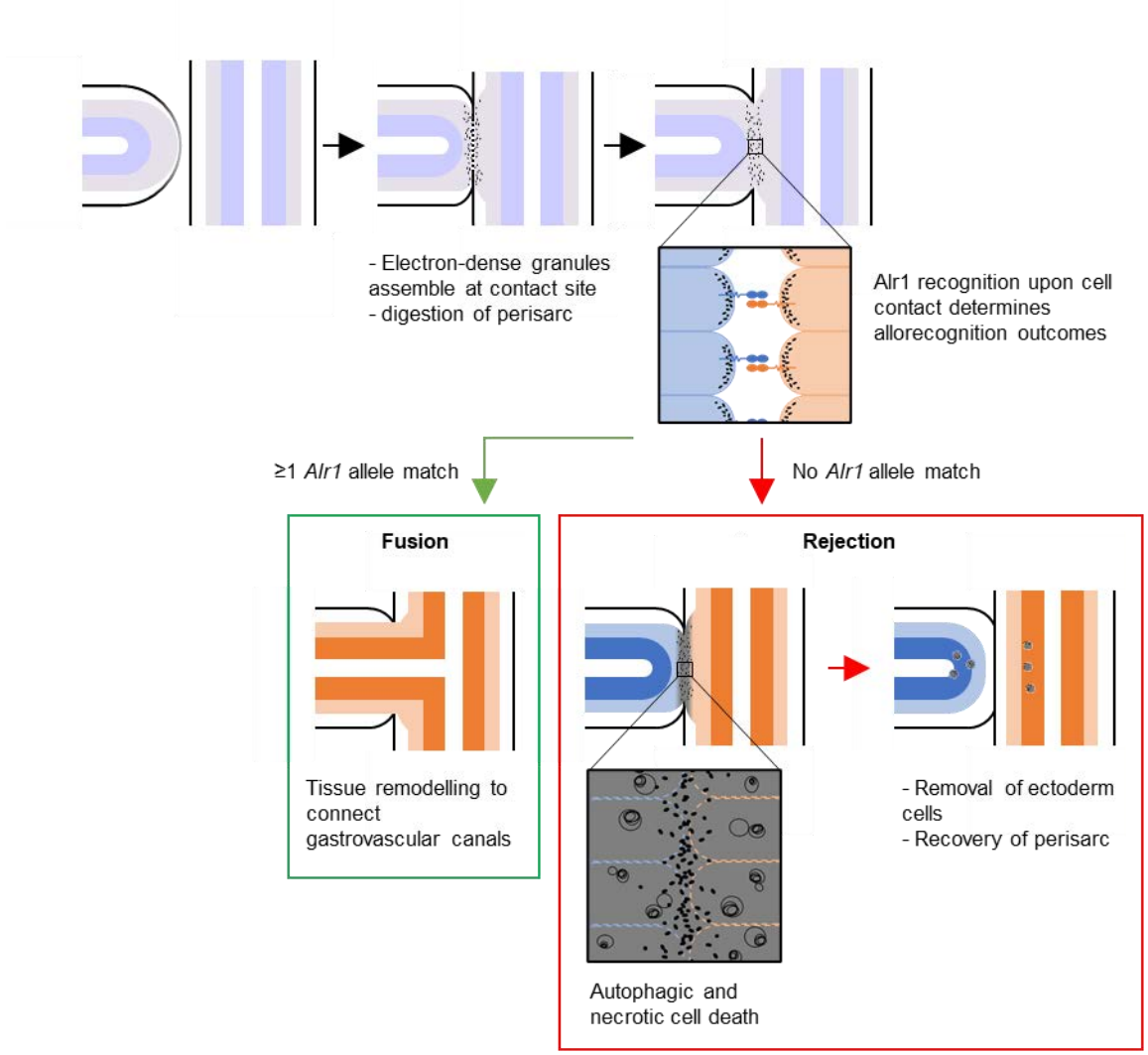

Figure 3.17. Summary of allorecognition responses in *C. radiatum* stolons.

Chapter 4: Allorecognition in *C. radiatum* medusae

TEM observation was performed in collaboration with Dr. Miwa Tamura-Nakano (Research Institute National Center for Global Health and Medicine).

Introduction

Sessile colonies adapt allorecognition to defend against invasion of non-self materials due to the occasional contact with other individuals in the nature. However, as discussed in Chapter 3, allorecognition determinant *Alr1* is expressed not only in stolons and mat tissue, but in all tissue types examined, including eggs, embryos and planula larvae in *Hydractinia* (Nicotra et al., 2009; Rosa et al., 2010). Besides stolons, allorecognition was also examined in polyps. Graft between polyps from colonies that exhibited transitory fusion remained fused throughout the 24-hour assay but ectoderm at the contact zone appeared to be granular (Cadavid et al., 2004). Autophagy was also observed at the contact zone by TEM (Buss et al., 2012).

Apart from *Hydractinia*, allorecognition was also examined in different forms of *Podocoryne* (Tardent & Bührer, 1982). *Podocoryne* is hydroid jellyfish, like *C. radiatum*, having both polyp and medusa stages. Graft between polyps showed allorecognition, by which incompatible polyp graft was resorbed by the host. Such resorption was not observed in compatible grafts. For medusae, manubria were exchanged and grafted onto the umbrella of another individual. Grafting between both compatible and incompatible medusae resulted in healthy chimeras, suggesting *Podocoryne* medusae do not possess allorecognition.

In this study, I detected *Alr1* transcript not only in stolons, but also in medusae in *C. radiatum*. *C. radiatum* also possesses the free-swimming medusa stage, which is capable of sexual reproduction. *C. radiatum* medusa shares typical morphological features with other jellyfish (Figure 4.1). It has a bell-shaped gelatinous umbrella of ~2 mm, with a manubrium

suspended from the centre and tentacles attached to the margin of the umbrella. Manubrium is a stalk-like structure with a mouth (also as anus) for predation and discharge of waste, and a gastrovascular cavity for digestion. Digested nutrients are transferred to other body parts by the gastrovascular canals on the umbrella. *C. radiatum* medusae have separate sexes. Manubria bear gonads that produce either sperm in male or eggs in female. *C. radiatum* produce and release eggs and sperm daily in response to light.

To investigate if *C. radiatum* medusae also possess allorecognition, I performed two graft assays: (1) umbrella-manubrium graft—grafting an exogenous manubrium onto the host umbrella; (2) manubrium half-half graft—grafting two amputated manubria together. In both forms of grafting, grafts remain fused for a prolonged period and shared gastrovascular system, disregarding histocompatibility (determined by *Alr1* genotypes and stolon allorecognition outcomes). In umbrella-manubrium grafts, formation of ring-shaped scars around incompatible manubrium grafts on the umbrella was observed. Progressive tissue overgrowth and excessive formation of gastrovascular canals, with lysosomal vesicles in the ectodermal muscle lining was observed within the scars. While these scars were frequently observed in grafts between wild types, these scars formed only occasionally but not always in grafts between inbred lines without *Alr1* allele match. The Alr-dependent allorecognition is either very weak in medusa or the ring-shaped scars might not be a direct consequence of allorecognition. Autophagy was also observed in the ectodermal gonad cells at the contact region in the manubrium half-half grafts. But the autophagy was likely to be a part of the gametogenesis processes. Overall, *C. radiatum* medusae do not have effective allorecognition as the stolons.

Results

C. radiatum medusae tolerated chimera formation

To investigate if *C. radiatum* medusae exhibit allorecognition, I performed umbrella-manubrium graft in which manubrium of an individual was transplanted onto the umbrella of another individual, producing a jellyfish with both its own manubrium and the graft manubrium (Figure 4.2A). Grafts between both compatible and incompatible individuals (compatibility is defined by the allorecognition outcomes in stolon encounters) produced stable chimeras that both manubria remained attached to the umbrella and were functional, i.e. could feed and spawn, over a long period of time (longest period observed was 2 months, which is comparable to the average lifespan of *C. radiatum* medusae). There was no observable difference in the health conditions between compatible and incompatible grafts. While obvious rejection was not observed, circular scars (hereinafter referred to as ring-shaped scars) with extensive gastrovascular canals formed around where the graft manubria were attached on the host umbrella (Figure 4.2B-C). Size and degree of tissue overgrowth varied between individuals.

For both compatible and incompatible grafts, graft manubria retained the ability of feeding and remained healthy over a long period of time. New gastrovascular canals connecting the graft manubria to the nearby radial canals on the host umbrella were always observed (Figure 4.3A). To inspect if material transport occurred between the graft manubrial and the hosts, only the host manubrium was fed with DiI-stained brine shrimp and transport of fluorescent materials was observed five hours after feeding (Figure 4.3B-D). Fluorescence was diffused in both host and graft manubrial (Figure 4.3B). Magnified microscopic observation showed travelling of fluorescent materials across the gastrovascular canals connecting the host and the graft (Figure 4.3C-D). Regardless of histocompatibility,

gastrovascular systems of hosts and grafts connected and allowed transfer of materials, enabling the graft manubria to function like the host ones.

Hyperplasia and tissue overgrowth at ring-shaped scars in incompatible grafts

Formation of ring-shaped scars was observed only in the incompatible grafts, being a potential indicator of allorecognition. Further morphological observation was performed to examine the nature of the ring-shaped scars. DAPI staining showed that ring-shaped scars have increased cell density, suggesting scar formation might be a result of hyperplasia (Figure 4.4A). High magnification of the ring-shaped scar showed that the scar was not canal but an assembly of disorganised cells, with incorporation of some pigments. Observation of incompatible grafts over a three-week period revealed that ring-shaped scars expanded in size and became more obvious with extensive formation of gastrovascular networks within the scars (Figure 4.4B,C). These newly formed tissues, especially those close to the graft, thickened over time and were pigmented, like the manubrium tissue. The growth of these tissues usually stopped at the ring-shaped scars, forming a circular pattern around the graft.

Cell death in both compatible and incompatible grafts

Umbrella-manubrium grafts were observed under TEM to investigate the cellular morphologies of compatible and incompatible grafts. For identification of morphological changes in the grafts, I first made observations of a normal medusa (Figure 4.5). Manubrium was composed of endodermal gastrovascular cavity, enfolded by the ectodermal gonads attached to the basement membrane (Figure 4.5B). Endoderm has relatively electron-dense cytoplasm with large lipid droplets and lysosomes with crystal structures, like that in stolons. Ectodermal cell layer extended from the gonads on the umbrella beyond the width of the manubrium. Lysosomal vesicles were present at the peripheral cells, which might be part of

the gametogenesis processes. The ectodermal cells were replaced by aligned striated muscles in other parts of the umbrella away from the manubrium (Figure 4.5C).

In compatible grafts, uniform adhesion of graft manubria onto the host umbrella was observed around the gastrovascular cavity (Figure 4.6B,C&D). However, in the areas with contact between the graft gonads and the host umbrella, large lysosomal vesicles were observed (Figure 4.6F-H). Lysosomal vesicles in the graft gonad cells might be of the same source as those observed in the typical gonads (Figure 4.5B). However, lysosomal vesicles and disturbed membrane structures were also present in the host umbrella muscle cells (Figure 4.6H). These structures were observed 2 weeks after graft, so were unlikely to be due to wounding introduced during grafting.

In incompatible grafts, graft manubrium also showed smooth adhesion to the host umbrella (Figure 4.7B,H&I). Ectodermal cell layer also extended on the umbrella as in compatible grafts. Apoptotic cells were observed at the periphery, which might be the source of the lysosomal vesicles observed in the gonads (Figure 4.7C). Protrusions, presumably part of the ring-shaped scar, on the inner side of umbrella near the graft were observed (Figure 4.7D). Protrusions were composed of deformed muscle cells with large lysosomal vesicles (Figure 4.7E,F). The thickening of the tissue might be a result of swelling of the muscle cell layer. These adjacent swelling muscle cells might explain why ring-shaped scars appeared "double-lined". Protrusions with closely adjacent endodermal luminal structures were also observed near the graft manubrium, showing the newly formed gastrovascular canals (Figure 4.7G,J&K). Large lysosomal vesicles were also present in the muscle cell layer (Figure 4.7K).

Overall, lysosomal vesicles were observed in both compatible and incompatible graft, which might not be related to allorecognition. However, protrusions in the muscle cell layer and formation of additional gastrovascular canals were only observed in incompatible grafts,

defining the cellular morphology of the ring-shaped scars.

Autophagy inhibitor suppressed tissue overgrowth inside ring-shaped scars

Lysosomal vesicles were commonly observed in the grafts, at the contact region between the graft gonadal cells and the graft umbrella, and also in the deformed muscle cells. Accumulation of lysosomal vesicles is a common feature of programmed cell death, including autophagy. To see if these lysosomal vesicles were associated with autophagy, I test the effect of 3-Methyladenine (3-MA) on the incompatible grafts. 3-MA is an inhibitor of class III phosphoinositide 3-kinase (PI3K) and is a widely used inhibitor of autophagy. 3-MA was applied to the grafts since the day of grafting. While ring-shaped scars were formed on both control (Figure 4.8A,B) and 3-MA treated grafts (Figure 4.8C,D), 3-MA treated grafts had significantly less tissue growth inside the ring-shaped scars compared to that in the control grafts. Thickening of radial canals near the grafts was observed but there was almost no new gastrovascular canals or new tissue generated. This suggested the association of autophagy, or PI3K, with the tissue overgrowth in ring-shaped scars.

Formation of ring-shaped scars was not a direct consequence of allorecognition

High frequencies of ring-shaped scars were observed in manubrium grafts between genetically distinct incompatible wild types but not in grafts between the same strains (compatible isogenic individuals), suggesting ring-shaped scars might be an indicator of allorecognition. Allorecognition in stolons is entirely genetically determined. To investigate the relationship between ring-shaped rings and allorecognition, umbrella-manubrium graft assays were performed in the inbred lines (Table 4.1). Surprisingly, while ring-shaped scars were only observed in grafts without Alr1 allele match, i.e. incompatible in stolon encounters, they were not always formed in these grafts. In some combinations, e.g. F0 ♀

and F3 ♂, F0 ♀ and F5 ♀, only small scars were formed in low rates (>10%). The low scar formation rates were also not correlated with the genotypes of Alr2 or IgSF2. Sex also did not affect the scar formation rates.

While the formation of ring-shaped scars was not decided by *Alr* genes, it was likely to be, at least partially, genetically dependent. Ring-shaped scars were formed in high rates in grafts between the genetically distinct wild types, but they were not observed in the grafts between the wild types and the F1 individuals, showing the shared genetics might suppress the scar formation.

However, formation of ring-shaped scars was probably not completely determined by genetics. Conditions of ring-shaped scars, e.g. formation, size, varied when just host and donor were reversed. In several combinations (F0 ♀ and F0 ♂, F0 ♀ and F2 ♀, F0 ♀ and F4 ♂), ring-shaped scars were only stably formed in specific host-donor combinations but not the vice-versa. Note that sample numbers in some combinations might be too small to be representative. However, in the combinations between the wild types, clear tendency of formation of larger scars and more tissue growth was observed in the "host: F0 ♀, donor: F0 ♂" combination. This tendency suggested there might possibly be hierarchy in the genetic determination of ring-shaped scar formation.

To see if formation of ring-shaped scars occurred in genetically distinct individuals or was only limited to F0 ♀ and F0 ♂ (GNW and Chu), graft assays were also conducted with the additional wild type OGW (Table 4.2). Similar to that in the GNW-Chu inbred lines, grafts between OGW isogenic individuals did not cause scar formation. Grafts between OGW and the other two wild types occasionally had scars formed, with high formation rates only when OGW being the hosts.

Table 4.1. Ring-shaped scar formation in inbred line umbrella-manubrium grafting assays. Successful: individuals with graft manubria remaining attached 1 week post graft.

		Genotype										
Host	Donor	*Alr1*		Match	*Alr2*		Match	*IgSF2*		Match	Total	Successful	Scar
F0 ♀	F0 ♀	AA	AA	2	AA	AA	2	AA	AA	2	4	4	0
F0 ♂	F0 ♂	CD	CD	2	CC	CC	2	CC	CC	2	12	11	0
F0 ♀	F1 ♀	AB	AC	1	AA	AC	1	AA	AC	1	8	8	0
F1 ♀	F0 ♀	AC	AA	1	AC	AA	1	AC	AA	1	8	7	0
F0 ♂	F1 ♀	CD	AC	1	CD	AC	1	CD	AC	1	4	3	0
F9 ♂	F8 ♀	AA	AC	1	AA	AC	1	AA	AC	1	4	2	0
F0 ♀	F0 ♂	AA	CD	0	AA	CC	0	AA	CC	0	20	18	18
F0 ♂	F0 ♀	CD	AA	0	CC	AA	0	CC	AA	0	16	16	10
F0 ♀	F2 ♀	AA	CD	0	AA	AC	1	AA	AC	1	12	11	2
F2 ♀	F0 ♀	CD	AA	0	AC	AA	1	AC	AA	1	8	5	4
F0 ♀	F3 ♂	AA	CD	0	AA	CC	0	AA	AC	1	12	12	1
F0 ♀	F4 ♂	AA	CD	0	AA	CC	0	AA	AC	1	20	17	4
F4 ♂	F0 ♀	CD	AA	0	CC	AA	0	AC	AA	1	4	4	3
F0 ♀	F5 ♀	AA	CC	0	AA	CC	0	AA	AA	2	20	20	3
F5 ♀	F0 ♀	CC	AA	0	CC	AA	0	AA	AA	2	4	1	0
F0 ♂	F9 ♂	CD	AA	0	CC	AA	0	CC	AA	0	4	1	1
F9 ♂	F0 ♂	AA	CD	0	AA	CC	0	AA	CC	0	4	4	4
F5 ♀	DD	CC	DD	0	CC	AC	1	AA	AC	1	8	6	1
DD	F5 ♀	DD	CC	0	AC	CC	1	AC	AA	1	8	7	1

Table 4.2. Ring-shaped scar formation in umbrella-manubrium grafting assays with an additional wild type.

		Genotype					
Host	Donor	*Alr1*		Match	Total	Successful	Scar
OGW	OGW	EF	EF	2	4	3	0
F0 ♀	OGW	AA	EF	0	4	4	0
OGW	F0 ♀	EF	AA	0	4	3	3
F0 ♂	OGW	CD	EF	0	4	3	1
OGW	F0 ♂	EF	CD	0	4	3	3

No ring-shaped scar formation in interspecific grafts

Ring-shaped scar formation was likely to be induced by grafting between genetically distinct individuals instead of allorecognition. In this sense, grafting between different species might also cause the scar formation. To test this hypothesis, grafting was performed

between *C. radiatum* wild types (F0 ♀/ F0 ♂) and the close relative species *C. pacificum* (B4-1 ♀/ B3-9 ♂). Successful rates were noticeably low (Table 4.3) compared to that between *C. radiatum*, probably due to the differences between body sizes of the two species (*C. pacificum* were larger). *C. pacificum* were also relatively active and sensitive to light, increasing the difficulty in grafting. In the successful grafts, no ring-shaped scar was formed (Figure 4.9). While the grafts were always in contact with at least one of the host radial canals, there was no sign of formation of new canals. The top parts of the graft manubria were smooth without extension. Connection of gastrovascular canals and material transfer between the hosts and the grafts were not validated. The small contact area also explained the high separation rates of the host and the graft manubria. Interspecific grafting did not cause the formation of ring-shaped scars, suggesting the factor(s) inducing scar formation is/are species-specific.

Table 4.3. Umbrella-manubrium grafting assays between *C. radiatum* and *C. pacificum*.

Host	Donor	Total	Successful	Scar
C. radiatum F0 GNW ♀	*C. pacificum* B4-1 ♀	16	1	0
C. pacificum B4-1 ♀	*C. radiatum* F0 GNW ♀	16	2	0
C. radiatum F0 Chu ♂	*C. pacificum* B3-9 ♂	16	10	0
C. pacificum B3-9 ♂	*C. radiatum* F0 Chu ♂	16	0	0

Manubrium half-half grafting generated stable chimeras with no rejection response

Grafting was also conducted by joining the upper and lower halves of the manubria from two individuals (named manubrium half-half graft) (Figure 4.10A) to see if contact of manubria leads to allorecognition, or extra tissue growth as on the umbrella. Grafting between compatible and incompatible individuals resulted in stable chimeras that showed normal health conditions (could feed and spawn) for prolonged periods (longest observation period was 3 weeks) (Figure 4.10B-F). Grafts between different sexes released both eggs and

sperm, showing gonads remained functional. Graft regions could barely be observed except the differences in the shapes between the female and male gonads (Figure 4.10E,F). Fusion of grafts were rapid. As soon as 1 day post graft, graft regions, especially the endoderm and mesoglea, were already not detectable even in paraffin sections (Figure 4.10G).

Grafts 1 week post graft were scrutinised under TEM to examine the morphologies in compatible and incompatible grafts. Compatible grafts showed smooth fusion even in the ectoderm, though deformed cells with lysosomal vesicles were present on the periphery (Figure 4.11A-D). The lysosomal vesicles contained needle-like crystal structures, which were different from those in the endodermal cells. These lysosomal vesicles and deformed cells were commonly observed on the outer layers of gonads. In incompatible grafts, endoderm and mesoglea exhibited perfect fusion with no distinguishable margin (Figure 4.11F,H,J), while there were gaps remained between the ectodermal gonads. The gaps were filled with lysosome containing deformed cells, resembling those observed on gonad surfaces. The fusion of the ectoderm was likely to be prohibited due to the difference in tissue types and the cell damage/death observed at the ectoderm gaps was probably because these regions were recognised as the peripheries of the gonads. Overall, manubria did not display allorecognition nor abnormal tissue growth upon contact with genetically distinct tissues.

Discussion

C. radiatum medusae showed only weak or no *Alr*-dependent allorecognition

In contrast to the stolons, *C. radiatum* medusae showed tolerance of chimerism between genetically distinct individuals. Chimeric grafts were stably formed with no observable effect on health or functionality, and showed no sign of separation. Indeed, in umbrella-manubrium grafts, expansion of tissues from the grafts on the host umbrella

proceeded with time, securing the connection between the host and the graft manubria. In manubrium half-half grafts, grafts were attached together with perfectly fused mesoglea and endoderm. The results were in line with the previous observation in *Podocoryne* (Tardent & Bührer, 1982), showing tolerance of chimerism in medusae.

The absence of allorecognition in medusae is logically expectable in light of survival benefit. Stolons in sessile colonies are likely to encounter others in the nature, so the decision between fusion and rejection is important in balancing the benefit gained from increasing body size and the risk of germ/somatic cell parasitism. Allorecognition is therefore crucial as a protective mechanism. On the other hand, free-living medusae generally have low chance in contacting, or forming chimeras, with other individuals in the nature. Allorecognition is therefore not retained or not acquired in medusae.

However, while acute rejection response, like detachment of graft, was not observed, ring-shaped scars appeared on host umbrella specifically in genetically distinct grafts. These scars might be a potential sign of response to incompatibility. Ring-shaped scars were only, but not always, formed in grafts between individuals without *Alr1* match. It is uncertain if the formation of ring-shaped scars was partially dependent on *Alr1*, or some of the factors that determined the scar formation coincidently inherited with *Alr1*. Ring-shaped scars were only stably formed in grafts between wild types. Further experiments and genetic analysis were necessary to determine the determinants of scar formation.

While there is no evidence of *Alr*-dependence allorecognition in medusae, transcript expression was detected by both RNA-seq and in-situ hybridisation. Protein expression was not successfully detected (customised antibodies failed to detect *Alr1*). If Alr proteins are expressed and presented on cell surface, it is expectable that recognition by homophilic binding of *Alr* occurs. However, as no consistent phenotype associated with *Alr* genotypes was detected, medusae do not possess effective downstream pathways that lead to the

allorecognition responses in stolons. Absence of mechanisms regulating chitin/perisarc is expected in medusae, as medusae do not have similar chitinous exoskeletons. However, immediate rejection responses—necrotic and autophagic responses observed in stolon epithelial cells in contact with incompatible individuals—were also not detected. It shows that these cell death responses may also be limited to stolon cells. The inconsistent ring-shaped scar formation might be possibly a sign of weak rejection induced by the mismatching of Alr. However further experiment is needed to provide evidence of the dependency.

Conditions of ring-shaped scars formed varied between samples, even they were generated with medusae collected from the same colonies, i.e. genetically identical, at the same time. In my observations, the scars tended to form when the initial contact areas between the host umbrella and graft manubria were large, showing the scar formation might be induced by cellular contact. Furthermore, possible hierarchy was observed in the scar formation, as scars were likely to form or become more obvious when specific strains being the donors. In generally, scars formed when the grafts were from medusae of larger body size. Scars tended to form in grafts between inbred lines when wild types were the donors and larger scars were formed in grafts between the wild types when the F0 ♂ (Chu) were the donors. Wild types were typically larger and healthier than the inbred lines (in terms of lifespan and spawning) and F0 ♂ (Chu) is larger in size than F0 ♀ (GNW). The tendency of scar formation might be a result of genetic hierarchy or the differences in health or physiological conditions of different strains.

Tissue overgrowth in ring-shaped scars resembled neoplasia

Excessive tissue growth extended from the graft manubria were observed inside the ring-shaped scars. Noticeably, increased interconnecting gastrovascular canals were formed. This form of tissue overgrowth from the grafts resembled neoplasia morphologically.

Neoplasia refers to abnormal growth of new tissue, generally contributing to tumour formation. Neoplasia is typically an outcome of accumulative genetic alterations that generate phenotypical effects on the cell differentiation and proliferation. Many of these mutations on their own are neutral or even beneficial, and are therefore inherited through generations (Greaves, 2015; Merlo et al., 2006; Zahir et al., 2020). In the medusa graft, the differences between the genetic profiles of the wild types might have resembled phenotypic effects of accumulation of mutations. The wild types used in this study might have their own formulas in coordinating physiological processes, including development, growth and homeostasis, in their own manners. When tissues of these strains were artificially put together in the graft experiments, the discrepancies caused malfunction in regulating the tissue growth, leading to the neoplasia-like condition.

The abnormal overgrown tissues appeared to be expanded from grafts. However, if the tissues were derived from the invaded graft manubrium cells or the host umbrella cells under the stimuli exerted by the graft was not determined. Though not observed in *C. radiatum*, umbrella of the Hydrozoan jellyfish *Clytia hemisphaerica* (*Clytia*) showed ability of regenerating a full manubrium (Sinigaglia et al., 2020). Removal of manubria in *C. radiatum* leaded to unrepairable injuries and successful healing was not observed before the umbrella weakened due to starvation as they could not feed without the maniubria (own observation). *C. radiatum* might have lower regenerative capacity. However, the manubrium-to-umbrella size ratio is much higher in *C. radiatum* (the diameter of a manubrium is around 1/4 of that of the umbrella), which might also explain the incapability of regeneration. On the other hand, regeneration of umbrella was never observed in disconnected manubria. To investigate if specific cell types or locally expressed molecules in the manubria were required for the scar formation, I tried to graft only the upper or the lower portions of the donor manubria (Figure 4.12). Ring-shaped scars were formed in all samples showing scar

formation was probably not triggered by cells or molecules specific to the top of manubrium, though manubria exhibited rapid reorganisation and regeneration so the amputation might not be meaningful. Further experiments that can identify the source of the newly formed tissues, e.g. grafting using transgenic fluorescent strains, would be helpful in understanding the underlying mechanisms of the tissue overgrowth.

Ring-shaped scars and tissue overgrowth

The ring-shaped scars appeared to be swollen host umbrella muscle cells with lysosomal vesicles. The scars were circular and centred by the contact region with graft manubrium. Therefore, the scars were suspected to form due to the diffusion of some undetermined factors. While gastrovascular canals were extensively formed inside the scars, the scars themselves were not canals. The observation that the overgrowth of tissues stopped at the ring-shaped scars might suggest that the factors caused the scar formation were continually expressed, on the assumption that the same factors caused the tissue overgrowth. It might also be possible that the scars had a limiting effect on the tissue growth.

In *Clytia*, reorganisation of subumbrellar radial muscle layer was observed associated with the regeneration of manubria in medusae with manurbia amputated (Sinigaglia et al., 2020). Disorganization followed by reorganisation of muscle fibres so that they were convergent to the prospective sites of manubrium regeneration occurred prior to the new manubrium regeneration. The additional graft manubria in *C. radiatum* graft experiments might have confused the jellyfish and “mistakenly” activate a similar remodelling/regeneration mechanism. The scars might mark the margin of the areas of muscle reorganisation and the tissue overgrowth might be a product from the attempt to regenerate manubrium. Although connection to neighbouring radial canals was commonly observed in all intraspecfic grafts, aggressive tissue growth was only seen in grafts with ring-

shaped scars. This observation is also in line with the observation in *Clytia* that the reorganisation of muscle was essential to manubrium regeneration. The remodelling and regeneration of *Clytia* medusae were dependent on the Wnt signalling, which is also a potential direction for further investigation.

Large lysosomal vesicles were frequently observed in the ring-shaped scars, there was no clear clue about the source of these structures. Lysosomal vesicles were also observed in the host muscle cells in compatible grafts without ring-shaped scars. Tissue damage might possibly be caused by contact between different tissue types or maybe the extra weight of graft injured the umbrella. Autophagy inhibition by 3-MA treatment suppressed the tissue overgrowth showing the association with autophagy, or PI3K. Autophagy was reported to regulate regeneration and remodelling in various invertebrates (Song et al., 2020; Tettamanti et al., 2009). However, other autophagic features, e.g. phagosomes, autophagosomes, were not observed. 3-MA was also reported to upregulate apoptosis, either by a reduction of autophagy or inhibition of PI3K that suppresses apoptosis (Franke et al., 1997). It was reported in mammals that 3-MA promoted apoptosis and suppressed cell proliferation via the PI3K/AKT pathway (Li et al., 2017). Further analysis of conservation of PI3K/AKT pathway in *C. radiatum* and detection of different types of cell death may provide more information on the relationship between autophagy/cell death and the scar formation.

PI3K/AKT pathway was also reported to regulate Vascular endothelial growth factor C (VEGF-C) expression in lymphangiogenesis in human oral squamous cell carcinoma (Chen et al., 2012). VEGF-C, as suggested by its name, is a proangiogenic factor that frequently associated with tumor angiogenesis and lymphangiogenesis in vertebrates. VEGF protein family is a highly conserved across metazoan and VEGF-C-like protein was identified in *Podocoryne* with a role in tentacle and gastrovascular canal formation (Seipel et al., 2004; Rauniyar, Bokharaie & Jeltsch, 2023). In *C. radiatum*, homolog sequence of VEGF-C-like

protein was also identified by BLAST and VEGF inhibitor PTK787/ZK 222584 (1-[4-chloroanilino]-4-[4-pyridylmethyl] phthalazine succinate) (Wood et al., 2000) was found to suppress radial canal branching (Ohmura, master's thesis), showing vascularisation by VEGF pathway is conserved in *C. radiatum*. The inhibition of VEGF via inhibition of PI3K might also explain the reduction in gastrovascular tissue growth in the ring-shaped scar under 3-MA treatment.

Materials and Methods

Medusa graft assays

Healthy medusae (around 4- to 6-week-old) fed on the day before the experiment day were used in the graft assays. In umbrella-manubrium graft assay, manubria from the donor jellyfish were amputated by cutting open the top of the umbrella. The amputated manubria were inserted into the host jellyfish umbrella and were pinned with thin glass needles, produced by pulling heated glass capillary manually, on 2% agarose/ASW inside 4-well plates (as in Figure 4.2A). Host tentacles were amputated to ease handling. Grafts were unpinned >36 hours after grafting. Excessive feeding was avoided on the first few days after grafting to avoid the two manubria inside the umbrella attacking each other. In manubrium half-half graft assay, manubria were disconnected from the umbrella in the same way as described above and were dissected into half. Upper and lower halves were threaded on a glass needle (produced as described above) and were pressed towards each other by small agarose cubes (as in Figure 4.11A). Material transport in umbrella manubrium was examined by feeding the only one of the manubria (usually the host manubria as their mouth were centred at the opening of the umbrella and were easy to feed) with brine shrimp (*Artemia* nauplii) pre-soaked in DiI (D3911, Invitrogen)/ASW solution for 30 minutes. Grafts were

observed with Axiophot 2 (Zeiss, Germany) 4 hours after feeding. DAPI (4',6-diamidino-2-phenylindole) staining were performed with 4% paraformaldehyde fixed medusae (RT, 30 minutes). Medusae were first relaxed in a 1:1 mixture of 7% (w/v) $MgCl_2 \cdot 6H_2O$ and ASW for 10 minutes before fixation. Fixed medusae were stained with 0.5 µg/ml DAPI/PBS (RT, 10 minutes). Umbrella was cut open to spread flat for observation. Images were obtained with Olympus BX51.

3-MA treatment

3-MA was applied at 3 mM since grafting. Samples were fed daily followed by changed of ASW supplied with freshly thawed 3-MA. 3-MA was dissolved in ASW at 20 mM and stocked as aliquots at -30°C. Frozen stocks were thawed with heating to ensure complete dissolution.

TEM imaging

Samples were prepared as described in Chapter 2, except medusae were relaxed in a 1:1 mixture of 7% (w/v) $MgCl_2 \cdot 6H_2O$ and ASW for 10 minutes before fixation. Semi-thin sections at 1 µm were stained with 0.5 % toluidine blue.

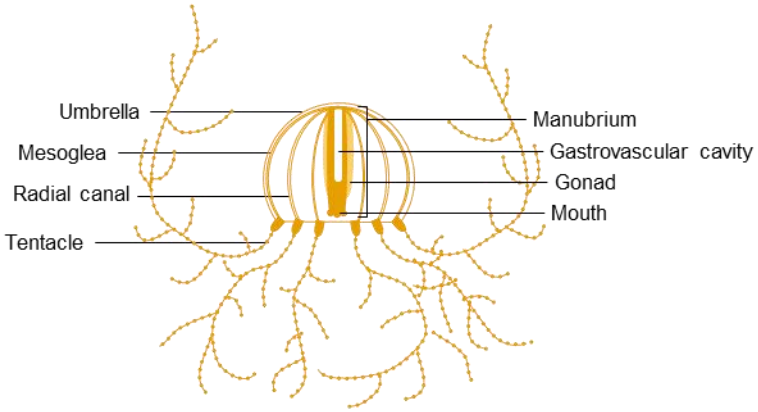

Figure 4.1. Illustration of *C. radiatum* medusa.

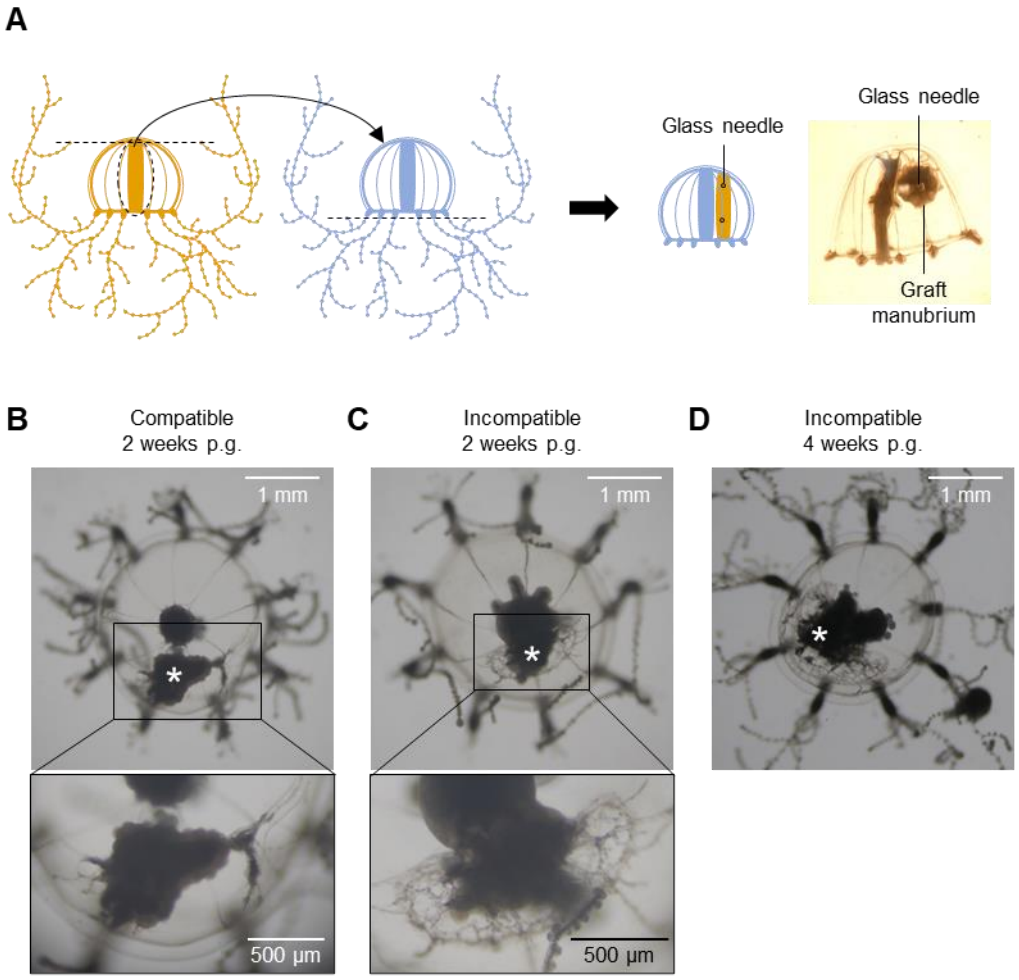

Figure 4.2. Allorecognition in *C. radiatum* medusae. (A) Schematic illustration of umbrella-manubrium grafting experiment. (B) Compatible graft (host: F0 ♀ , donor: F0 ♀) 2 weeks post graft. (C) Incompatible graft (host: F0 ♂, donor: F0 ♀) 2 weeks post graft. (D) Incompatible graft (host: F0 ♀, donor: F0 ♂) 4 weeks post graft. Black arrow: connections of gastrovascular canal extended from graft and host radial canal. Asterisk: graft. p.g.: post graft.

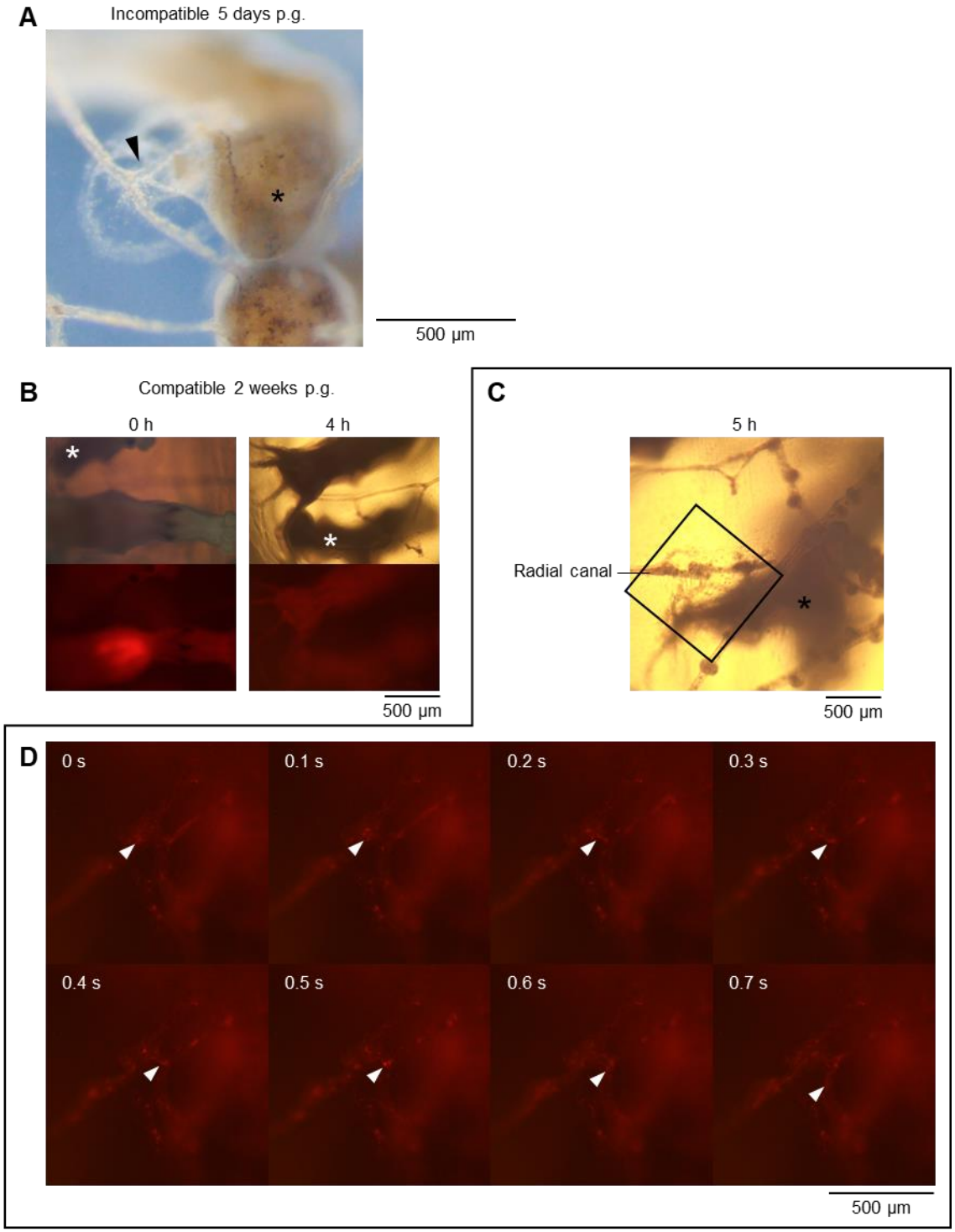

Figure 4.3. Transport of materials between host medusae and graft manubria. (A) Close-up of incompatible graft (host: F0 ♂, donor: F0 ♀) 5 days post graft. Black arrow: connections of gastrovascular canal extended from graft and host radial canal. (B-D) Compatible graft (host: F0 ♀, donor: F0 ♀) with only the host medusa fed with DiI-stained brine shrimp. (C-D) Transport of materials in the gastrovascular system. Area shown in (D) is boxed in (C). White arrows track one of the fluorescent materials in the gastrovascular canal. Asterisk: graft.

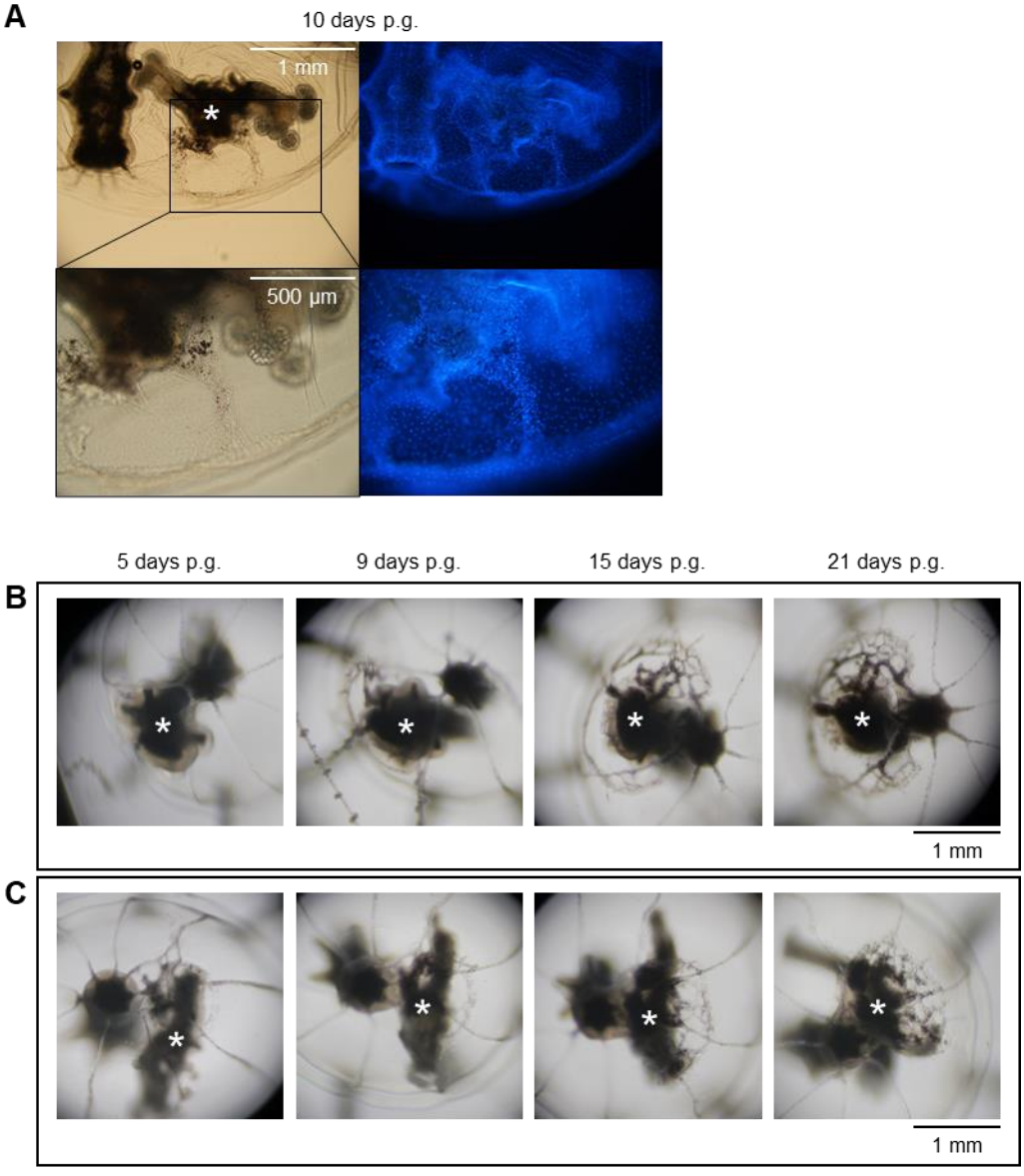

Figure 4.4. Ring-shaped scar formation in incompatible umbrella-manubrium grafts. (A) DAPI staining of ring-shaped scar 10 days post graft (4% paraformaldehyde-fixed). Host: F0 ♀, donor: F0 ♂. (B,C) Representative images showing ring-shaped scar formation over 21 days post graft. A: host: F0 ♀, donor: F0 ♂. B: host: F0 ♂, donor: F0 ♀. Asterisk: graft. p.g.: post graft.

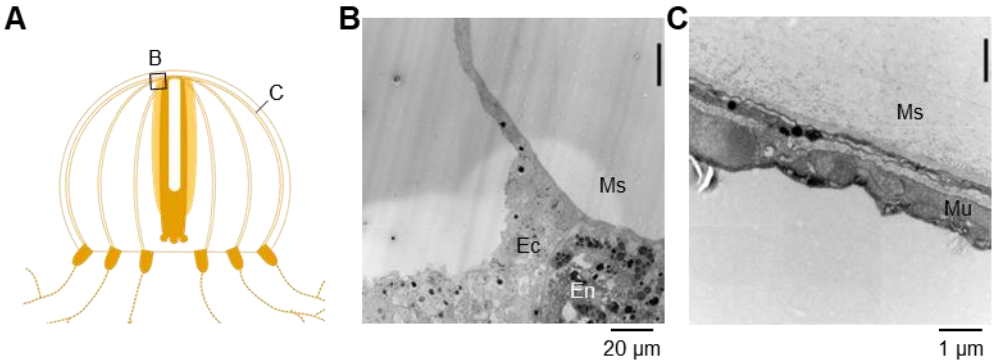

Figure 4.5. TEM observation of *C. radiatum* medusa morphology. (A) Illustration of a medusa showing the approximate position of (B) and (C). (B-C) TEM images of F0 ♀ medusa. (B) Connecting region between umbrella and manubrium. (C) Close-up of umbrella cross-section. Ec: ectoderm; En: endoderm; Ms: mesoglea; Mu: muscle.

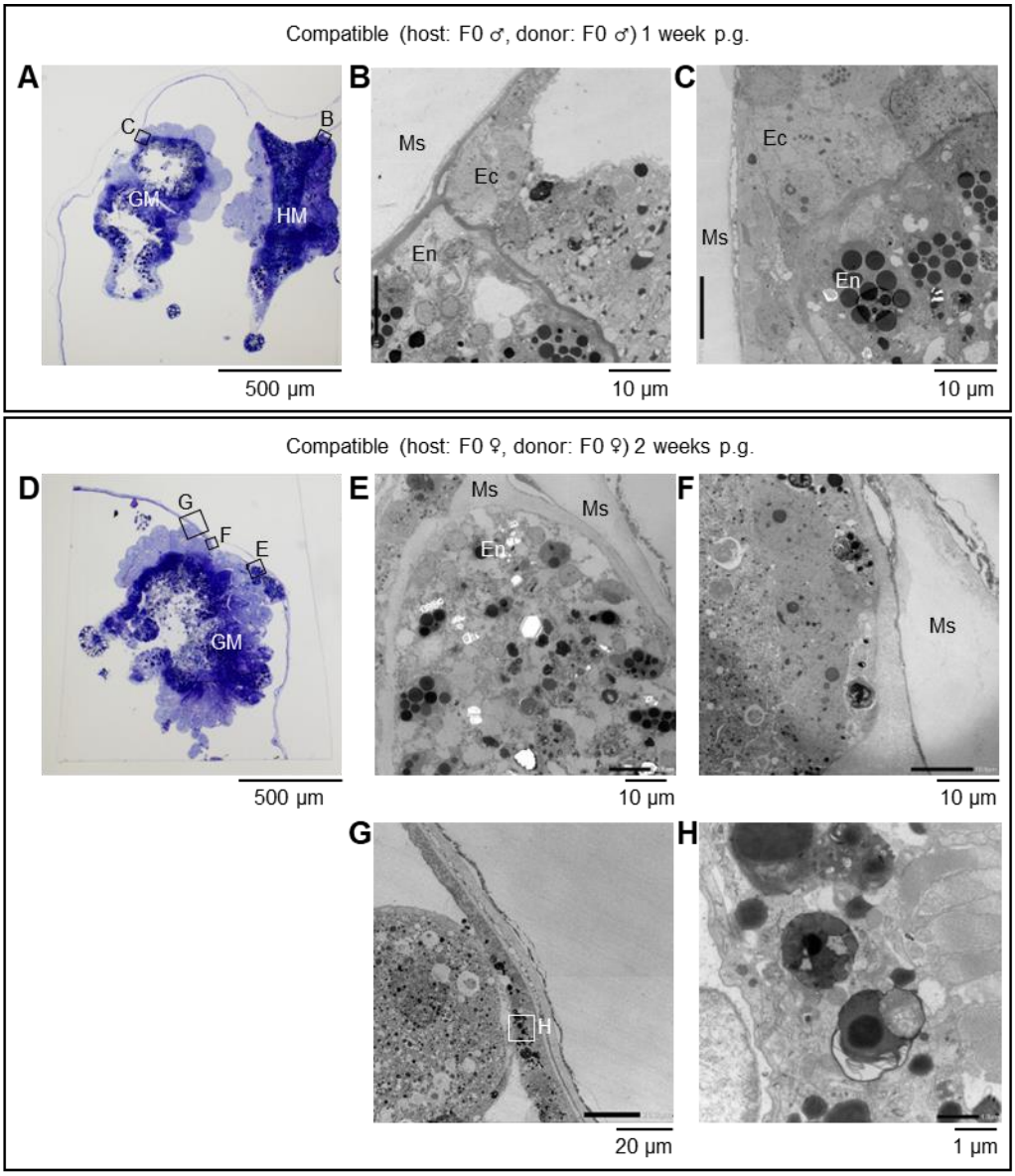

Figure 4.6. TEM observation of compatible umbrella-manubrium grafts. (A-C) Representative images showing TEM observation of compatible manubrium graft (host: F0 ♂, donor: F0 ♂) 1 week post graft. (A) Semi-thin section stained with 0.5 % toluidine blue. Region of host manubrium connecting to the host umbrella is enlarged in (B). Region of graft manubrium connecting to the host umbrella is enlarged in (C). (D-H) Representative images showing TEM observation of compatible manubrium graft (host: F0 ♀, donor: F0 ♀) 2 weeks post graft. (D) Semi-thin section stained with 0.5 % toluidine blue. Regions of graft manubrium connecting to the host umbrella is enlarged in (E-H). HM: host manubrium; GM: graft manubrium.

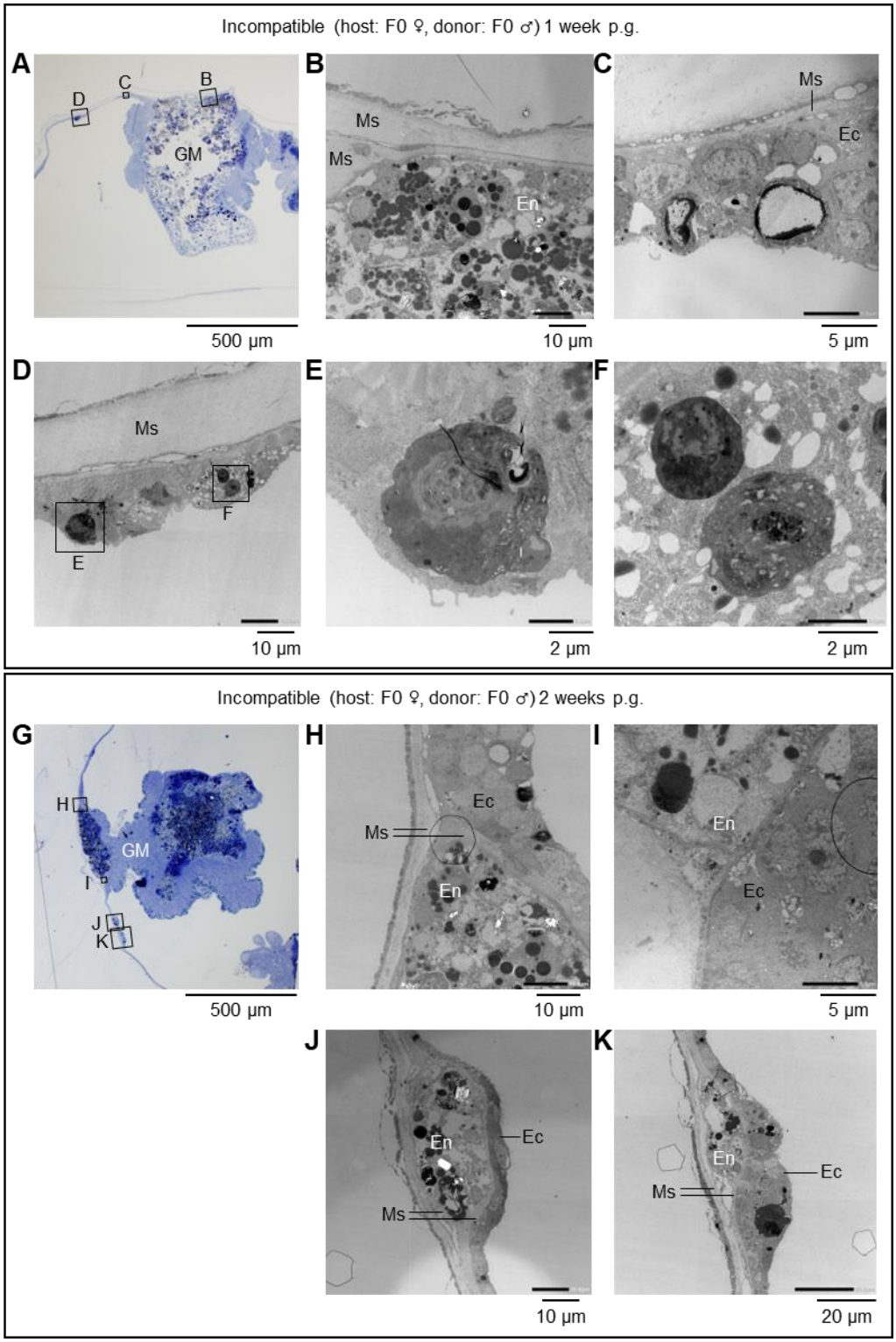

Figure 4.7. TEM observation of incompatible umbrella-manubrium grafts. (A-F) Representative images showing TEM observation of incompatible manubrium graft (host: F0 ♀, donor: F0 ♂) 1 week post graft. (A) Semi-thin section stained with 0.5 % toluidine blue. Region of graft manubrium connecting to the host umbrella is enlarged in (B) and (C). (D-F) Tissue grown on host manubrium. Magnified images of large lysosomes are shown in (E) and (F). (G-K) Representative images showing TEM of incompatible manubrium graft (host: F0 ♀, donor: F0 ♂) 2 weeks post graft. (G) Semi-thin section stained with 0.5 % toluidine blue. (H,I) Region of graft manubrium connecting to the host umbrella. (J,K) Tissue grown on host manubrium.

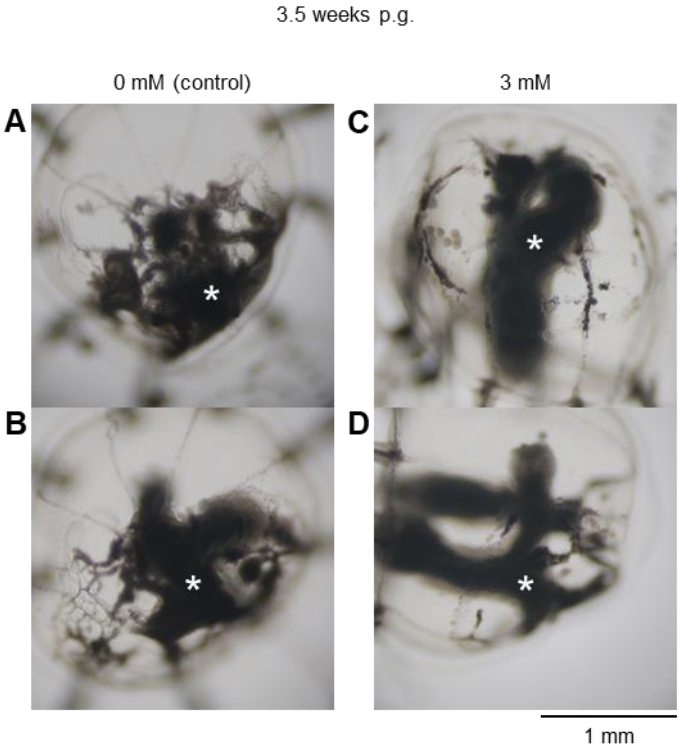

Figure 4.8. 3-MA suppressed tissue overgrowth in ring-shaped scars in incompatible manubrium grafts. (A,B) Representative images showing ring-shaped scar in incompatible graft (host: F0 ♀, donor: F0 ♂) without 3-MA treatment 3.5 weeks post graft. (C,D) Representative images showing ring-shaped scar in incompatible graft (host: F0 ♀, donor: F0 ♂) with 3-mM 3-MA treatment 3.5 weeks post graft.

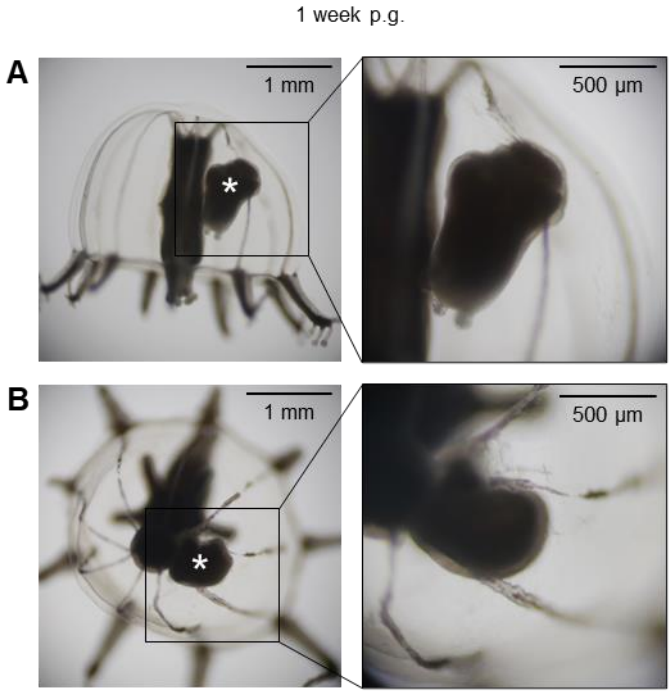

Figure 4.9. No formation of ring-shaped scar in interspecific umbrella-manubrium grafts. (A,B) Representative images showing xenografts 7 days post graft. A: host: *C. radiatum* F0 ♀, donor: *C. pacificum* B4-1 ♀. B: host: *C. radiatum* F0 ♂, donor: *C. pacificum* B3-9 ♂. Asterisk: graft.

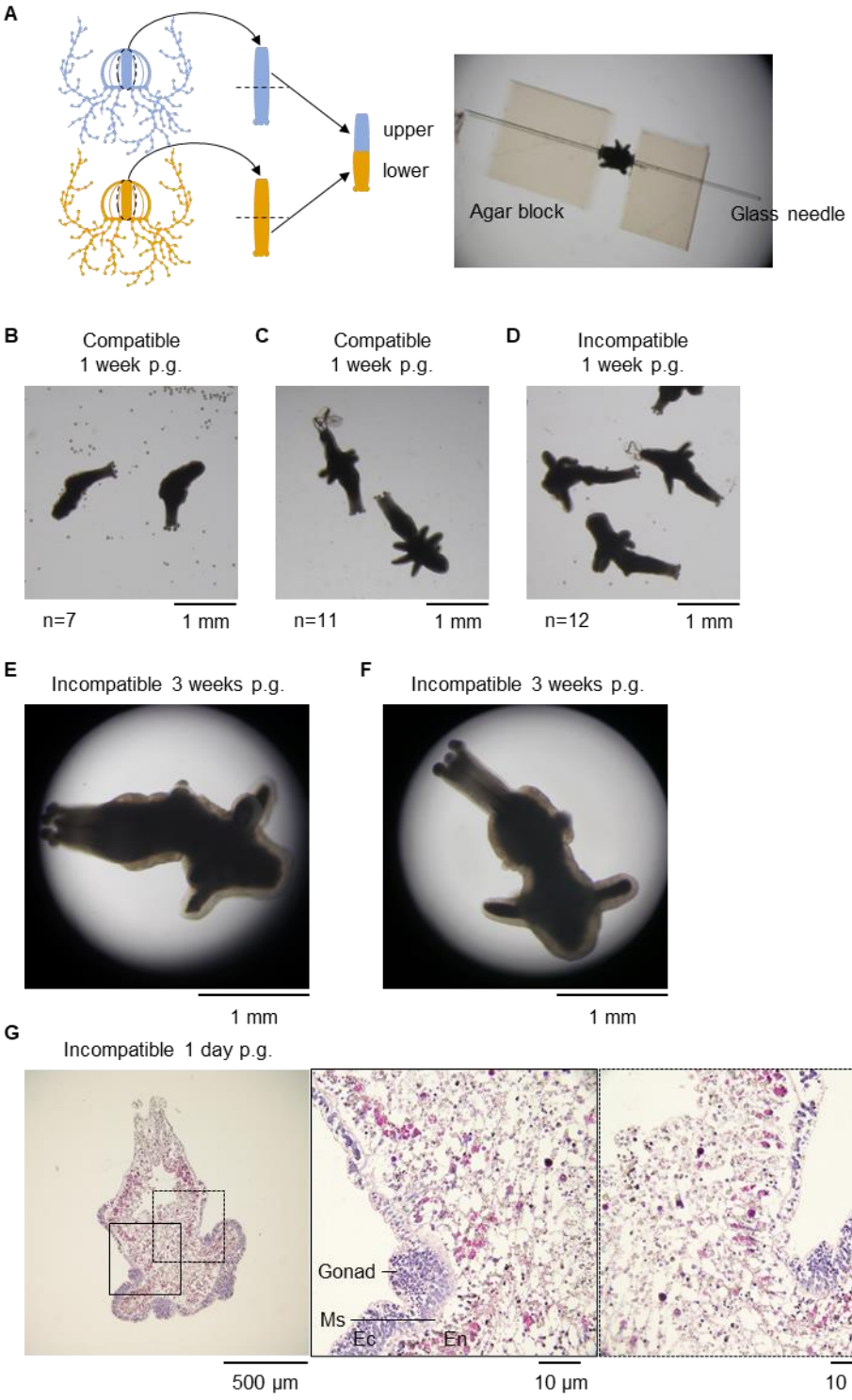

Figure 4.10. Manubrium half-half graft. (A) Schematic illustration of manubrium half-half graft experiment. (B,C) Representative images showing compatible manubrium half-half grafts (B: upper: F0 ♀, lower: F0 ♀, C: upper: F0 ♂, lower: F0 ♂) 1 week post graft. (D) Representative image showing incompatible manubrium half-half grafts (upper: F0 ♂, lower: F0 ♀) 1 week post graft. (E,F) Representative image showing incompatible manubrium half-half grafts (upper: F0 ♂, lower: F0 ♀) 3 weeks post graft. (G) Representative image showing haematoxylin-eosin-stained cross-section of incompatible manubrium half-half grafts (upper: F0 ♂, lower: F0 ♀) 1 day post graft. n: sample number.

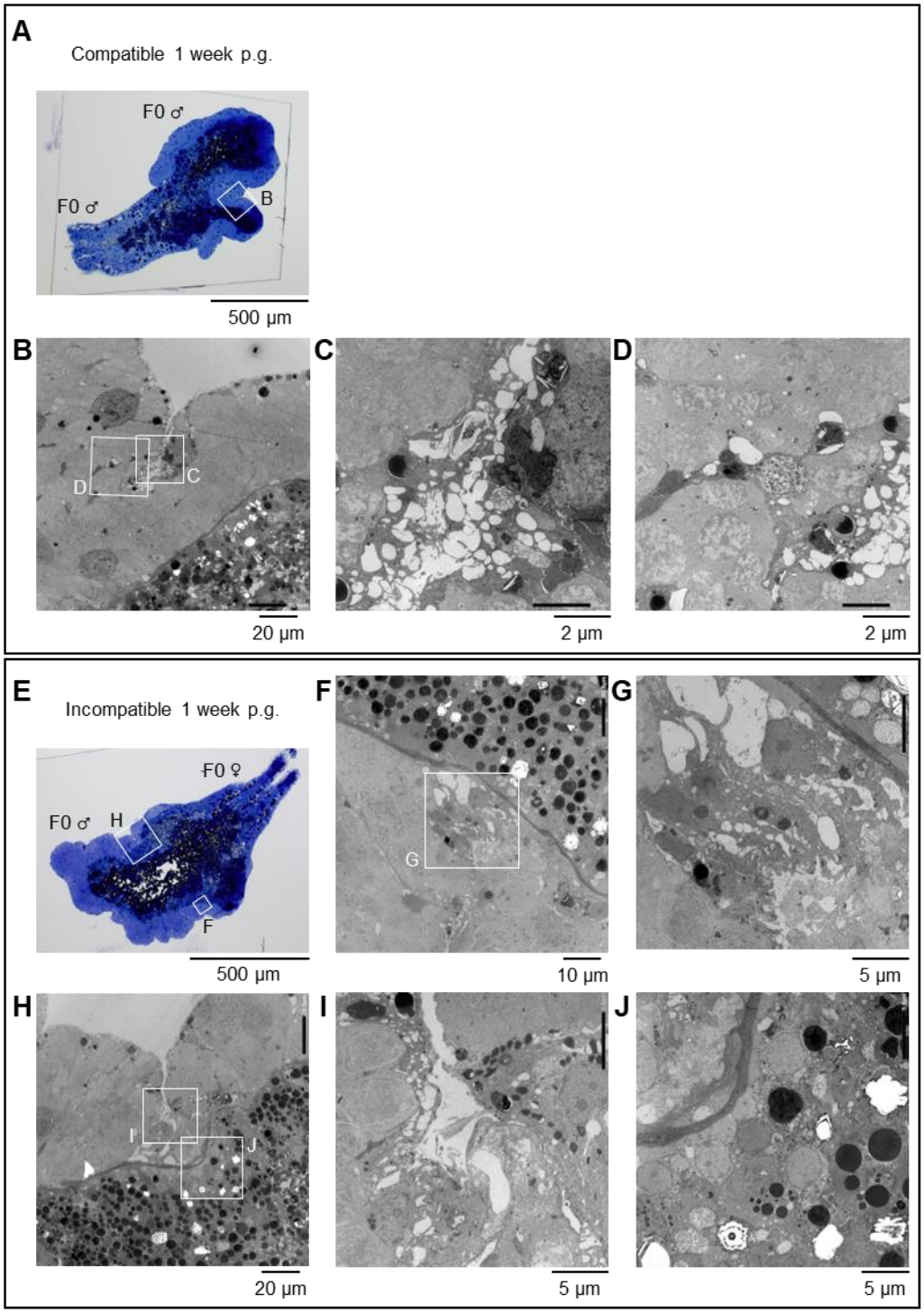

Figure 4.11. TEM observation of manubrium half-half grafts. (A-D) Representative images showing TEM observation of compatible manubrium half-half grafts (upper: F0 ♂, lower: F0 ♂) 1 week post graft. (A) Semi-thin section stained with 0.5 % toluidine blue. Connecting zone is enlarged in (B-D). (E-J) Representative images showing TEM observation of compatible manubrium half-half grafts (upper: F0 ♂, lower: F0 ♀) 1 week post graft. (E) Semi-thin section stained with 0.5 % toluidine blue. Connecting zone is enlarged in (F-J).

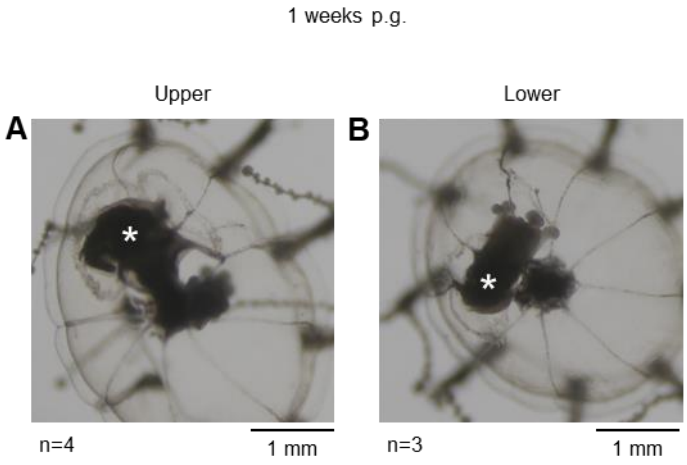

Figure 4.12. Umbrella-manubrium grafting with upper or lower portions of manubria induced ring-shaped scar formation. (A) Incompatible graft (host: F0 ♀, donor: F0 ♂) with upper portion of donor manubrium 1 weeks post graft. (B) Incompatible graft (host: F0 ♀, donor: F0 ♂) with lower portion of donor manubrium 1 weeks post graft. Asterisk: graft.

Chapter 5: Conclusions

Overall in this study, I established *C. radiatum* as a new animal model for allorecognition research. *Hydractinia* has been almost the only research model for Hydrozoan allorecognition for decades. There is so far lack of information about the evolutionary aspects of allorecognition in Hydrozoan. The introduction of the new research model in this study, with comprehensive characterisation of allorecognition in *C. radiatum*, both genetically and morphologically, provides valuable information for evaluating the evolution of Hydrozoan allorecognition.

Morphological analysis of allorecognition responses in stolons, documented in Chapter 2, showed that *C. radiatum* displayed clearly distinguishable and effective allorecognition responses: fusion and rejection. Fusion was defined by the rapid connection of gastrovascular canals upon cellular contact. Rejection was characterised by locally induced autophagic and necrotic cell death, and the separation of stolons by the reconstruction of the exoskeleton perisarc. The morphological characterisation of allorecognition responses in *C. radiatum* stolons demonstrated that fusion between compatible individuals is conserved across all studied Hydrozoan species, i.e. *Hydractinia*, *Podocoryne* and *C. radiatum*. While all three Hydrozoans also displayed "rejection", defined as the capability to prevent fusion between incompatible stolons, mechanisms and outcomes differ among species. *Hydractinia* has the most aggressive rejection responses involving killing the opponents with nematocysts. *Podocoryne* and *C. radiatum* showed relatively mild responses. Reconstruction of perisarc to block the stolons after the initial contact was first observed in *C. radiatum*. Genetic analysis featured in Chapter 3 identified the *C. radiatum Alr*-related genes, which are the first recognised and characterised *Alr* family genes outside *Hydractinia*, showing evidence of conservation. Only ortholog of *Hydractinia Alr1* was identified in *C. radiatum* and it

appeared to be the single determinant of allorecognition outcomes in the inbred lines, showing *C. radiatum* might possibly possesses a simpler genetic mechanism in determining allorecognition compared to *Hydractinia*. Chapter 4 showed *C. radiatum* medusae have only weak allorecognition. Medusae overall had high tolerance towards chimera formation, between both "compatible" and "incompatible" individuals, in terms of *Alr1*-dependent allorecognition. While there is no vigorous rejection response, e.g. separation of grafted tissues, ring-shaped scars were formed only in grafts without *Alr1* allele match, which suggested presence of potential weak *Alr*-dependent allorecognition responses in medusae.

Alr1 expression at transcript level was confirmed in both stolons and medusae. However, only stolons displayed clear allorecognition responses that effectively allow fusion between compatible colonies but not between incompatible ones. Medusae showed toleration towards chimera formation between incompatible individuals. Although the formation of ring-shaped scars might be a sign of weak allorecognition responses, allorecognition-induced cellular responses, including autophagic and necrotic cell death, were not observed at the contact regions in medusa grafts. These mechanisms appeared to be acquired only in stolons or were lost in medusa form. PI3K/autophagy inhibitor 3-MA treatment showed that the tissue overgrowth in the ring-shaped scars depended on PI3K/autophagy pathway. Autophagy was also observed in stolon allorecognition. It was not clear if analogous pathways were induced in stolons and medusae. Comparison of characterised allorecognition responses in stolons and medusae were summarized in Figure 5.

In conclusion, this study provided genetic and morphological information of *C. radiatum* allorecognition, facilitating not only comparative evaluation of Hydrozoan allorecognition across species, but also that between *C. radiatum* stolons and medusae. All in all, *C. radiatum* is a promising model animal for invertebrate allorecognition.

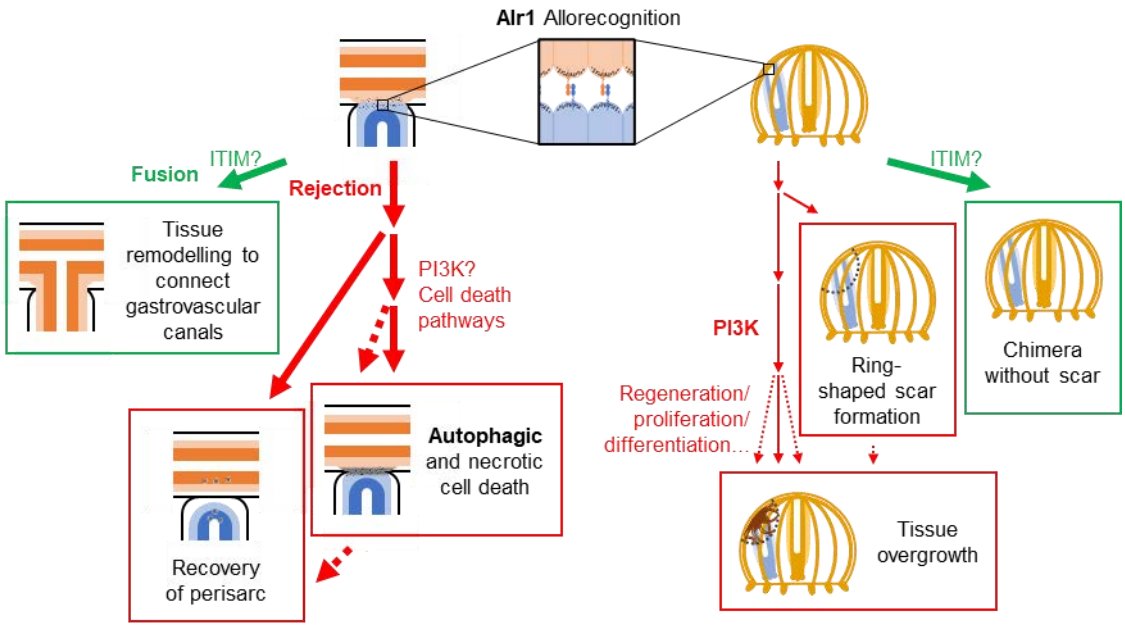

Figure 5. Schematic illustration of comparison between allorecognition in stolons and medusae.

References

Barrow, A. D., & Trowsdale, J. (2006). You say ITAM and I say ITIM, let's call the whole thing off: the ambiguity of immunoreceptor signalling. *European journal of immunology*, *36*(7), 1646-1653.

Barrow, A. D., Astoul, E., Floto, A., Brooke, G., Relou, I. A., Jennings, N. S., Smith, K. G., Ouwehand, W., Farndale, R. W., Alexander, D. R., & Trowsdale, J. (2004). Cutting edge: TREM-like transcript-1, a platelet immunoreceptor tyrosine-based inhibition motif encoding costimulatory immunoreceptor that enhances, rather than inhibits, calcium signaling via SHP-2. *Journal of immunology* (Baltimore, Md. : 1950), *172*(10), 5838–5842. https://doi.org/10.4049/jimmunol.172.10.5838

Bastiaans, E., Debets, A. J., & Aanen, D. K. (2015). Experimental demonstration of the benefits of somatic fusion and the consequences for allorecognition. Evolution, 69(4), 1091-1099.

Ben-Shlomo R. (2008). The molecular basis of allorecognition in ascidians. *BioEssays : news and reviews in molecular, cellular and developmental biology*, *30*(11-12), 1048–1051. https://doi.org/10.1002/bies.20848

Bentlage, B., & Collins, A. G. (2021). Tackling the phylogenetic conundrum of Hydroidolina (Cnidaria: Medusozoa: Hydrozoa) by assessing competing tree topologies with targeted high-throughput sequencing. *PeerJ*, *9*, e12104.

Bonner, J. T. (1998). The origins of multicellularity. Integrative Biology: Issues, News, and Reviews: Published in Association with The Society for Integrative and Comparative Biology, *1*(1), 27-36.

Bosch, T. C. G. and David, C. N. (1986). Immunocompetence in Hydra: epithelial cells recognize self-non-self and react against it. *J. Exp. Zool*. *238*,225-234.

Boya, P., González-Polo, R. A., Casares, N., Perfettini, J. L., Dessen, P., Larochette, N., ... & Kroemer, G. (2005). Inhibition of macroautophagy triggers apoptosis. *Molecular and cellular biology*, *25*(3), 1025-1040.

Buss, L. W. (1990). Competition within and between encrusting clonal invertebrates. *Trends in Ecology & Evolution*, *5*(11), 352-356.

Buss, L. W., & Yund, P. O. (1988). A comparison of recent and historical populations of the colonial hydroid Hydractinia. *Ecology*, *69*(3), 646-654.

Buss, L. W., Anderson, C., Westerman, E., Kritzberger, C., Poudyal, M., Moreno, M. A., & Lakkis, F. G. (2012). Allorecognition triggers autophagy and subsequent necrosis in the cnidarian Hydractinia symbiolongicarpus. *PLoS One*, *7*(11), e48914.

Buss, L. W., McFadden, C. S., & Keene, D. R. (1984). Biology of hydractiniid hydroids. 2. Histocompatibility effector system/competitive mechanism mediated by nematocyst discharge. *The Biological Bulletin*, *167*(1), 139-158.

Cadavid, L. F., Powell, A. E., Nicotra, M. L., Moreno, M., & Buss, L. W. (2004). An invertebrate histocompatibility complex. *Genetics*, *167*(1), 357-365.

Campbell, R. D. (1976). Elimination of Hydra interstitial and nerve cells by means of colchicine. *Journal of cell science*, *21*(1), 1-13.

Cannon, J. P., Haire, R. N., & Litman, G. W. (2002). Identification of diversified genes that contain immunoglobulin-like variable regions in a protochordate. *Nature immunology*, *3*(12), 1200-1207.

Carpenter, M. A., Powell, J. H., Ishizuka, K. J., Palmeri, K. J., Rendulic, S., & De Tomaso, A. W. (2011). Growth and long-term somatic and germline chimerism following fusion of juvenile Botryllus schlosseri. *The Biological Bulletin*, *220*(1), 57-70.

Chen, J. C., Chang, Y. W., Hong, C. C., Yu, Y. H., & Su, J. L. (2012). The role of the VEGF-C/VEGFRs axis in tumor progression and therapy. *International journal of molecular*

sciences, *14*(1), 88-107.

Cunningham, C. W., Buss, L. W., & Anderson, C. (1991). Molecular and Geologic Evidence of Shared History between Hermit Crabs and the Symbiotic Genus Hydractinia. *Evolution*, *45*(6), 1301–1316. https://doi.org/10.2307/2409881

De Tomaso A. W. (2006). Allorecognition polymorphism versus parasitic stem cells. Trends in genetics : TIG, 22(9), 485–490. https://doi.org/10.1016/j.tig.2006.07.001

De Tomaso, A. W. (2009). Sea squirts and immune tolerance. *Disease models & mechanisms*, *2*(9-10), 440-445.

De Tomaso, A. W. (2014). Allorecognition, germline chimerism, and stem cell parasitism in the colonial ascidian, Botryllus schlosseri. *Biological Theory*, *9*, 423-430.

De Tomaso, A. W., & Weissman, I. L. (2003). Initial characterization of a protochordate histocompatibility locus. *Immunogenetics*, *55*, 480-490.

De Tomaso, A. W., Nyholm, S. V., Palmeri, K. J., Ishizuka, K. J., Ludington, W. B., Mitchel, K., & Weissman, I. L. (2005). Isolation and characterization of a protochordate histocompatibility locus. *Nature*, *438*(7067), 454-459.

Franke, T. F., Kaplan, D. R., & Cantley, L. C. (1997). PI3K: downstream AKTion blocks apoptosis. *Cell*, *88*(4), 435-437.

Gloria-Soria, A., Moreno, M. A., Yund, P. O., Lakkis, F. G., Dellaporta, S. L., & Buss, L. W. (2012). Evolutionary genetics of the hydroid allodeterminant alr2. *Molecular biology and evolution*, *29*(12), 3921-3932.

Greaves, M. (2015). Evolutionary determinants of cancer. *Cancer discovery*, *5*(8), 806-820.

Grosberg R. and Plachetzki D. (2010) Marine Invertebrates: Genetics of Colony Recognition. In: Breed M.D. and Moore J., (eds.) *Encyclopedia of Animal Behavior*, *volume 2*, pp. 381-388 Oxford: Academic Press.

Halaby, D. M., Poupon, A., & Mornon, J. P. (1999). The immunoglobulin fold family: sequence analysis and 3D structure comparisons. *Protein engineering*, *12*(7), 563-571.

Huene, A. L., Sanders, S. M., Ma, Z., Nguyen, A. D., Koren, S., Michaca, M. H., ... & Nicotra, M. L. (2022). A family of unusual immunoglobulin superfamily genes in an invertebrate histocompatibility complex. *Proceedings of the National Academy of Sciences*, *119*(40), e2207374119.

Hwang, D. S., Masic, A., Prajatelistia, E., Iordachescu, M., & Waite, J. H. (2013). Marine hydroid perisarc: A chitin-and melanin-reinforced composite with DOPA–iron (III) complexes. *Acta biomaterialia*, *9*(9), 8110-8117.

Ivker, F. B. (1972). A hierarchy of histo-incompatibility in Hydractinia echinata. *The Biological Bulletin*, *143*(1), 162-174.

Karadge, U. B., Gosto, M., & Nicotra, M. L. (2015). Allorecognition proteins in an invertebrate exhibit homophilic interactions. *Current Biology*, *25*(21), 2845-2850.

Klug, M., Tardent, P., Smid, I., & Holstein, T. (1984). Presence and localization of chitinase in Hydra and Podocoryne (Cnidaria, Hydrozoa). *Journal of Experimental Zoology*, *229*(1), 69-72.

Kuznetsov, S. G., & Bosch, T. C. (2003). Self/nonself recognition in Cnidaria: contact to allogeneic tissue does not result in elimination of nonself cells in Hydra vulgaris. *Zoology*, *106*(2), 109-116.

Kuznetsov, S. G., Anton-Erxleben, F., & Bosch, T. C. (2002). Epithelial interactions in Hydra: apoptosis in interspecies grafts is induced by detachment from the extracellular matrix. *Journal of experimental biology*, *205*(24), 3809-3817.

Laird, D. J., De Tomaso, A. W., & Weissman, I. L. (2005). Stem cells are units of natural selection in a colonial ascidian. *Cell*, *123*(7), 1351-1360.

Lange, R. G., Dick, M. H., & Müller, W. A. (1992). Specificity and early ontogeny of historecognition in the hydroid Hydractinia. *Journal of Experimental Zoology*, *262*(3), 307-316.

Lange, R., Plickert, G., & Müller, W. A. (1989). Histoincompatibility in a low invertebrate, Hydractinia echinata: analysis of the mechanism of rejection. *Journal of Experimental Zoology*, *249*(3), 284-292.

Li, S., Chen, J. W., Xie, X., Tian, J., Deng, C., Wang, J., ... & Li, F. (2017). Autophagy inhibitor regulates apoptosis and proliferation of synovial fibroblasts through the inhibition of PI3K/AKT pathway in collagen-induced arthritis rat model. *American journal of translational research*, *9*(5), 2065.

Mali, B., Möhrlen, F., Frohme, M., & Frank, U. (2004). A putative double role of a chitinase in a cnidarian: pattern formation and immunity. *Developmental & Comparative Immunology*, *28*(10), 973-981.

McFadden, C. S. (1986). Laboratory evidence for a size refuge in competitive interactions between the hydroids Hydractinia echinata (Flemming) and Podocoryne carnea (Sars). *The Biological Bulletin*, *171*(1), 161-174.

McKitrick, T. R., Muscat, C. C., Pierce, J. D., Bhattacharya, D., & De Tomaso, A. W. (2011). Allorecognition in a basal chordate consists of independent activating and inhibitory pathways. *Immunity*, *34*(4), 616-626.

Mendoza-Becerril, M. A., Marian, J. E. A., Migotto, A. E., & Marques, A. C. (2017). Exoskeletons of Bougainvilliidae and other Hydroidolina (Cnidaria, Hydrozoa): structure and composition. *PeerJ*, *5*, e2964.

Mendoza-Becerril, M. A., Maronna, M. M., Pacheco, M. L., Simões, M. G., Leme, J. M., Miranda, L. S., ... & Marques, A. C. (2016). An evolutionary comparative analysis of the medusozoan (Cnidaria) exoskeleton. *Zoological Journal of the Linnean Society*, *178*(2), 206-

225.

Merlo, L. M., Pepper, J. W., Reid, B. J., & Maley, C. C. (2006). Cancer as an evolutionary and ecological process. *Nature reviews cancer*, *6*(12), 924-935.

Mokady, O., & Buss, L. W. (1996). Transmission genetics of allorecognition in Hydractinia symbiolongicarpus (Cnidaria:Hydrozoa). *Genetics*, *143*(2), 823–827. https://doi.org/10.1093/genetics/143.2.823

Mueller, W. A., & Rinkevich, B. (2020). Cell Communication-mediated nonself-recognition and-intolerance in representative species of the animal kingdom. *Journal of Molecular Evolution*, *88*(6), 482-500.

Murphy, K., Travers, P. & Walport, M. (2008). *Janeway's im Munobiology*, *Vol. 15*. Garland Science. Taylor & Francis Group, LLC, pp. 655–708.

Nicotra, M. L. (2019). Invertebrate allorecognition. *Current Biology*, *29*(11), R463-R467.

Nicotra, M. L. (2022). The Hydractinia allorecognition system. *Immunogenetics*, *74*(1), 27-34.

Nicotra, M. L., Powell, A. E., Rosengarten, R. D., Moreno, M., Grimwood, J., Lakkis, F. G., ... & Buss, L. W. (2009). A hypervariable invertebrate allodeterminant. *Current Biology*, *19*(7), 583-589.

Niklas, K. J. (2014). The evolutionary-developmental origins of multicellularity. *American journal of botany*, *101*(1), 6-25.

Nyholm, S. V., Passegue, E., Ludington, W. B., Voskoboynik, A., Mitchel, K., Weissman, I. L., & De Tomaso, A. W. (2006). fester, A candidate allorecognition receptor from a primitive chordate. *Immunity*, *25*(1), 163-173.

Pellettieri, J., Fitzgerald, P., Watanabe, S., Mancuso, J., Green, D. R., & Alvarado, A. S. (2010). Cell death and tissue remodeling in planarian regeneration. *Developmental*

biology, *338*(1), 76-85.

Powell, A. E., Nicotra, M. L., Moreno, M. A., Lakkis, F. G., Dellaporta, S. L., & Buss, L. W. (2007). Differential effect of allorecognition loci on phenotype in Hydractinia symbiolongicarpus (Cnidaria: Hydrozoa). *Genetics*, *177*(4), 2101-2107.

Rauniyar, K., Bokharaie, H., & Jeltsch, M. (2023). Expansion and collapse of VEGF diversity in major clades of the animal kingdom. *Angiogenesis*, 1-25.

Ravetch, J. V., & Lanier, L. L. (2000). Immune inhibitory receptors. *Science*, *290*(5489), 84-89.

Renkema, G. H., Boot, R. G., Au, F. L., Donker-Koopman, W. E., Strijland, A., Muijsers, A. O., ... & Aerts, J. M. (1998). Chitotriosidase, a chitinase, and the 39-kDa human cartilage glycoprotein, a chitin-binding lectin, are homologues of family 18 glycosyl hydrolases secreted by human macrophages. *European Journal of Biochemistry*, *251*(1-2), 504-509.

Rinkevich, B. (2002). Germ cell parasitism as an ecological and evolutionary puzzle: hitchhiking with positively selected genotypes. *Oikos*, *96*(1), 25-30.

Rodriguez-Valbuena, H., Gonzalez-Muñoz, A., & Cadavid, L. F. (2022). Multiple Alr genes exhibit allorecognition-associated variation in the colonial cnidarian Hydractinia. *Immunogenetics*, *74*(6), 559-581.

Rosa, S. F., Powell, A. E., Rosengarten, R. D., Nicotra, M. L., Moreno, M. A., Grimwood, J., ... & Buss, L. W. (2010). Hydractinia allodeterminant alr1 resides in an immunoglobulin superfamily-like gene complex. *Current Biology*, *20*(12), 1122-1127.

Rosengarten, R. D., & Nicotra, M. L. (2011). Model systems of invertebrate allorecognition. *Current Biology*, *21*(2), R82-R92.

Schnitzler, C. E., Chang, E. S., Waletich, J., Wong, W. Y., Nguyen, A. D., Barreira, S., ... & Baxevanis, A. D. (2023). The genome of the colonial hydroid Hydractinia reveals

their stem cells use a toolkit of genes shared with all animals. bioRxiv, 2023-08.

Seipel, K., Eberhardt, M., Müller, P., Pescia, E., Yanze, N., & Schmid, V. (2004). Homologs of vascular endothelial growth factor and receptor, VEGF and VEGFR, in the jellyfish Podocoryne carnea. *Developmental dynamics: an official publication of the American Association of Anatomists*, *231*(2), 303-312.

Sferrazza, G., Corti, M., Brusotti, G., Pierimarchi, P., Temporini, C., Serafino, A., & Calleri, E. (2020). Nature-derived compounds modulating Wnt/β-catenin pathway: A preventive and therapeutic opportunity in neoplastic diseases. *Acta Pharmaceutica Sinica B*, *10*(10), 1814-1834.

Shenk, M. A., & Buss, L. W. (1991). Ontogenetic changes in fusibility in the colonial hydroid Hydractinia symbiolongicarpus. *Journal of Experimental Zoology*, *257*(1), 80-86.

Sinigaglia, C., Peron, S., Eichelbrenner, J., Chevalier, S., Steger, J., Barreau, C., ... & Leclère, L. (2020). Pattern regulation in a regenerating jellyfish. *Elife*, *9*, e54868.

Song, Q., Liu, H., Zhen, H., & Zhao, B. (2020). Autophagy and its role in regeneration and remodeling within invertebrate. *Cell & Bioscience*, *10*(1), 1-16.

Stoner, D. S., & Weissman, I. L. (1996). Somatic and germ cell parasitism in a colonial ascidian: possible role for a highly polymorphic allorecognition system. *Proceedings of the National Academy of Sciences*, *93*(26), 15254-15259.

Tachibana, K., Matsumoto, M., Minowa, A., & Deguchi, R. (2020). Isolation and Characterization of Feeding-Deficient Strains in Inbred Lines of the Hydrozoan Jellyfish Cladonema pacificum. *Zoological science*, *37*(3), 263-270.

Tardent, P., & Bührer, M. (1982). Intraspecific tissue incompatibilities in the metagenetical Podocoryne carnea M. Sars (Cnidaria, Hydrozoa). *Progress in clinical and biological research*, *85*, 295-308.

Tardent, P., & Jauch, U. (1983). An ultrastructural study of homoclonal and

heteroclonal encounters between stolons in Podocoryne carnea M. Sars (Hydroidea, Athecata). *Mechanisms of Ageing and Development*, *21*(3-4), 257-272.

Tettamanti, G., Carata, E., Montali, A., Dini, L., & Fimia, G. M. (2019). Autophagy in development and regeneration: role in tissue remodelling and cell survival. *The European Zoological Journal*, *86*(1), 113-131.

Tsuji, H., Nishimura, S., Inui, T., Kado, Y., Ishikawa, K., Nakamura, T., & Uegaki, K. (2010). Kinetic and crystallographic analyses of the catalytic domain of chitinase from Pyrococcus furiosus–the role of conserved residues in the active site. *The FEBS journal*, *277*(12), 2683-2695.

Underhill, D. M., & Goodridge, H. S. (2007). The many faces of ITAMs. *Trends in immunology*, *28*(2), 66-73.

Vandepas, L. E. (2018). Chitin the Good Fight–Identification and Description of Chitin and Its Genes in Cnidaria (Doctoral dissertation).

Vandepas, L. E., Tassia, M. G., Halanych, K. M., & Amemiya, C. T. (2023). Unexpected Distribution of Chitin and Chitin Synthase across Soft-Bodied Cnidarians. *Biomolecules*, *13*(5), 777.

Wang, J. H. (2013). The sequence signature of an Ig-fold. Protein & cell, 4, 569-572.

Westman, J., Grinstein, S., & Marques, P. E. (2020). Phagocytosis of necrotic debris at sites of injury and inflammation. *Frontiers in immunology*, *10*, 3030.

Wood, J. M., Bold, G., Buchdunger, E., Cozens, R., Ferrari, S., Frei, J., ... & Marmé, D. (2000). PTK787/ZK 222584, a novel and potent inhibitor of vascular endothelial growth factor receptor tyrosine kinases, impairs vascular endothelial growth factor-induced responses and tumor growth after oral administration. *Cancer research*, *60*(8), 2178-2189.

Zahir, N., Sun, R., Gallahan, D., Gatenby, R. A., & Curtis, C. (2020). Characterizing the ecological and evolutionary dynamics of cancer. *Nature genetics*, *52*(8), 759-767.

Zapata, F., Goetz, F. E., Smith, S. A., Howison, M., Siebert, S., Church, S. H., ... & Cartwright, P. (2015). Phylogenomic analyses support traditional relationships within Cnidaria. *PloS one*, *10*(10), e0139068.

Zhang, X. D., Qi, L., Wu, J. C., & Qin, Z. H. (2013). DRAM1 regulates autophagy flux through lysosomes. *PLoS one*, *8*(5), e63245.

Appendix 1: TEM morphological observation of *C. radiatum*

During the observation of allorecognition responses by TEM, valuable high-resolution images characterising *C. radiatum* morphology were obtained. These images are organised in this appendix chapter.

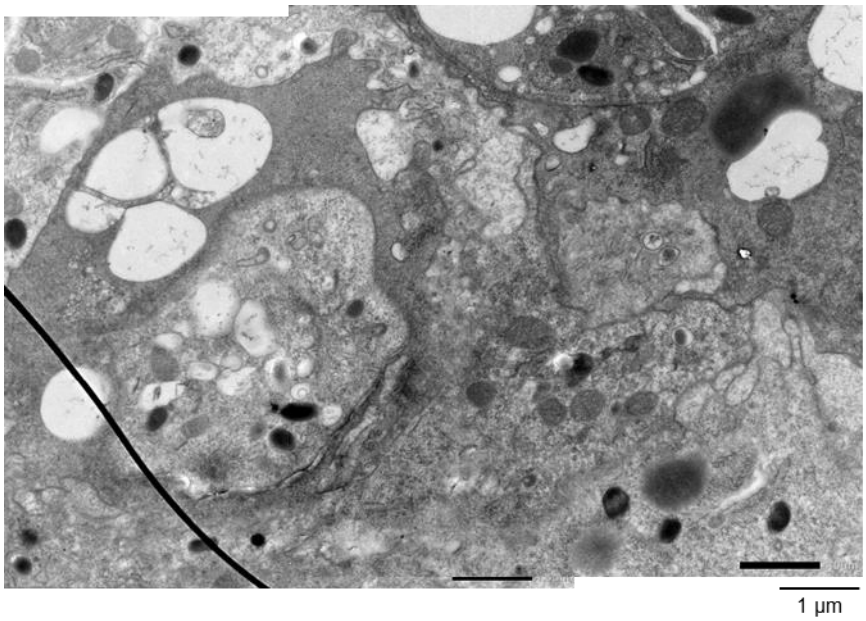

Appendix figure A1.1. Additional image of phagocytotic cells in stolons.
Manually stitched images of phagocytotic cells observed in incompatible encounter (attacking: F0♀, defending: F0 ♂) at 3 hours post-encounter. The phagocytotic cells had vesicles with engulfed cellular materials, smooth homogenous cytoplasm and outward cell projections.

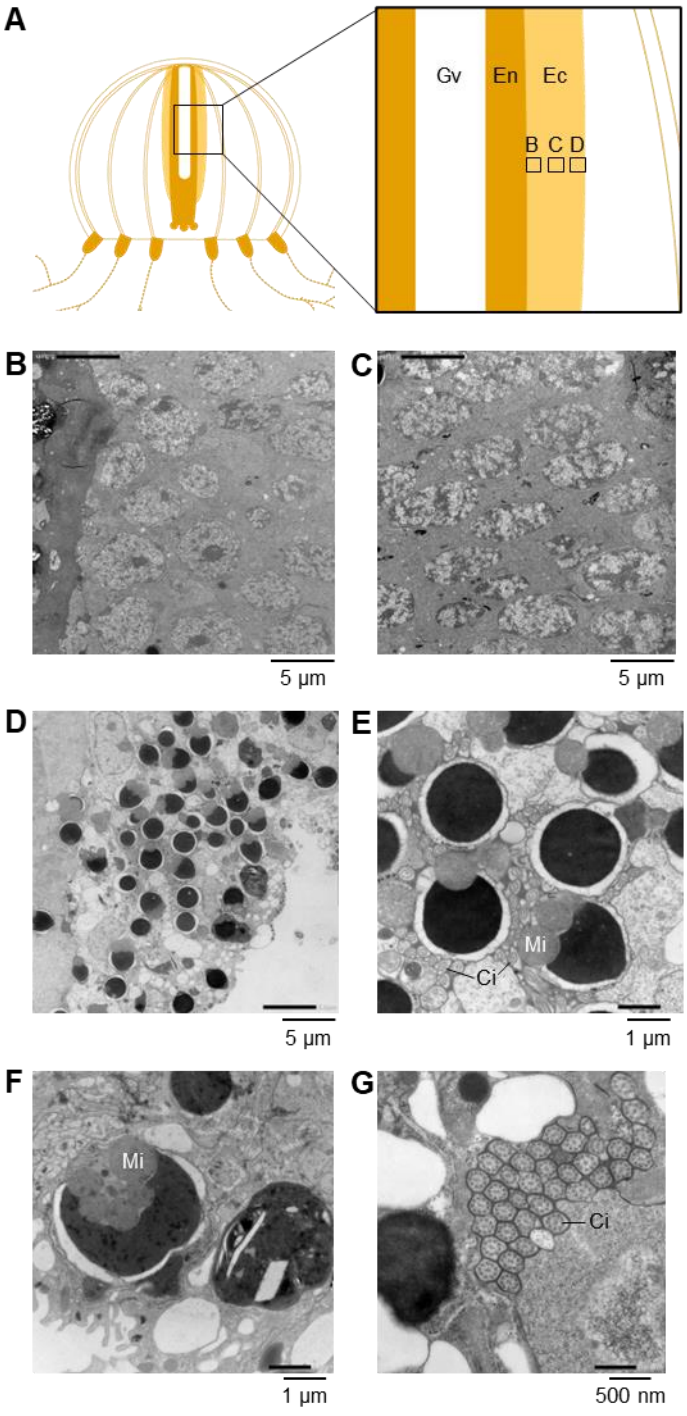

Appendix figure A1.2. Spermatogenesis in *C. radiatum*. (A) Illustration showing the approximate positions of (B-D). (B,C) Early spermatogia. (D,E) spermatozoa at the gonad surface. (F) Spermatozoon with five mitochondria (Mi) attached. (G) Cilia in spermatocytes. Ec: ectoderm, En: endoderm, Gv: gastrovascular cavity, Ci: cilium.

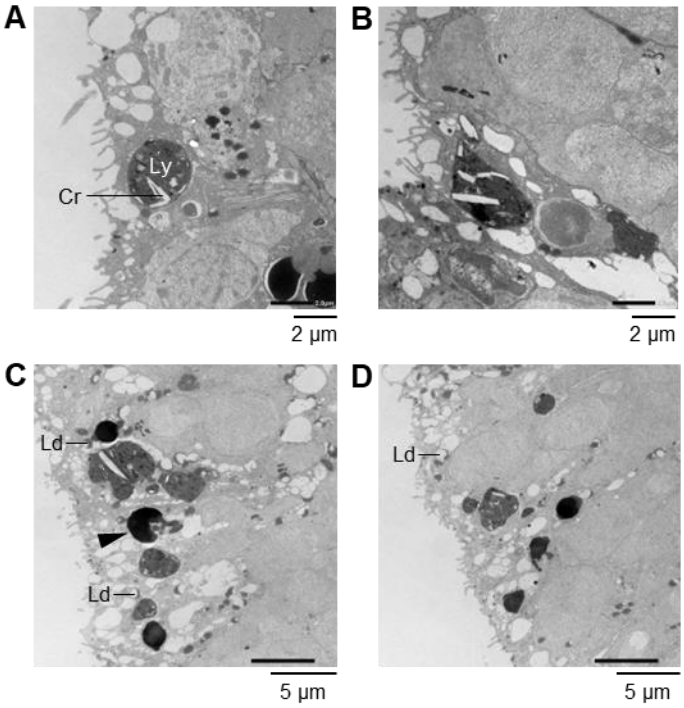

Appendix figure A1.3. Large lysosomal vesicles at the male gonad surface. (A-D) representative images of the large crystal (Cr)-containing lysosomal vesicles (Ly) observed at the surface of male gonad. They were often observed with deformed spermatozoa (black arrow) and lipid droplet (Ld).

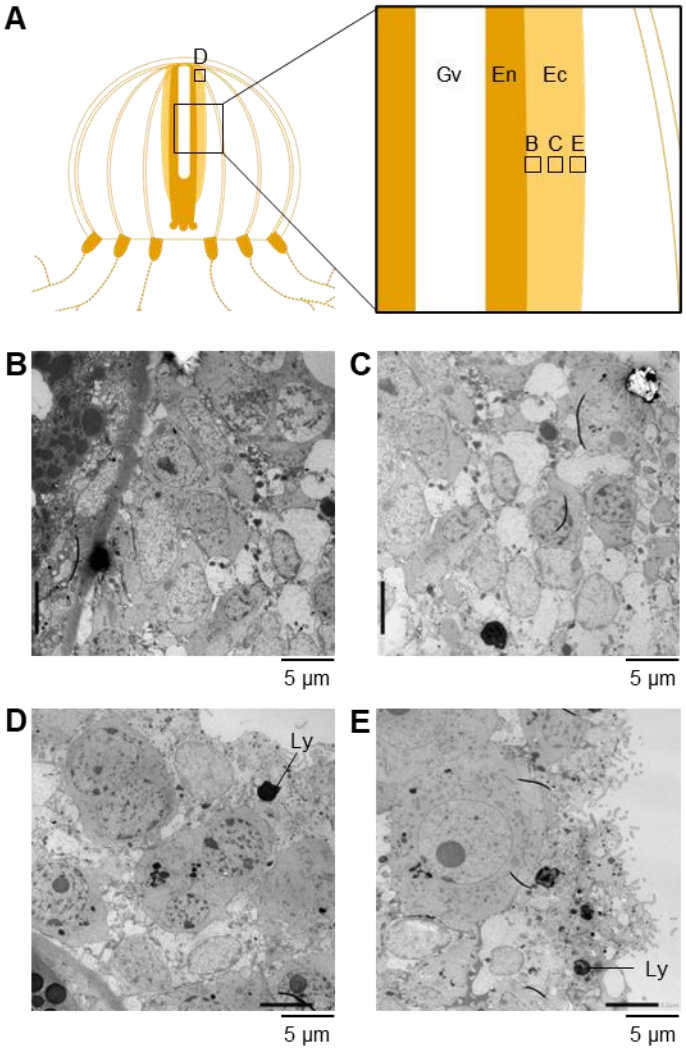

Appendix figure A1.4. Oogenesis in *C. radiatum*. (A) Illustration showing the approximate positions of (B-E). (B,C,D) Primary oogonia. (E) Oocyte with nucleolated nucleus and lysosomal vesicles at the surface.

Appendix 2: Establishment of *C. radiatum* experimental protocols

In-situ hybridisation is a powerful tool to detect transcript expression by visualising the expression patterns in whole-mount or sectioned tissues. However, protocols adapted from other animal models did not work on *C. radiatum* stolons, mainly due to the impermeability of the perisarc exoskeleton. Here in this appendix chapter, I summarise the optimisation work on the whole-mount stolon in-situ hybridisation protocol.

CrChit1 candidate 1 was used as the detection target for the optimisation as clear signals were consistently detected in the endoderm. However, there were two main problems affecting the qualities of the assay results: (1) uneven signals and obviously denser signals at edges or regions with "openings"; (2) general high background signals, especially at closed structures, e.g. stolon tips. I suspect that the chitinous skeleton perisarc limited the permeability of reagents, including RNA-probes, antibodies, washing buffer, etc., during the assays, leading to the uneven lack of access or accumulation of the reagents in the samples. Therefore, different pre-treatments were tested to improve the permeability of samples:

(1) 0.2N HCl (RT 20 min)—reported to improve background signals by eliminating endogenous alkaline phosphatase, 1N HCl RT was applied to gram-positive bacteria to dissolve cell wall;
(2) 80°C (in Hybridisation Buffer) (30 min)—reported to improve background signals by eliminating endogenous alkaline phosphatase;
(3) 2.5-10 mg/ml Lysozyme (RT 20-30 min)—2.5 mg/ml was applied to gram-positive bacteria to dissolve cell wall;
(4) Physical cut by razor blade—reported in recent paper described partial dissection of the perisarc with a scalpel enhance permeability in immunohistochemistry in hydroid stolons.

Experiment results (Appendix figure A2.1) showed that clear signals were detected in

0.2N HCl treated samples. 80°C treatment did not improve signal/noise ratio. Lysozyme treatment did not improve evenness of signals. Only introduction of physical cuts by razon blade significantly allow expression signals to be detected throughout the samples. It is in line with the hypothesis that the uneven signals were due to the impermeability of the perisarc. As the permeability was dependent on the manually introduced physical cuts, the assay results depended heavily on manipulation techniques. Cuts must be evenly introduced at intervals as small as possible. The cuts often produced damages to the morphology of the samples, limiting the accuracy and reliability of the assay results, especially for signal detection at specific structures, e.g. stolon encounter region, stolon tips. Further optimisation is desired to improve the assay result quality.

References

Furukawa, K., Hoshino, T., Tsuneda, S., & Inamori, Y. (2006). Comprehensive analysis of cell wall-permeabilizing conditions for highly sensitive fluorescence in situ hybridization. *Microbes and environments*, *21*(4), 227-234.

Kosevich, I. A. (2023). Ultrastructural and immunocytochemical evidence of a colonial nervous system in hydroids. *Frontiers in Neural Circuits*, *17*.

Vauti, F., Stegemann, L. A., Vögele, V., & Köster, R. W. (2020). All-age whole mount in situ hybridization to reveal larval and juvenile expression patterns in zebrafish. *PloS one*, *15*(8), e0237167.

Wolenski, F. S., Layden, M. J., Martindale, M. Q., Gilmore, T. D., & Finnerty, J. R. (2013). Characterizing the spatiotemporal expression of RNAs and proteins in the starlet sea anemone, Nematostella vectensis. *Nature protocols*, *8*(5), 900-915.

大西章博, 長野晃弘, 藤本尚志, 高橋力也, 牛久保明邦, & 鈴木昌治. (2003). FISH

(fluorescence in situ hybridization) 法を適用したコンポスト好熱性細菌の検出技術の開発. *環境技術*, *32*(12), 976-985.

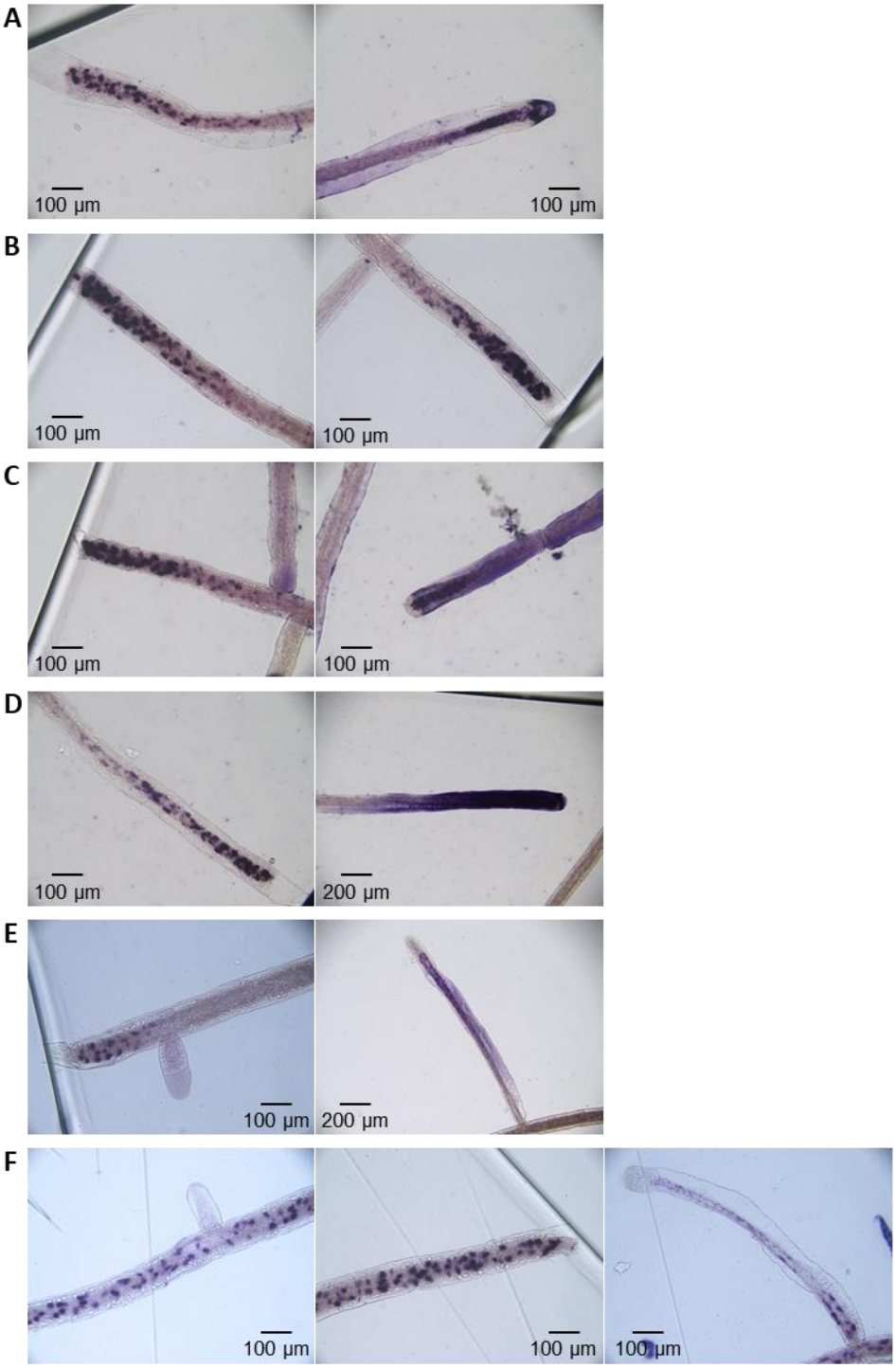

Appendix figure A2.1. Optimisation of whole-mount stolon in-situ hybridisation protocol.
Samples with pre-treatments as stated below:
(A) 0.2N HCl (20 min)
(B) 0.2N HCl (20 min), 80°C (in Hybridisation Buffer) (30 min)
(C) 2.5 mg/ml Lysozyme (RT 30 min), 0.2N HCl (20 min)
(D) 2.5 mg/ml Lysozyme (RT 30 min), 0.2N HCl (20 min), 80°C (in Hybridisation Buffer) (30 min)
(E) 0.2N HCl (20 min), 10 mg/ml Lysozyme (RT 20 min)
(F) 0.2N HCl (20 min), physical cut by razor blade

Appendix 2.2 Whole-mount stolon in-situ hybridisation protocol (v5 20230921)

Fixation

4% PFA/1X PBS (4°C, use within 1 month) 4°C O/N

1X PBST RT 10 min × 3

Preparation: Fresh 100% MeOH

MeOH series: 25% MeOH/1X PBST, 50% MeOH/1X PBST, 75% MeOH/1X PBST

Dehydration—reduces background (eliminate endogenous AP?), increases permeability?

25% MeOH/1X PBST RT 10 min

50% MeOH/1X PBST RT 10 min

75% MeOH/1X PBST RT 10 min

100% MeOH RT 10 min

100% MeOH → can store long-term at -30°C

Preparation: Prepare 0.3% H2O2/MeOH: 50 µl 35% H2O2 + 5 ml MeOH (1/116X dilution)

MeOH series: 25% MeOH/1X PBST, 50% MeOH/1X PBST, 75% MeOH/1X PBST

Bleaching

0.3% H2O2/MeOH RT 30 min

Preparation: Switch on 55°C oven, 80°C heat block

Pre-hybridisation buffer → RT, 55°C

Thaw frozen Pro K stock (-30°C)
→ prepare 10 µg/ml Pro K/1X PBST: 1 mg/ml Pro K stock→ 1/100X dilution in 1X PBST

Prepare 0.1 M TEA buffer: 1 M TEA buffer (pH 8.0) → 1/10X dilution in Milli-Q

100% MeOH RT 5 min

Rehydration

75% MeOH/1X PBST RT 5 min

50% MeOH/1X PBST RT 5 min

25% MeOH/1X PBST RT 5 min

1X PBST RT 5 min × 2

Stolon: Introduce cuts on stolons by pressing with razor blade to increase permeability.

HCl Treatment—eliminates endogenous alkaline phosphatase, enhances perisarc permeability

0.2N HCl RT 20 min

Milli-Q RT 5 min

Proteinase K Treatment—increases permeability

10 µg/ml Pro K/1X PBST RT 40 min

1X PBST RT 5 min

Re-fixation

4% PFA/1X PBS RT 20 min

1X PBST RT 5 min × 3

Acetylation—reduces non-specific background by neutralising positive charges in the samples

0.1M TEA buffer RT 5 min

0.3% Acetic anhydride/0.1 M TEA buffer (+ 30 µl Acetic anhydride/10 ml just before use, half-life in aq. is only a few min., mix vigorously) RT 5 min

0.6% Acetic anhydride/0.1 M TEA buffer (+ 60 µl Acetic anhydride/10 ml just before use, half-life in aq. is only a few min., mix vigorously) RT 5 min

1X PBST RT 5 min × 2

Pre-hybridisation

RT Pre-hybridisation buffer RT 15 min

55°C Pre-hybridisation buffer 55°C 1 hr

Hybridisation

Preparation: Dilute DIG-RNA probes to 0.5-1 µg/ml with Hybridisation buffer
→ denature at 80°C 5 min → on ice → 55°C

DIG-RNA probes in Hybridisation buffer 55°C 18-24 hr

Preparation: Wash buffer 1, Wash buffer 2, 2X SSC+T, 0.2X SSC+T → 55°C

Post-hybridisation wash

Wash buffer 1 55°C 30 min

Wash buffer 2 55°C 30 min

2X SSC+T 55°C 30 min

0.2X SSC+T 55°C 30 min

0.2X SSC+T 55°C → RT 15 min

Alkaline phosphatase-conjugated antibody incubation and detection

MABT RT 10 min × 2

Preparation: Prepare 2% Blocking buffer: 10% Blocking buffer/MABT (4°C) → 1/5X dilution in MABT

2% Blocking buffer RT 2 hr

Preparation: Prepare Anti-DIG AP Ab solution: Anti-DIG AP Fab fragments (Roche) (4°C) → 1/2000X dilution in MABT

Anti-DIG AP Ab solution 4°C O/N (12-16 hr)

MABT RT 10 min × 6

MABT RT ~1 hr - O/N (4°C) × ~4 (total ≥ 10 times)

Preparation: Prepare AP buffer -Mg, AP buffer + Levamisole: 100 mM Levamisole stock (-20°C) → 1/20X dilution in AP buffer (final conc.: 5 mM)

AP buffer -Mg RT 5 min

AP buffer + Levamisole RT 5 min × 2

Preparation: Prepare NBT/BCIP solution: NBT/BCIP stock solution (Roche) (4°C) → 1/100X dilution in AP buffer + Levamisole

NBT/BCIP solution RT 20 min~ (in dark; check every 10 min under microscope)

1X PBST RT 5 min × 2

99.5% EtOH RT 10 min (better signal/noise)

1X PBST RT 5 min × 2

Counterstain with 10 µg/ml **DAPI/PBST** RT 10 min (in dark)

1X PBST RT 5 min × 2

4% PFA/1X PBS RT 30 min

1X PBST RT 10 min × 2

Mount samples on glass slides with **Fluro-KEEPER** (nacalai) (or Glycerol mounting medium)

Reagents:

10X PBS (D-PBS) RT

Reagent/Stock	Quantity (100 ml)	Final conc.
D-PBS powder (D5652)	1 bottle	10X
Milli-Q	→ 100 ml	

4% PFA/1X PBST 4°C (use within 1 month)

Reagent/Stock	Quantity (40 ml)	Final conc.
16% paraformaldehyde (RT or -30°C)	10 ml	4%
10X PBS	4 ml	1X
Milli-Q	→ 40 ml	

1X PBST RT

Reagent/Stock	Quantity (500 ml)	Final conc.
10X PBS	50 ml	1X
Tween-20	500 µl	0.1%
Milli-Q	→ 500 ml	

0.2 N HCl RT

Reagent/Stock	Quantity (50 ml)	Final conc.
Conc. HCl (35%; 11.3 N)	890 µl*	0.2 N
Milli-Q	→ 50 ml	

*transfer with a marked glass pipette

1 M TEA buffer (pH 8.0) Adjust with ~3 ml conc. HCl (pH paper); RT

Reagent/Stock	Quantity (50 ml)	Final conc.
Triethanolamine (TEA)*	7.46 g	1 M
Milli-Q	→ 50 ml	

*TEA is extremely viscous. Weigh out 7.46 g in a 50-ml tube (transfer with 5-ml pipette).

20X SSC (pH 7.0) Adjust with HCl; RT

Reagent/Stock	Quantity (500 ml)	Final conc.
NaCl	87.65 g	3 M
Sodium citrate	44.1 g	0.3 M
Milli-Q	→ 500 ml	

50X Denhardt's reagent 4°C

Reagent/Stock	Quantity (50 ml)	Final conc.
Ficoll 400	0.5 g	1%
Polyvinylpyrrolidone (PVP)	0.5 g	1%
Bovine serum albumin (BSA) (4°C)	0.5 g	1%
Milli-Q	→ 50 ml	

Pre-hybridisation buffer -30°C

Reagent/Stock	Quantity (100 ml)	Final conc.
20X SSC	25 ml	5X
Formamide	50 ml	50%
tRNA (-30°C)	5 mg	50 µg/ml
Heparin (4°C)	5 mg	50 µg/ml
Denhardt's reagent (50X) (4°C)	4 ml	2X
Tween-20	100 µl	0.1%
Milli-Q	→100 ml	

Hybridisation buffer -30°C

Reagent/Stock	Quantity (100 ml)	Final conc.
Dextran sulphate	10 g	10%
20X SSC	25 ml	5X
Deionised formamide (-30°C)	50 ml	50%
tRNA (-30°C)	5 mg	50 µg/ml
Heparin (4°C)	5 mg	50 µg/ml
Denhardt's reagent (50X) (4°C)	4 ml	2X
Tween-20	100 µl	0.1%
Milli-Q	→100 ml	

Wash buffer 1 RT

Reagent/Stock	Quantity (100 ml)	Final conc.
20X SSC	25 ml	5X
Formamide	50 ml	50%
Tween-20	100 µl	0.1%
Milli-Q	→100 ml	

Wash buffer 2 RT

Reagent/Stock	Quantity (100 ml)	Final conc.
20X SSC	10 ml	2X
Formamide	50 ml	50%
Tween-20	100 µl	0.1%
Milli-Q	→100 ml	

2X SSC+T RT

Reagent/Stock	Quantity (50 ml)	Final conc.
20X SSC	5 ml	2X
20% Tween-20	250 µl	0.1%
Milli-Q	→50 ml	

0.2X SSC+T RT

Reagent/Stock	Quantity (50 ml)	Final conc.
20X SSC	0.5 ml	0.2X
20% Tween-20	250 µl	0.1%
Milli-Q	→50 ml	

Maleic acid buffer (MABT) (pH 7.5) Adjust pH with ~4 g NaOH pellet; RT

Reagent/Stock	Quantity (500 ml)	Final conc.
Maleic acid	5.8 g	100 mM
NaCl	4.38 g	150 mM
Tween-20	500 µl	0.1%
Milli-Q	→500 ml	

1 M Tris-HCl (pH 9.5) Adjust pH with HCl (pH paper); RT

Reagent/Stock	Quantity (500 ml)	Final conc.
Tris base	60.55 g	1 M
Milli-Q	→500 ml	

5 M NaCl RT

Reagent/Stock	Quantity (50 ml)	Final conc.
NaCl	14.61 g	5 M
Milli-Q	→50 ml	

1 M MgCl2 RT

Reagent/Stock	Quantity (50 ml)	Final conc.
MgCl2	10.165 g	1 M
Milli-Q	→50 ml	

100 mM Levamisole -30°C

Reagent/Stock	Quantity (5 ml)	Final conc.
Levamisole hydrochloride (WM=240.75)	0.1205 g	100 mM
Milli-Q	→5 ml	

AP buffer +/-Mg (a.k.a. NT(M)T buffer) (MgOH precipitate, pH decreases by time, make fresh, syringe-filtered)

Reagent/Stock	Quantity (50 ml)	Final conc.
1 M Tris-HCl (pH 9.5)	5 ml	0.1 M
(1 M MgCl2	2.5 ml	50 mM)
5 M NaCl	1 ml	0.1 M
Tween-20	500 µl	1%
Milli-Q	→ 50 ml	

WASTE:

K: PFA, Acetic anhydride/TEA, MABT, NBT/BCIP

f-OH: MeOH, H_2O_2/MeOH,

f-N: formamide